VINICIUS DELGADO DA ROCHA

MOLECULAR EVOLUTION OF TWO PATHOGENICITY-ASSOCIATED GENE FAMILIES ACROSS THE DOTHIDEOMYCETES CLASS OF FUNGI

Tese apresentada à Universidade Federal de Viçosa, como parte das exigências do Programa de Pós-Graduação em Genética e Melhoramento, para obtenção do título de *Doctor Scientiae*.

Orientador: Luiz Orlando de Oliveira

VIÇOSA - MINAS GERAIS
2023

Ficha catalográfica elaborada pela Biblioteca Central da Universidade Federal de Viçosa - Campus Viçosa

T
R672m
2023

Rocha, Vinícius Delgado da, 1995-
Molecular evolution of two pathogenicity-associated gene families across the Dothideomycetes class of fungi / Vinícius Delgado da Rocha. – Viçosa, MG, 2023.
1 tese eletrônica (123 f.): il. (algumas color.).

Texto em inglês.
Orientador: Luiz Orlando de Oliveira.
Tese (doutorado) - Universidade Federal de Viçosa, Departamento de Bioquímica e Biologia Molecular, 2023.
Inclui bibliografia.
DOI: https://doi.org/10.47328/ufvbbt.2023.467
Modo de acesso: World Wide Web.

1. Fungos fitopatogênicos. 2. *Corynespora*. 3. Evolução (Biologia). 4. Genômica. 5. Filogenia. 6. Fitopatógenos. I. Oliveira, Luiz Orlando de, 1961-. II. Universidade Federal de Viçosa. Departamento de Bioquímica e Biologia Molecular. Programa de Pós-Graduação em Genética e Melhoramento. III. Título.

CDD 22. ed. 579.564

Bibliotecário(a) responsável: Bruna Silva CRB-6/2552

VINICIUS DELGADO DA ROCHA

MOLECULAR EVOLUTION OF TWO PATHOGENICITY-ASSOCIATED GENE FAMILIES ACROSS THE DOTHIDEOMYCETES CLASS OF FUNGI

Tese apresentada à Universidade Federal de Viçosa, como parte das exigências do Programa de Pós-Graduação em Genética e Melhoramento, para obtenção do título de *Doctor Scientiae*.

APROVADA: 20 de julho de 2023.

Assentimento:

Vinicius Delgado da Rocha
Autor

Luiz Orlando de Oliveira
Orientador

AGRADECIMENTOS

A Deus pela vida, sabedoria e coragem ao longo dessa jornada.

À Universidade Federal de Viçosa (UFV) e ao programa de Pós-Graduação em Genética e Melhoramento (PPGGM) que contribuíram para fornecer ensino e condições de trabalho para realização este curso de doutorado.

À Coordenação de Aperfeiçoamento de Pessoal de Nível Superior – Brasil (CAPES) – Código de Financiamento 001.

Ao Conselho Nacional de Desenvolvimento Científico e Tecnológico (CNPq) pela concessão da bolsa.

À Fundação de Amparo à Pesquisa do Estado de Minas Gerais (FAPEMIG) pelo apoio financeiro – Projeto (APQ-00150-17).

Ao Instituto de Biotecnologia Aplicada à Agropecuária (BIOAGRO) pela disponibilidade de espaço para realização deste trabalho.

À minha família, de modo especial, aos pais Juvêncio e Amália, tia Nildete e irmã Gabriele pelo amor e carinho, por sempre estar ao meu lado.

Ao Prof. Luiz Orlando de Oliveira, pela orientação, disposição e ensinamentos para escrita científica.

À Dr. Thaís Dal'Sasso pelas orientações na área de Bioinformática e pelos ensinamentos durante atividades laboratoriais com fungos fitopatógenos.

Ao Prof. Maximiller Dal-Bianco Lamas Costa pelos ensinamentos na montagem dos experimentos de RT-qPCR.

Aos meus colegas do Laboratório de Biologia Molecular e Filogeografia. Obrigado a todos pela conivência e amizade.

A todos que contribuíram diretamente e indiretamente para a conclusão desta importante etapa.

ABSTRACT

ROCHA, Vinicius Delgado da, D.Sc., Universidade Federal de Viçosa, July, 2023. **Molecular evolution of two pathogenicity-associated gene families across the Dothideomycetes class of fungi**. Adviser: Luiz Orlando de Oliveira.

The Dothideomycetes class of fungi comprises over 19,000 described species, which are distributed into 23 orders. Generally, Dothideomycetes species have a cosmopolitan distribution and exhibit high ecological diversity, with distinct trophic modes (saprotrophic, pathogenic, endophytic, and mycorrhizal). Within the Dothideomycetes, one notable feature is the presence of many plant-pathogenic species, such as *Corynespora cassiicola* (Pleosporales) that causes diseases in economically important crops. Using data genomic data from 79 Dothideomycetes species (15 orders) and 61 *C. cassiicola* isolates, we investigated the evolutionary history of two pathogenicity-associated gene families: Pectin methylesterase (PME) and Deuterolysin metalloprotease (M35). We conducted phylogenic reconstructions and gene genealogies to uncover evolutionary patterns in both PME and M35. In *C. cassiicola* (isolate CC_29), we assessed gene expression patterns of members of each family, PME and M35, during the process of soybean infection. For the PME family, we recovered three major clades across the Dothideomycetes. Among these three clades, two (PME1 and PME2) have experienced duplications and sequent gene retention events, whereas the other clade (PME3) likely has evolved through biased gene loss. Each *C. cassiicola* isolate displayed five PME genes. The five PME haplogroups in *C. cassiicola* showed varying levels of genetic diversity and may have undergone distinct selective pressures. For the M35 family, the number of genes varied from zero to seven per genome across the Dothideomycetes. Specifically, some species within the order Botryophaeriales exhibited a higher numbergenesM35 genes. The majority of *C. cassiicola* isolates display three M35 genes per genome. In *C. cassiicola*, either gene retention episodes or gene loss characterized each of the four sub-clades within the M35 family. All genes of each family, PME and M35, were expressed in *C. cassiicola* during the interaction with soybean plants, suggesting that they are functional and may contribute to fungal infection.

Keywords: *Corynespora*. Genomics. Gene duplication. Molecular phylogeny. Plant-pathogens

RESUMO

ROCHA, Vinicius Delgado da, D.Sc., Universidade Federal de Viçosa, julho de 2023. **Evolução molecular de duas famílias gênicas associadas à patogenicidade na classe de fungos Dothideomycetes**. Orientador: Luiz Orlando de Oliveira.

A classe Dothideomycetes compreende mais de 19.000 espécies de fungos distribuídas em 23 ordens. As espécies de Dothideomycetes geralmente têm distribuição cosmopolita e exibem alta diversidade ecológica, com diferentes modos tróficos (saprotrófico, patogênico, endofítico e micorrízico). Na classe Dothideomycetes, há muitas espécies fitopatogênicas, incluindo *Corynespora cassiicola* (Pleosporales), que causa doenças em culturas comerciais. Neste estudo, dados genômicos de 79 espécies de Dothideomycetes (15 ordens) e 61 isolados de *C. cassiicola* foram usados para investigar a história evolutiva de duas famílias gênicas associados à patogenicidade: Pectina metilesterase (PME) e Deuterolisina metaloprotease (M35). Foram realizadas reconstruções filogenéticas e genealogias de gene para descobrir padrões evolutivos tanto em PME quanto em M35. Para *C. cassiicola* (isolado CC_29), foram avaliados os padrões de expressão de genes em cada família, PME e M35, durante o processo de infecção de soja. Na família PME, foram identificados três clados principais em Dothideomycetes. Entre esses três clados, dois (PME1 e PME2) passaram por eventos de duplicação com subsequente retenção gênica, enquanto o outro clado (PME3) provavelmente evoluiu por perda gênica tendenciosa. Cada isolado de *C. cassiicola* exibiu cinco genes de PME. Os cinco haplogrupos de PME em *C. cassiicola* mostraram diferente níveis de polimorfismo e podem ter evoluído sob pressões seletivas distintas. Na família M35, o número de genes variou de zero a sete por genoma em Dothideomycetes. Espécies da ordem Botryophaeriales exibiram um maior número de genes de M35. A maioria dos isolados de *C. cassiicola* exibiu três genes de M35 por genoma. Em *C. cassiicola*, episódios de retenção gênica ou perda gênica caracterizam cada um dos quatro sub-clados dentro da família M35. Os genes de cada família, PME e M35, foram expressos em *C. cassiicola* durante a interação com plantas de soja, sugerindo que eles são funcionais e podem contribuir para a infecção fúngica.

Palavras-chave: *Corynespora*. Genômica. Duplicações gênicas. Filogenia molecular. Fitopatógenos

SUMÁRIO

THESIS STRUCTURE AND GENERAL OBJECTIVES

THESIS STRUCTURE AND GENERAL OBJECTIVES

The thesis is organized into two chapters.

The first chapter explored the evolutionary history of the Pectin methylesterase (PME) gene family across the Dothideomycetes class of fungi. To conduct an extensive analysis of PMEs within the class Dothideomycetes, we used genomic data from 79 Dothideomycetes species, which belong to 15 orders. These species exhibit different trophic modes (saprotrophs, pathotroph, and symbiotroph). Additionally, we also studied PMEs specifically in *Corynespora cassiicola*, which is a highly polyphagous plant-pathogenic fungus. We obtained genomic data from 61 *C. cassiicola* isolates and included also a recently sequenced genome of *Corynespora smithii*. The expression levels of PME genes were evaluated in *C. cassiicola* in a period from 0 to 8 days post-inoculation on soybean leaves. Our study addressed to uncover evolutionary mechanisms that explain the distribution and diversification patterns of PME genes in both Dothideomycetes and *C. cassiicola*.

The second chapter investigated the evolutionary history of the Deuterolysin metalloprotease (M35) gene family across Dothideomycetes. This chapter followed a similar methodology previously used in the first chapter. We retrieved genomic data from 79 Dothideomycetes species and 61 *C. cassiicola* isolates. Subsequently, we used genomic tools to unravel evolutionary forces that drove the origin and diversity of M35 genes among Dothideomycetes species. We also examined the expression profiles of M35 genes in *C. cassiicola* during the soybean infection.

CHAPTER I

Unveiling the evolutionary history of the Pectin methylesterase (PME) gene family in the Dothideomycetes class of fungi

Unveiling the evolutionary history of the Pectin methylesterase (PME) gene family in the Dothideomycetes class of fungi

Vinicius Delgado da Rocha[a], Thaís Carolina da Silva Dal'Sasso[b], Maximiller Dal-Bianco Lamas Costa[a], Luiz Orlando de Oliveira[a]

[a]Departamento de Bioquímica e Biologia Molecular, Universidade Federal de Viçosa, Viçosa, Brazil.
[b]Departamento de Genética, Universidade de São Paulo/Escola Superior de Agricultura "Luiz de Queiroz", Piracicaba, Brazil

Corresponding author: :Luiz Orlando de Oliveira
Email: luiz.ufv@hotmail.com

Abstract

Once deposited in the plant cell wall, pectin undergoes demethylesterification by endogenous pectin methylesterases (PMEs), which play various roles in growth and development, including defense against pathogen attacks. Pathogen PMEs can alter pectin's methylesterification pattern, increasing its susceptibility to degradation by other fungal pectinases and thus playing a critical role as virulence factors during early infection stages. To investigate the evolutionary history of PMEs in the Dothideomycetes class of fungi, we obtained genomic data from 15 orders (79 species) and added genomic data from 61 isolates of *Corynespora cassiicola*. Our analyses involved maximum likelihood phylogenies, gene genealogies, and selection analyses. Additionally, we measured PME gene expression levels of *C. cassiicola* using soybean as a host through RT-qPCR assays. We recovered 145 putative effector PMEs and 57 putative non-effector PMEs across the Dothideomycetes. The PME gene family exhibits a small size (up to 5 members per genome) and comprises three major clades. The evolutionary patterns of the PME1 and PME2 clades were largely shaped by duplications and recurring gene retention events, while biased gene loss characterized the small-sized PME3 clade. The presence of five members in the PME gene family of *C. cassiicola* suggests that the family may play a key role in the evolutionary success of *C. cassiicola* as a polyphagous plant pathogen. The haplogroups Cc_PME1.1 and Cc_PME1.2 exhibited an accelerated rate of evolution, whereas Cc_PME2.1, Cc_PME2.2, and Cc_PME2.3 seem to be under strong purifying selective constraints. All five PME genes were expressed during infection of soybean leaves, with the highest levels during from six to eight days post-inoculation. The highest relative expression level was measured for CC_29_g7533, a member of the Cc_PME2.3 clade, while the remaining four genes had relatively lower levels of expression.

Keywords: *Corynespora*, gene retention, molecular evolution, plant pathogens, putative effectors

1.INTRODUCTION

The cell wall plays a crucial role in plants' defense against biotic stresses such as pathogenic viruses, bacteria, fungi, and oomycetes (Panstruga et al., 2009). The cell wall provides: physical strength that requires breakdown for the progression of the infection, undergoes reinforcement and repair during the invasion, and is a reservoir of antimicrobial compounds, which are released during degradation (Hückelhoven, 2008; Miedes et al., 2014). The composition of the plant cell wall varies among different plant species, tissues, and developmental stages; however, carbohydrate-based polymers (such as cellulose, hemicellulose, lignin, and pectin) and structural proteins are major components (Vorwerk et al., 2004). In the plant cell wall, a cellulose-hemicellulose network is embedded in a cohesive pectin matrix (Lionetti et al., 2012) that can hinder the progress of the pathogen's growth into plant tissues.

The complex polysaccharide pectin is found in both the primary cell wall and the middle lamellae of plants (Caffal and Mohnen, 2009). In dicots and non-graminaceous monocots, pectin can account for up to 30% of the total polysaccharides, while in monocots, it accounts for only 10% (Caffal and Mohnen, 2009). Homogalacturonan (HG) is one of the main components of pectin, constituting approximately 65% of the total pectin (Mohnen et al., 2008). HG is a linear homopolymer of α-D galacturonic acid residues linked in a 1→4 pattern and can be methyl-esterified at C-6 carboxyl (Mohnen et al., 2008). Methyl-esterification occurs in the medial cisterns of the Golgi, and HG is then exported to the cell wall in a highly methyl-esterified form, comprising about 80% of the total HG (Wolf et al., 2009).

Pectin methylesterases (PMEs) are enzymes that specifically hydrolyze the methyl ester bond at C-6 of α-D galacturonic acid residues in the HG linear chain (Jolie et al., 2010). HG, once deposited in the cell wall, can be demethylesterified by plant PMEs, leading to pectin remodeling in the cell wall to serve various roles in growth and development (Pelloux et al., 2007). The demethylesterification pattern determines the texture and rigidity of the cell wall (Pelloux et al., 2007). PMEs are ubiquitous, being found in plants, fungi, oomycetes, insects, nematodes, and some bacteria (Markovič and Janeček, 2004; Vicente et al., 2019; Mingora et al., 2015).

Currently, PMEs are classified into the Carbohydrate Esterase family 8 (CE8) according to the CAZymes (*Carbohydrate Active-Ezymes*) database (Drula et al.,

2022). The protein structure of PMEs exhibits a typical PME domain (PF01095; IPR000070), with six residues involved in the active site (Pelloux et al., 2004). These residues are located within four amino acid segments: QAVAL (residue Q), QDTL (residues Q and D), DFIFG (residue D), and LGRPW (residues R and W) (Markovič and Janeček, 2004; Pelloux et al., 2004). Notably, crystal structures of PMEs from various organisms, such as fungi (*Aspergillus niger*), plants (*Daucus carota*), insects (*Sitophilus oryzae*), and bacteria (*Erwinia chrysanthemi*), have revealed a conserved parallel β-helix structure (Kent et al., 2016).

Fungal PMEs play a crucial role in the invasion of plant tissues during fungal infection by altering the methylesterification pattern of pectin (Sella et al., 2016). Specifically, they convert highly methylesterified pectin into a less methylesterified form (Valete-Collet et al., 2003), disrupting the cohesive pectin matrix that surrounds the cellulose-hemicellulose network and softening the plant cell wall. This less methylesterified form of pectin is also more susceptible to degradation by other pectinases, such as fungal polygalacturonases (PGs) that are active on pectin regions that have undergone intense demethylesterification by PMEs (Valete-Collet et al., 2003). The combined activities of fungal pectinolytic enzymes result in the deconstruction of the middle lamella, which normally promotes cell-to-cell adhesion in plant tissues (Reignault et al., 2007). This deconstruction facilitates pathogenic fungi in breaching the plant cell wall and establishing infection.

Evidence-based studies have suggested that pathogen PMEs may serve as key virulence factors during the early phases of infection and disease development. For example, functional analysis of the oomycete *Phytophthora capsici* showed that the gene Pcpme6 encodes for a PME capable of degrading the cell wall and plasma membrane of pepper leaves, resulting in the formation of necrotic lesions (Feng et al., 2010). Knockout of PME genes has been shown to significantly reduce the virulence of plant pathogenic fungi, as observed in both the necrotrophic pathogen *Botrytis cinerea* (Valete-Collet et al., 2003) and the hemibiotrophic *Fusarium graminearum* (Sella et al., 2016). A previous study examined proteomes of 103 fungal species from four phyla, namely Ascomycota, Basidiomycota, Chytridiomycota, and Zygomycota, and showed that a small number of PMEs (up to 8) were present in most fungal species (Zhao et al., 2013). The genome of the oomycetes *Phytophthora spp*. was found to have up to 19 copies of the PME gene (Mingora et al., 2015; Horowitz et al., 2015). Both studies indicate that the PME

family likely underwent expansion through multiple gene duplication events in both fungi and oomycetes.

Although PMEs certainly play a crucial role in plant-pathogen interactions, the evolutionary history of PME gene families in fungi has not yet been investigated. The remarkable characteristics of the Dothideomycetes (Ascomycota) render this class of fungi an interesting subject for studying the evolutionary history of the PME gene families. The Dothideomycetes are believed to have evolved in the range between 100 and 220 million years ago (Liu et al., 2017) and currently contain 23 orders, with over 19,000 described species (Wijayawardene et al., 2017; Haridas et al., 2020). Geographically, the Dothideomycetes are widely distributed, with members found on every continent (Ohm et al., 2012). Many species of *Dothideomycetes* are known for their tolerance to extreme climatic conditions and can be found associated with various hosts or substrates, including water, soil, rock, plants, and animals (Hyde et al., 2013; Haridas et al., 2020). An array of distinct trophic modes (saprotrophs, pathotroph, and symbiotroph) indicates a large ecological diversity across the Dothideomycetes (Haridas et al., 2020). The Pleosporales, the largest order within Dothideomycetes, comprise approximately a quarter of all Dothideomycetes species (Kirk et al., 2008; Zhang et al., 2012). Together with the Capnodiales and the Botryosphaeriales, the Pleosporales harbor many genera capable of causing devastating diseases in important crops worldwide (Ohm et al., 2012). High-quality genomic resources for *Dothideomycetes* are readily available in public repositories, with a majority of them derived from plant pathogens and plant-associated species (Dal'Sasso et al., 2023). Moreover, a robust molecular phylogenetic framework based on a set of 1,851 single-copy orthologs has been established to determine the genealogical relationships among 79 species across the Dothideomycetes (Dal'Sasso et al., 2023).

Among the Dothideomycetes, *Corynespora cassiicola* (Pleosporales, Corynesporascaceae) is a polyphagous pathogen capable of infecting over 400 plant species (Déon et al., 2014; Rondon and Lawrence, 2021), and even humans (Looi et al., 2017). In recent decades, *C. cassiicola* has become a major concern for the production of economically important crops worldwide (Rondon and Lawrence, 2021). This species is responsible for a disease known as target spot, which causes severe losses in soybean, cotton, and tomato crops (Mackenzie et al., 2018; Sumabat et al., 2018; Rondon and Lawrence, 2021). Corynespora Leaf Fall, caused

by *C. cassiicola*, is one of the most devastating diseases in *Hevea brasiliensis* (rubber tree), leading to massive defoliation of the trees (Déon et al 2012). *Corynespora cassiicola* has an abundance of genomic resources available (Dal'Sasso et al., 2022), including additional genomes of closely-related species like *Corynespora smithii* (Dal'Sasso et al., unpublished). *Corynespora cassiicola* displays a large repertoire of putative effectors (Lopez et al., 2018; Dal'Sasso et al., 2021). Effectors are molecules that facilitate infection by manipulating host cell physiology and structure (Lo Presti et al. 2015). Whitin the set of putative effectors of *C. cassiicola*, enzymes capable of degradation host cell components have been identified, including carbohydrate esterases (Lopez et al., 2018; Dal'Sasso et al., 2021), class of enzymes in which PMEs are incorporated.

We anticipated that investigating the genomes of the Dothideomycetes class of fungi, as well as studying the genomes of *C. cassiicola*, would yield valuable information about the evolutionary history, diversification, and maintenance of the PME gene family across both higher and lower taxonomic ranks.

Our study initially involved retrieving genomic data for predicted PME gene family members from 79 species of Dothideomycetes using a custom pipeline. Subsequently, these members were categorized into putative effector PMEs or putative non-effector PMEs. Additionally, we reconstructed the phylogenetic relationships among the predicted PME paralogs retrieved from Dothideomycetes, with the hypothesis that PMEs have an ancient origin in fungi and that independent PME clades may have evolved due to polymorphisms and gene duplication events that accumulated over time. We considered that biased patterns could drive PME gene evolution, resulting in imbalanced numbers of members in different clades, as unequal processes of gene retention or gene loss following gene duplication could be clade-dependent.

We further investigated the evolution of the PME gene family at the species level by reconstructing the phylogenetic relationships of PME genes present in the genomes of 61 isolates of *C. cassiicola*, with the additional isolate of *C. smithii*. Additionally, we analyzed signatures of positive selection in the PMEs of *C. cassiicola* and conducted analyses using RT-qPCR assays to uncover the expression profile of the PME gene family during the course of infection in soybean, an economically important host. This investigation provided insights into the likely

mechanisms that contributed to the evolution of PMEs in the Dothideomycetes and *C. cassiicola*, in special.

2.MATERIAL AND METHODS

2.1 Data assembly and gene prediction

Our data collection strategy aimed to encompass a broad range of species within the Dothideomycetes class of fungi, including *Corynespora cassiicola*, a polyphagous plant pathogenic fungus with a cosmopolitan distribution. The protein sequences utilized in this study were obtained from MycoCosm (Grigoriev et al., 2013), and consisted of 79 species of Dothideomycetes representing 15 orders (Supplementary Table S1), previously employed in a recent phylogenomic study (Dal'Sasso et al., 2023). Additionally, protein sequences from two species of Eurotiomycetes (*Aspergillus nidulans* and *Aspergillus fumigatus*) were included to enhance the taxonomic diversity of the analyses.

To conduct subsequent analyses, we utilized a total of 61 isolates of C. cassiicola (Supplementary Table S2). Genome sequences from 14 isolates were retrieved from GenBank, while predicted coding-DNA sequences (CDSs) and protein sequences for a set of 44 isolates were obtained from a previous study (Dal'Sasso et al., 2022). We also included CDSs and protein data from an additional three isolates of *C. cassiicola* (unpublished data from Dal'Sasso et al.,). Lastly, we obtained CDSs and protein data from the *Corynespora smithii* isolate CBS 139925 (unpublished data from Dal'Sasso et al.,), which is likely one of the species most closely related to *C. cassiicola* (Shoch et al., 2009; Voglmayr and Jaklitsch, 2017). For the molecular data downloaded from GenBank, gene prediction was performed using Augustus v3.2.2 (Stanke and Morgenstern, 2005), following the method described in a previous study (Dal'Sasso et al., 2022), with *C. cassiicola* isolate CCP serving as a pre-trained 'species model'.

2.2 Protein annotation and secretome prediction

To predict protein annotation and secretome, we used a previously described pipeline (Dal'Sasso et al., 2022). The predicted proteins were annotated using two software tools: PfamScan with Pfam database v33.0 (Mistry et al., 2021), and InterProScan v5.30.69 (Jones et al., 2014) with eight parameters, including SMART-7.1, SUPERFAMILY-1.75, ProDom-2006.1, CDD-3.16, TIGRFAM-15.0, Pfam v31.0, Coils-2.2.1, and Gene3D-4.2.0.

A protein was considered secreted if it was predicted to have a signal peptide (according to SignalP v4.1; Petersen et al., 2011) and no transmembrane domains (according to TMHMM v2.0c; Krogh et al., 2001). We used TargetP v.1.1b (Emanuelsson et al., 2000) to predict the subcellular localization of each secreted protein.

Finally, we predicted CAZymes (Carbohydrate Active-Enzymes) using HMMER v.3.3.2 (http://hmmer.org/) with profile hidden Markov models (HMMs) downloaded from dbCAN2 (Zhang et al., 2018) and an e-value cut-off $<1e^{-5}$ and coverage cut-off >0.35.

2.3 PME gene identification

We identified PME homologs with an e-value <0.001 using HMMER v.3.3.2 (http://hmmer.org/) with profile HMMs for the PME domain (PF01095) downloaded from Pfam database v33.0 (Mistry et al., 2021). A protein was considered a member of the PME family if it belonged to the CAZymes family 8 of Carbohydrate Esterase and contained a PME domain that was identified by at least two out of three software tools (PfamScan, InterproScan, and HMMER).

We categorized PMEs into two groups: putative effector PMEs and putative non-effector PMEs. To classify a PME protein as a putative effector, we established three criteria: the presence of a signal peptide as predicted by SignalP software, the absence of transmembrane domains as determined by TMHMM software, and the localization within the secretory pathway as predicted by TargetP software. PMEs that satisfied all three criteria were considered putative effectors, while those that failed any of the tests were classified as putative non-effector PMEs.

2.4 Data assembly and sequence alignment

We obtained four distinct datasets for the PME sequences. Dataset 'A' consisted of 182 full-length protein sequences (1002 amino acids) from 72 Dothideomycetes species and two *Aspergillus* spp. This dataset was specifically designed for Dothideomycetes. In contrast, three additional datasets were generated exclusively for *Corynespora* species. Dataset 'B' comprised 305 CDSs (2034 bp) from 61 isolates of *C. cassiicola*, including three CDSs from *C. smithii*. Dataset 'C' (305 CDSs; 2025 bp) and dataset 'D' (305 protein sequences; 675 aa) were obtained solely from 61 isolates of *C. cassiicola*.

The sequences were aligned using the L-INS-i algorithm, implemented in MAFFT v7.453 (Katoh and Standley, 2013). To ensure the alignment's quality, we removed PMEs that contained multiple PME domains or other domains. These proteins generally had highly divergent and excessively long sequences, which could potentially introduce high levels of noise into the alignment.

2.5 Maximum likelihood phylogeny

To reconstruct the phylogenetic relationships among PMEs in both Dothideomycetes and *C. cassiicola*, independent maximum likelihood (ML) analyses were conducted. Firstly, the full dataset A was used to analyze the PMEs in Dothideomycetes. Subsequently, dataset A was partitioned into three sub-datasets based on clades recovered in the preceding phylogenetic analysis, with each sub-dataset containing sequences from a single clade. To clarify the relationships among members of each clade, three independent phylogenies were performed, one for each clade. Finally, the full dataset B was used to analyze the relationships among PMEs in both *C. cassiicola* and *C. smithii*.

Before conducting the phylogenetic analyses, we determined the best evolutionary model for each dataset using Bayesian Information Criterion (BIC), which was implemented in ModelFinder 2 (Kalyaanamoorthy et al., 2017) within IQ-TREE (Nguyen et al., 2015). The following best-fit models were selected for each dataset: WAG+R7 for dataset A, either WAG+R6 or WAG+I+G4 for the sub-datasets of dataset A, and TPM3+F+I+G4 for dataset B. Phylogenetic analyses were conducted in IQ-TREE using ten independent runs and 1000 ultrafast bootstrap replicates, with a minimum correlation coefficient of 0.99 as the bootstrap convergence criterion (Hoang et al., 2018). The resulting consensus tree for each phylogenetic analysis was visualized using FigTree v1.2.4 (Rambaut 2009).

2.6 Genealogical network and nucleotide diversity

The median-joining network method (Bandelt et al., 1999) was used to infer gene genealogies among PMEs in *C. cassiicola*. Genealogical relationships were reconstructed in Network v.5.0.03 (Fluxus Technology Ltd) using default parameters, with indels removed as a source of information. The full dataset C was used to infer genealogical relationships for the entire set of PMEs from *C. cassiicola*. Subsequently, dataset C was partitioned into five sub-datasets based on

haplogroups identified in the previous analysis, with each sub-dataset containing sequences from a single haplogroup. Finally, genealogical relationships within each haplogroup were inferred.

For each haplogroup, measures of nucleotide diversity (segregating sites, S; number of haplotypes, H; haplotype diversity, Hd; nucleotide diversity, π; and average number of nucleotide differences, K) were estimated using DNAsp v6 (Rozas et al., 2017).

2.7 Analysis of positive selection

The ratio of nonsynonymous substitution (dN) to synonymous substitution (dS) rates, also known as the ω ratio, is an essential indicator of selective pressure on a gene (Hurst, 2002). When ω = 1, it denotes neutral evolution. Conversely, when ω < 1, it indicates purifying selection, while ω > 1 implies positive selection (Yang et al., 2000; Hurst, 2002). To investigate whether selection has influenced specific sites in PME proteins of *C. cassiicola* over time, we utilized the codeml tool within PAML v4.9h (Yang et al., 2007) to estimate the ω ratio at each site and identify any positively selected sites.

To identify potential evidence of positive selection in the PME family of *C. cassiicola*, we divided dataset C into five sub-datasets, with each containing sequences from a distinct haplogroup of PMEs in *C. cassiicola*. We ensured that any variation in ω was reflective of amino acid sites fixed in independent lineages (Rody and Oliveira 2018) by including three PME sequences from *C. smithii* in each sub-dataset. For these analyses, we excluded putative pseudogenes that lacked a start codon.

We employed four site-specific models, namely M1a (neutral), M2a (selection), M7 (beta), and M8 (beta & ω), to detect sites under selection. To remove ambiguous sites and alignment gaps, we used the command cleandata = 1. Along with the sequence file, PAML was provided with a file containing a phylogenetic tree created for each sub-dataset using IQ-TREE (Nguyen et al., 2015). We compared models M1a versus M2a and M7 versus M8 using likelihood ratio tests (LRT). To identify sites under positive selection (ω > 1, PP > 95%), we used the Bayes empirical Bayes (BEB) method, which calculated posterior probabilities (PP). To visualize the 3D structure of PME, we used PyMOL v2.5.2 (Schrödinger, LLC) and obtained the PDB format file from *Aspergillus niger* (accession number 5C1C). The protein structure

was presented as a cartoon diagram that highlighted putative positively selected sites.

2.8 Identification of conserved motifs

To uncover conserved motifs in the PME proteins of *C. cassiicola*, we utilized the MEME tool within the MEME suite v5.0.5 (Bailey et al., 2009), using the full dataset D as input. We set the maximum number of motifs to 10, the minimum and maximum motif lengths to 4 and 50, respectively, and kept all other parameters at their default settings.

2.9 Gene expression analysis

We investigated the expression profiles of PME genes during fungal infection of soybean using *C. cassiicola* isolate CC_29, which was collected from soybean leaves in Brazil and has publicly available genomic sequences (Dal'Sasso et al., 2021). The experiment followed a previously described methodology (Dal'Sasso et al., 2022). Briefly, soybean plants (cultivar BR/MG Conquista) were grown in a greenhouse and inoculated at the V3 developmental stage. A conidia solution (3.5 x 10^4 conidia/mL) with 0.01% Tween 20 was prepared from isolate CC_29 and used for inoculation. Four droplets of 20 µL each were spotted on the abaxial face of each leaflet from a leaf, and four disks (1.4 cm^2) were sampled at the inoculation spots from each leaflet at five points in time: 0, 2, 4, 6, and 8 days post-inoculation (dpi). Four biological replicates (four plants) were used for each time point, and controls were also included, in which plants were inoculated with distilled autoclaved water with 0.01% Tween 20.

The extraction of total RNA from each inoculated sample was carried out using TRIzol Reagent (Life Technologies), following the manufacturer's instructions. The RNA was then resuspended in 25 µL of distilled autoclaved water and stored at -80°C. The RNA concentrations were measured using a NanoDrop 2000 spectrophotometer (Thermos Fisher Scientific), and the RNA integrity was evaluated using a 1.5% (w/v) agarose gel. To remove any genomic DNA contamination, a total of 4 µg of RNA was treated with DNase I Amp Grade (Invitrogen). Subsequently, cDNA was synthesized from 4 µg of RNA using an M-MLV Reverse Transcriptase kit (Invitrogen) and stored at -20°C for later use.

Primers were designed for each of the five PME genes of *C. cassiicola* (isolate CC_29) using Primer3Plus (https://www.primer3plus.com/) and were subsequently evaluated for specificity using melt curve analysis. The primer sequences utilized for RT-qPCR are listed in Supplementary Table S3. The RT-qPCR experiments were carried out on a 7500 Real-Time PCR System (Applied Biosystems) with a final reaction volume of 10 µL, which included 5 µL of PowerUp SYBR Green Master Mix (Life Technologies), 2 µL of each primer (1.5 µM), and 1 µL of 2-fold diluted cDNA. The amplification protocol included an initial denaturation step of 50 °C for 2 min, followed by 95 °C for 10 min. This was then followed by 40 cycles of 94 °C for 15 seconds and 60 °C for 1 min. The RT-qPCR assays were designed using one reaction for each of four biological replicates and one reaction for the bulk of RNA derived from the four replicates.

The expression levels of each PME gene were determined using the $2^{-\Delta\Delta Ct}$ method (Livak and Schmittgen, 2001), with the β-tubulin gene used as the endogenous control for normalization. The data were analyzed for each PME gene independently using one-way ANOVA with Tukey's test in R v4.2.2 (https://www.r-project.org/). The relative expression values were presented as a heatmap generated using the *ggplot* package in R.

3. RESULTS

3.1 Genome-wide identification of PME genes

Our analysis identified a total of 202 PME genes across the 79 species of Dothideomycetes (Supplementary Table S1). There were seven PME genes in the genomes of *Aspergillus* ssp. Among the 202 predicted PME genes, 175 of them exhibited a single PME domain (PF01095), which was highly conserved among the predicted PMEs. However, 23 PMEs contained multiple PME domains (Supplementary Table S4), and four PMEs carried other domains in addition to a PME domain (Supplementary Table S5).

The number of PMEs among the species of Dothideomycetes varied from zero to five (Supplementary Figure S1 and Table S1). The highest number of PMEs was found in seven species from two orders: three species of Botryosphaeriales and four species of Pleosporales, including *C. cassiicola*. On the other hand, seven species from four orders had no PMEs: Capnodiales, with four species; Lineolatales (one species); Patellariales (one species); and Mytilinidiales (one species).

Within the order Capnodiales, a single PME gene was recovered in three species that exclusively infect monocot plants (Supplementary Figure S1 and Table S1). The analysis showed that PME genes were present in both pathogenic and non-pathogenic species (Supplementary Figure S1).

3.2 Prediction of putative effector PMEs in Dothideomycetes

Out of the 202 PMEs identified in the Dothideomycetes, 145 were predicted to be putative effectors, while the remaining 57 were predicted to be putative non-effectors (Supplementary Figure S1 and Table S1). The number of putative effector PME genes per species ranged from zero to four, with seven species having the highest numbers of putative effector PME genes: three from the Botryosphaeriales and four from the Pleosporales. When a species had up to two PME genes, there was a tendency for these genes to be putative effectors, although there were exceptions. Specifically, three species (*Hysterium pulicare*, *Rhytidhysteron rufulum*, and *Botryosphaeria dothidea*) contained exclusively putative non-effector PME genes. The main features of the putative non-effector PME genes were the absence of a peptide signal and large indels at their 5' regions. In the genome of *C. cassiicola* (isolate CCP), five PME genes were identified, three of which were predicted to be

putative effectors, and the remaining two were predicted to be putative non-effector genes.

3.3 Phylogeny of PME across the Dothideomycetes

The phylogenetic analyses were performed using only PME protein sequences that contained a single PME domain. The PME proteins that contained either multiple PME domains or additional domains were excluded from subsequent phylogenetic analyses due to their highly divergent and difficult-to-align sequences.

The ML phylogenetic tree was constructed using 175 PMEs from Dothideomycetes and five PMEs from *Aspergillus* ssp. to investigate the evolutionary relationships among 72 species of Dothideomycetes (Fig. 1A). The resulting tree divided the PMEs into three major clades, each with bootstrap values above 80. We will refer to those clades as the PME1, PME2, and PME3 clades. The PME1 and PME2 clades contained a large set of PMEs, representing a diverse range of species across the class Dothideomycetes. In contrast, the PME3 clade contained a small set of PMEs that were found among a limited number of species. To further explore the phylogenetic relationships within each of the major three clades, we produced three additional phylogenies, one for each clade.

The phylogenetic analysis of clade PME1 comprised 61 PMEs, including 47 putative effectors and 14 putative non-effectors, from 57 Dothideomycetes species and *Aspergillus* spp. (Fig. 1B). While the majority of the clade PME1 consisted of putative effectors, putative non-effectors were also present and spread throughout the phylogeny. The clade PME1 was further divided into two subclades, I and II, both of which received a bootstrap support value of 100. Subclade I contained 54 PMEs, including 42 putative effectors and 12 putative non-effectors, from ten orders (Acrospermales, Botryosphaeriales, Capnodiales, Dothideales, Histeriales, Mytilinidiales, Myriangiales, Pleosporales, Trypetheliales, and Venturiales). Subclade II, with fewer members, included seven PMEs, five of which were putative effectors and two were putative non-effectors, from four species of three orders (Aulographales, Pleosporales, and Venturiales) and *Aspergillus* spp. Within the clade PME1, *C. cassiicola* (isolate CCP) displayed two PMEs that were each classified into distinct subclades, which will be referred to as Cc_PME1.1 and Cc_PME1.2, respectively.

The most populous clade identified in this study was PME2, which comprised a total of 111 PMEs, 85 of which were putative effectors and 26 were putative non-effectors. These PMEs were obtained from 68 species of Dothideomycetes and *Aspergillus spp*. (Fig. 1C). Of the 68 species, 31 retained at least two PMEs within the clade PME2, most of which belonged to the *Botryosphaeriales* and *Pleosporales*. The PME2 clade was divided into two highly supported subclades, subclades A and B, both with bootstrap values of 100. Subclade A contained 93 members from 67 species of 11 orders (Acrospermales, Botryosphaeriales, Capnodiales, Eremomycetes, Dothideales, Histeriales, Mytilinidiales, Myriangiales, Microthyriales, Pleosporales, and Venturiales). Subclade B included 18 PMEs from 16 species of three orders (Acrospermales, Histeriales, and Pleosporales) and *Aspergillus* spp. Notably, *C. cassiicola* exhibited three PMEs across the clade PME2, namely Cc_PME2.1, Cc_PME2.2, and Cc_PME2.3, which were grouped into subclades A and B.

In contrast, the minor clade PME3 contained only 10 members, each from a distinct species (Fig. 1 D). These members were obtained from six orders (Aulographales, Eremomycetales, Hysteriales, Microthyriales, Pleosporales, and Venturiales) and contained six putative effectors and four putative non-effectors.

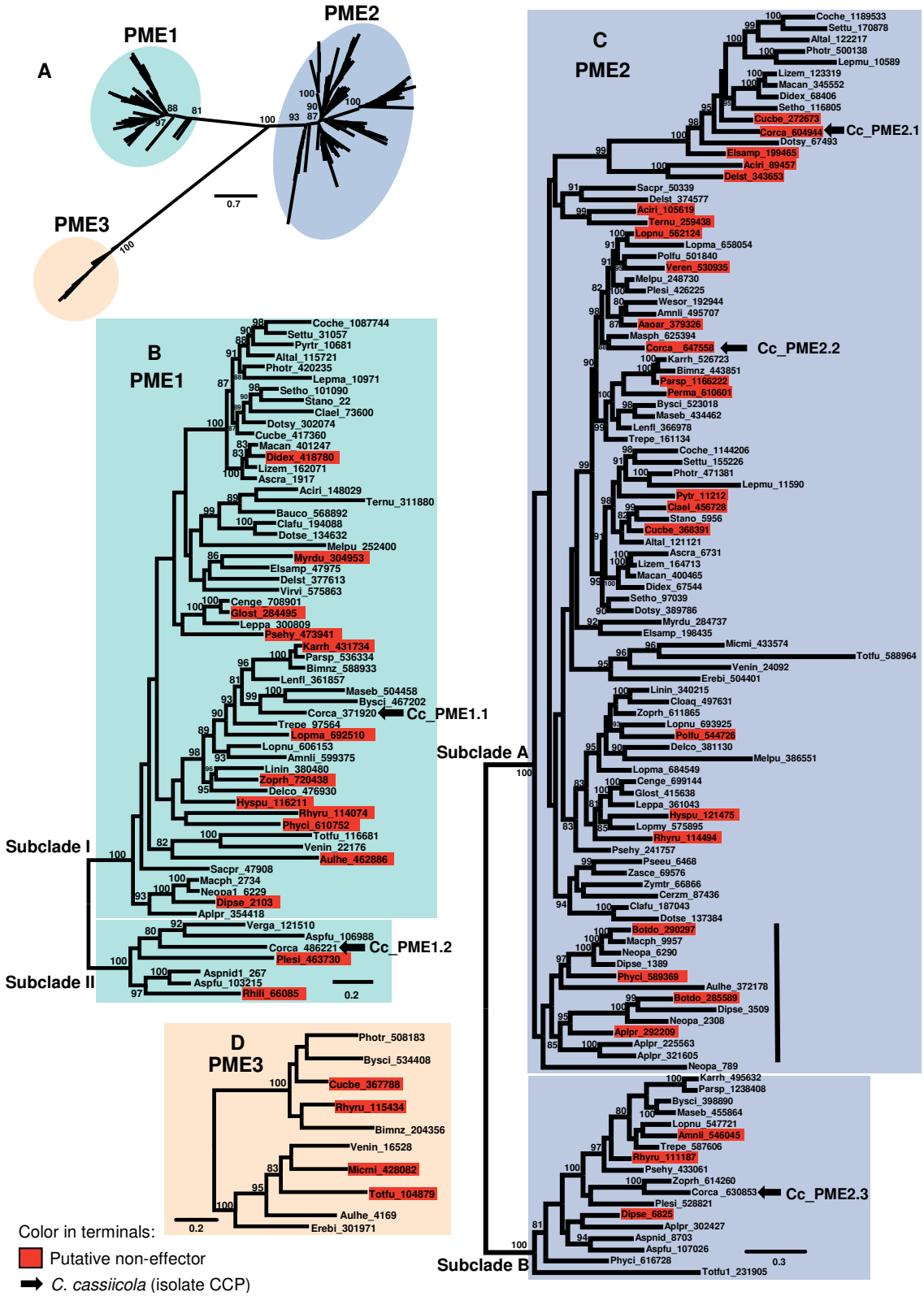

Figure 1. Phylogram of the maximum likelihood tree of the Pectin Methylesterase (PME) gene family across the Dothideomycetes. **A**. Overview of the unrooted consensus tree that was based on the full set of PMEs (182 protein sequences) obtained from Dothideomycetes (72 species) and *Aspergillus* ssp. (2 species). The three major clades in that tree were referred to as PME1, PME2, and PME3, respectively, as indicated. **B-D**. Independent phylogenetic reconstructions for each of the three major clades. **B**. The PME1 Clade. **C**. The PME2 Clade. **D**. The PME3 Clade. Nodal support values are given as bootstrap values above the branches when > 80. Branch lengths are drawn to scale. Scale bar corresponds to the expected number of substitutions per site. Arrows indicate the five predicted PME genes (Cc_PME1.1, Cc_PME1.2, Cc_PME2.1, Cc_PME2.2, and Cc_PME2.3) present in the genome of *Corynespora cassiicola* isolate CCP. Red terminals indicate putative PME genes that were regarded as non-effector genes. The vertical bar in the clade PME2 indicates the retention of duplicated genes that originated from ancient duplications within the order Botryosphaeriales.

3.4 Conserved amino acid segments in the PME gene family

The five amino acid segments (GxYxE, QAVAL, QDTL, DFIFG, and LGRPW) are known to be conserved among PMEs (Markovič and Janeček, 2004). The protein alignments (Supplementary Table S6) show that these five segments were conserved within each of the three clades (PME1, PME2, and PME3), with only a few amino acid replacements observed at sites 180, 202, and 293. These sites may also play a role in the active site. Interestingly, there was a distinct pattern of amino acid replacements among the three clades at these sites. For example, at site 180, the PME1 clade contained a polar amino acid residue (Proline, P), while the PME2 and PME3 clades contained a non-polar amino acid residue (Glutamine, Q). At site 202, the PME1 and PME2 clades shared a non-polar amino acid residue (Glutamine, Q), whereas the PME3 clade had a polar amino acid residue (Glycine, G). Finally, at site 293, a non-polar amino acid residue (Tryptophan, W) was shared among members of the PME1 and PME2 clades, whereas a non-polar amino acid residue (Asparagine, N) was found in all members of the PME3 clade. It is also interesting to note that members of the clade PME3 diverged substantially from other PME genes, accumulating mutations that resulted in amino acid substitutions (at sites 204, 289, 290, and 292) near amino acid residues located in the active site (Supplementary Table S6). Such substitutions were absent in members of the PME1 and PME2 clades.

3.5 The PME gene family of *Corynespora*

The genomes of 61 isolates of *C. cassiicola* yielded a total of 305 PME genes, with each isolate containing five predicted PME genes. Most of these genes (279 out of 305) were predicted to code for putative effectors. A ML phylogeny reconstructed the relationships among these 305 genes (using the CDSs), with highly supported nodes (bootstrap values > 95) for five major clades. Additionally, the phylogeny also contained three PME-encoding genes (CDSs) from *C. smithii* (Fig. 2A). Each clade was named after the PME gene it harbored and contained one of the five PMEs found in *C. cassiicola* isolate CCP: Cc_PME1.1, Cc_PME1.2, Cc_PME2.1, Cc_PME2.2, or Cc_PME2.3.

Three clades (Cc_PME1.1, Cc_PME2.1, and Cc_PME2.2) showed a sister relationship to PME genes from *C. smithii*, and each clade clustered a total of 61 PMEs, one from each isolate of *C. cassiicola*. Interestingly, PME genes-encoding putative effector proteins formed a single subclade within each clade: PME1.2 and PME2.3. Within the clade Cc_PME2.3, genes-encoding putative non-effectors contained a large deletion (243 bp) at the 5' region that eliminated the initiation codon (ATG). These putative non-effectors were obtained from isolates collected in Asia (China, Malaysia, Sri Lanka, and Thailand) from *Hevea brasiliensis*. It is also worth noting that all genes-encoding putative non-effector PMEs in *C. cassiicola* lacked predicted signal peptides.

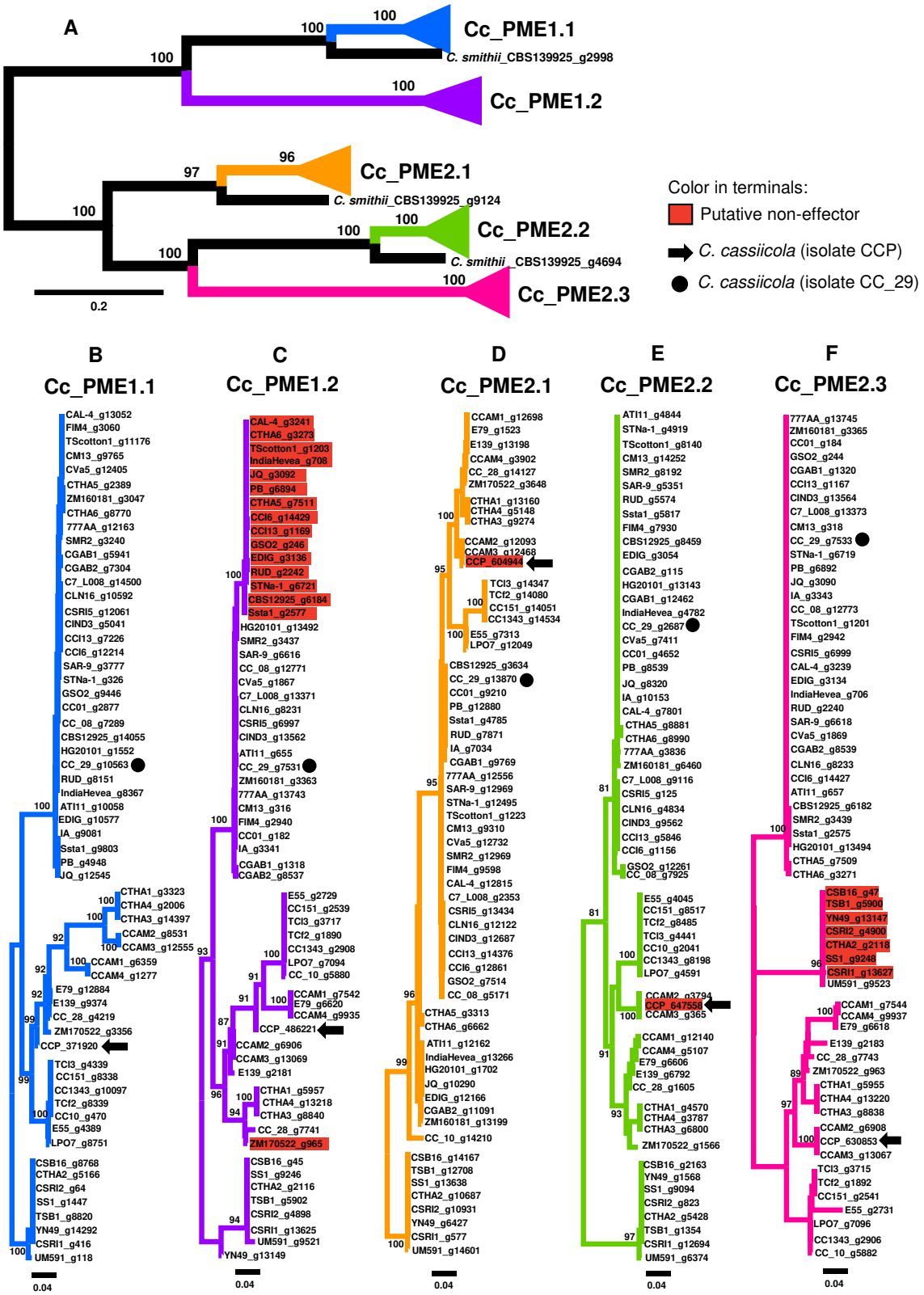

Figure 2. Phylograms of the maximum likelihood tree of the Pectin Methylesterase (PME) gene family across the 61 isolates of *Corynespora cassiicola* and *Corynespora smithii* isolate CBS 139925. The analysis was based on 308 coding DNA sequences (each of which was 2063 base pair long) of member of the PME gene family from 62 isolates. **A**. Overview of the full unrooted consensus tree, with five major clades collapsed into triangles. **B-F**. Expanded views show the composition of each major clade. **B**. Cc_PME1.1 (blue). **C**. Cc_PME1.2 (purple). **D**. Cc_PME2.2 (orange). **E**. Cc_PME2.3 (green). **F**. Cc_PME2.3 (pink). Nodal support values are given as bootstrap values above the branches, when > 80. Branch lengths are drawn to scale. Scale bar corresponds to the expected number of substitutions per site. Red terminals indicate putative PME genes that were regarded as non-effector genes. Placements of predicted the PME family members of isolates CCP and CC_29 are as indicated.

3.6 Genealogical relationships among PMEs of *Corynespora*

The haplotype networks depicted the genealogical relationships among 96 haplotypes recovered from 305 PME-encoding genes (CDSs) in 61 isolates of *C. cassiicola* (Fig. 3). The network that was based on the full set of PMEs exhibited five major haplogroups (Fig. 3A). Each of the five haplogroups corresponded to one of the five clades that were recovered in the phylogeny (Fig. 2). Thus, the five haplogroups were named according to their corresponding clades: Cc_PME1.1, Cc_PME1.2, Cc_PME2.2, Cc_PME2.2, and Cc_PME2.3, respectively.

Within the network, a large accumulation of mutational steps (>287 steps) separated the five haplogroups (Fig. 3A). The largest number of mutational steps (362 steps) separated haplogroup Cc_PME1.2 from haplogroup Cc_PME2.1. On the other hand, the distance between the haplogroup Cc_PME1.1 and haplogroup Cc_PME1.2 required the smallest number of mutational steps (287). The haplogroups CC_PME1.1 and Cc_PME2.3 occupied tip positions in the opposite extremities of the network. The haplogroup Cc_PME2.1 was located in the central position of the network.

We also constructed partial networks to describe the genealogical relationships among haplotypes within each haplogroup, which revealed interesting features (Fig. 3B-F). Haplogroups Cc_PME1.1 (Fig. 3B) and Cc_PME1.2 (Fig. 3C) contained a large number of member haplotypes, while haplogroups Cc_PME2.1 (Fig. 3D), Cc_PME2.2 (Fig. 3E), and Cc_PME2.3 (Fig. 3F) were comparatively small in size. There was a tendency for a large number of mutational steps to separate haplotypes within the Cc_PME1.1 haplogroup (up to 36 steps) and Cc_PME1.2 haplogroup (up to 34 steps). The placement of haplotypes within each haplogroup was not associated with either the geographical origin of the isolates or the host species. Haplotypes that coded for putative effector PMEs were distributed across four haplogroups: Cc_PME1.2 (haplotypes 1-6, 24), Cc_PME2.1 (haplotype 5), Cc_PME2.2 (haplotype 13), and Cc_PME2.3 (haplotype 9). At the tip position of the network, haplotypes that coded for putative non-effector PMEs were closely related to haplotypes that coded for putative effector PME.

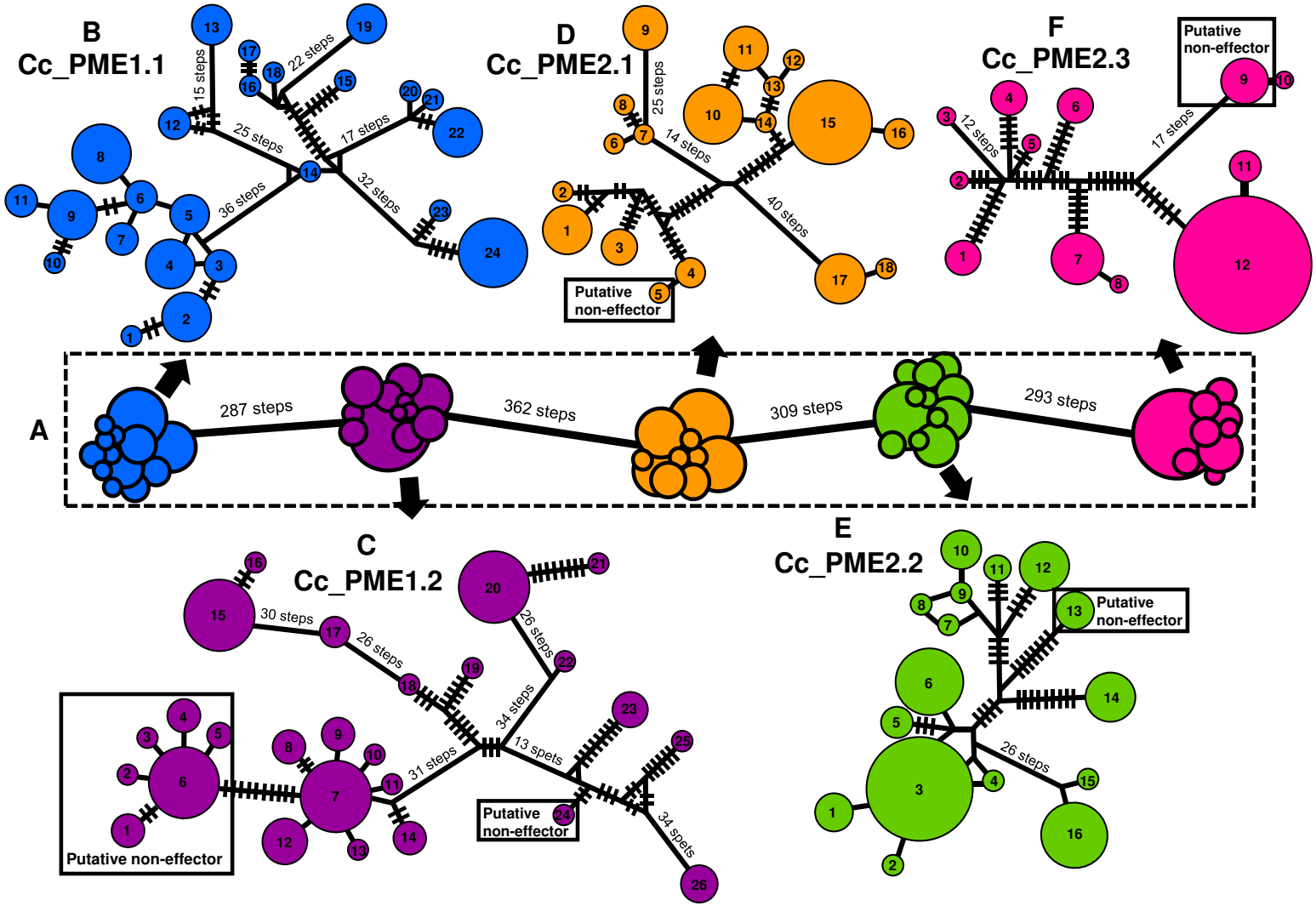

Figure 3. Genealogical relationships of the five haplogroups of Pectin Methylesterase (PME) gene family of *Corynespora cassiicola*. The analysis was based on the coding-DNA sequences (CDSs). **A.** The central box depicts the full median-joining network showing the five haplogroups. **B-F**. Expanded views show the composition of each haplogroup. **B.** Cc_PME1.1 (blue). **C.** Cc_PME1.2 (purple). **D** Cc_PME2.1 (orange). **E**. Cc_PME2.2 (green). **F** Cc_PME2.3 (pink). A circle represents a given haplotype (coded with number); circle size is proportional to the relative frequencies. Numbers of mutational steps are indicated with bars when more than one (unless indicated otherwise).

Measures of nucleotide diversities for each of the five PME haplogroups revealed that haplogroups Cc_PME1.1 and Cc_PME1.2 detained the highest levels of polymorphisms (π = 0.02925 and 0.04590, respectively), while the haplogroups Cc_PME2.1, Cc_PME2.2, and Cc_PME2.3 exhibited lower genetic differentiation levels (Table 1). The number of nucleotide differences (K) was very high among members of the haplogroup Cc_PME1.2 (49 nucleotides on average), whereas members of the haplogroup Cc_PME2.2 showed the lowest number of nucleotide differences (K = 13). Overall, these results suggest that there is a high level of genetic diversity within and among haplogroups of the PME-encoding genes in *C. cassiicola*.

Table1. Segregating sites (S), Number of haplotypes (H), haplotype diversity (Hd), Nucleotide diversity (π), and average number of nucleotide differences (K) for five Pectin Methylesterase (PME) haplogroups in *Corynespora cassiicola*.

Haplogroups	**S**	**H**	**Hd**	**π**	**K**
Cc_PME1.1	132	24	0.953	0.02925	35.54
Cc_PME1.2	170	26	0.954	0.04590	49.30
Cc_PME2.1	113	18	0.886	0.02694	26.10
Cc_PME2.2	63	16	0.838	0.01332	13.35
Cc_PME2.3	76	12	0.704	0.02105	15.79

3.7 Positively selected sites on the PMEs of *Corynespora*

We conducted four models (M1a, M2a, M7, and M8) using the codeml tool in PAML software to investigate the presence of amino acid sites under positive selection on PME proteins within each of the five PME clades of *C. cassiicola*. Our analysis revealed that two models of positive selection (M2a and M8) were statistically significant (LRT: P-value < 0.01), indicating that selection played a role in shaping the evolutionary history of the PME genes in *C. cassiicola*. Specifically, in the Cc_PME1.1 haplogroup, two sites were identified as putatively under positive selection by both M2a and M8, with a PP > 95% calculated by the BEB method. These two positively selected sites corresponded to amino acid residues 388N (asparagine) and 391W (tryptophan), located at the C-terminal region of the PME protein. While residue 388N was located within a loop region, residue 391W participated in a predicted α-helix structure (Fig. 4).

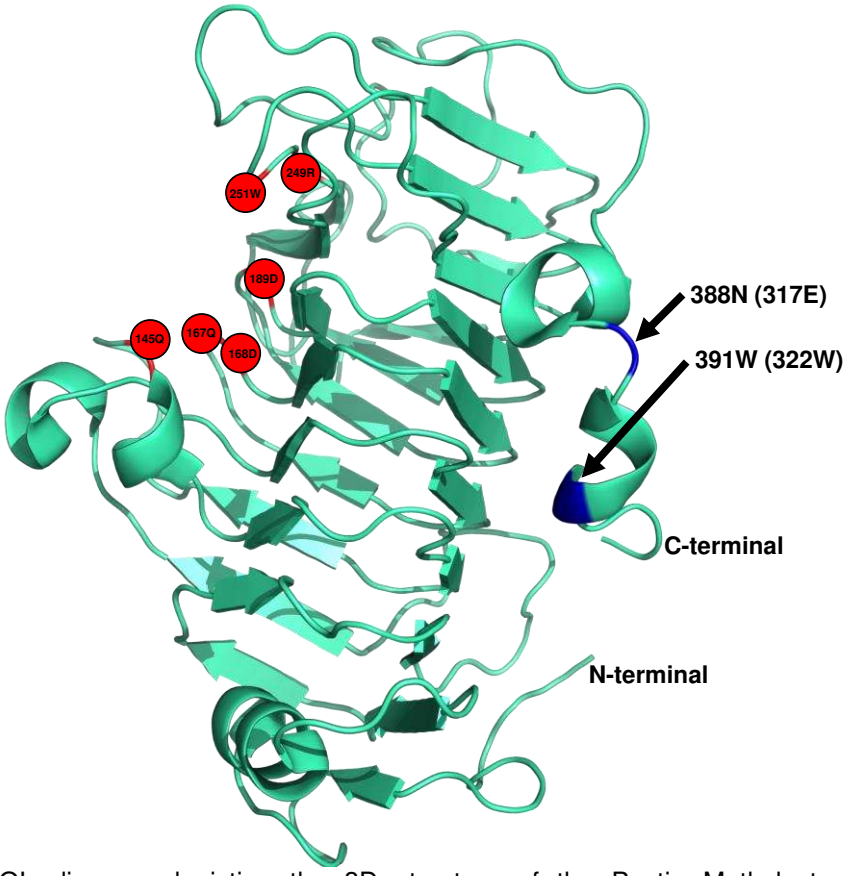

Figure 4. PyMOL diagram depicting the 3D structure of the Pectin Methylesterase (PME) of *Aspergillus niger*. Protein structure was retrieved from Protein Data Bank (PDB) accession number 5C1C. Arrows indicate relative locations of two positively selected sites in Cc_PME1.1 gene of *Corynespora cassiicola*. Circles indicate active site residues (145Q, 167Q, 168D, 189D, 249R, 251W, according to amino acid numbering for the PME of *Aspergillus niger*). Color codes: red, amino acid residues involved in the active site; blue, positively selected amino acid residues (388N and 394W) that were predicted by codeml/PAML with Bayes Empirical Baye PP> 95%. In parenthesis, the corresponding sites in the PME structure of *Aspergillus niger*.

3.8 Protein structure and conserved motifs of PMEs of *Corynespora*

A schematic diagram (Fig. 5A) illustrates the protein structure features of putative effector PMEs in *C. cassiicola*. On average, the putative effector PMEs ranged in length from 330 (Cc_PME2.3) to 472 (Cc_PME2.1) amino acid residues. The signal peptide was located at the N-terminal region and varied in length from 16 (Cc_PME2.2) to 27 (Cc_PME1.1) amino acid residues. The PME domain, as predicted by HMMER software, ranged in length from 188 (Cc_PME1.1) to 330 (Cc_PME2.2) amino acid residues, with an average length of 249 amino acid residues.

Using the MEME tool from the MEME suite software, we identified a total of three conserved motifs within PMEs, either putative effectors or putative non-effectors (Fig. 5B). The lengths of the motifs were 21 (motif II), 29 (motif I), and 34 (motif III) amino acid residues. All three motifs were located within the PME domain

and contained residues involved in the active site. Motif I contained residues 24Q and 25D, motif II contained residue 17D, and motif III contained residues 6R and 8W.

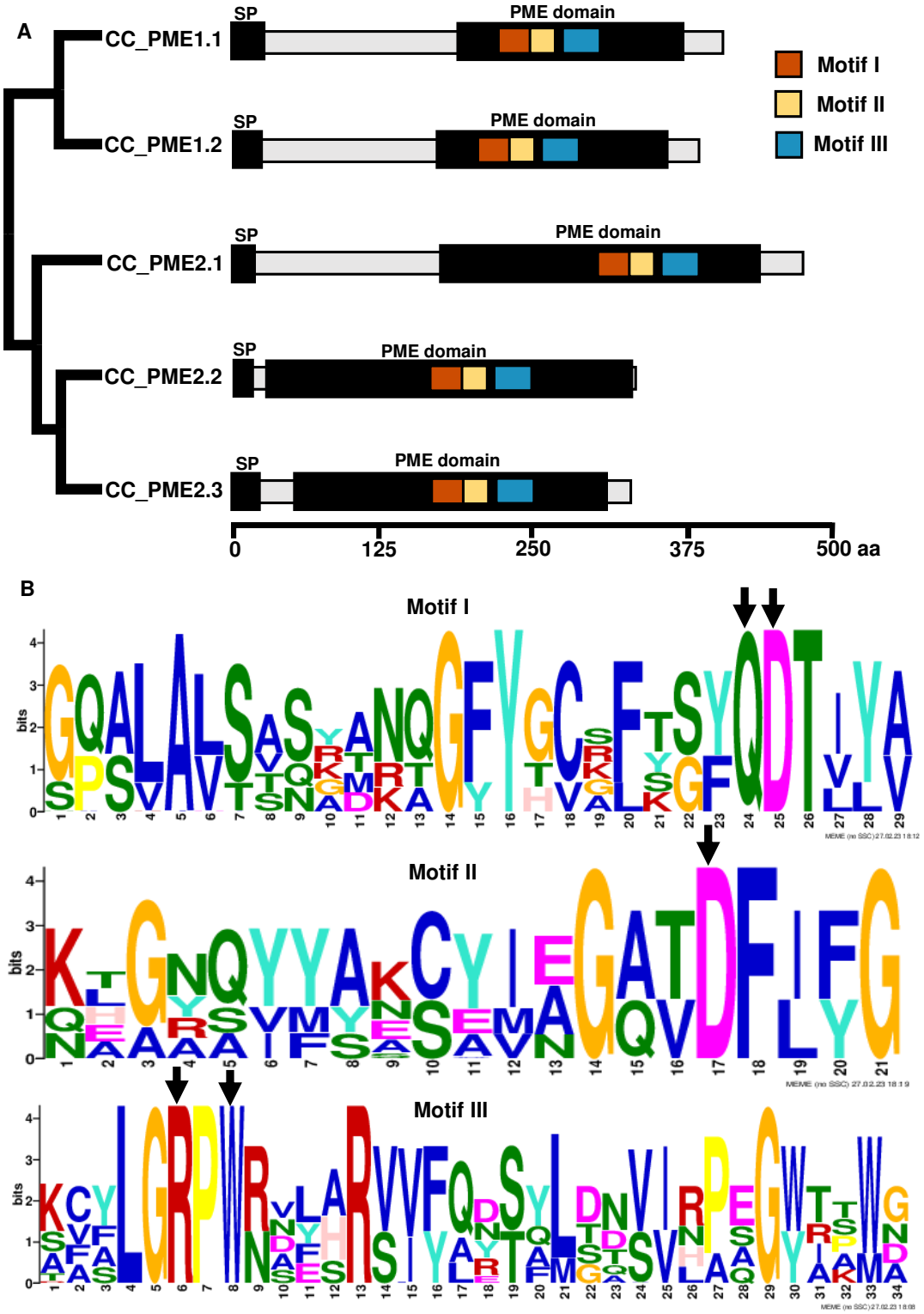

Figure 5. Structural overview of the five Pectin Methylesterase (PME) family members of *Corynespora cassiicola*. **A**. Schematic diagram showing the average length of putative effector PMEs, signal peptide (SP), predicted locations for the PME domain (PF01095) according to HMMER v. 3.3.2, and its three structural motifs. Protein lengths were drawn to scale. Scale bar indicates the number of amino acid residues. The scheme of the phylogenetic tree came from Figure 2. **B**. Consensus pattern within the three predicted motifs of PMEs of *C. cassiicola*. Arrows indicate amino acid residues involved in the active site.

3.9 Gene expression profiles of PMEs in *Corynespora*

The RT-qPCR assays provided insight into the expression profiles of the five PME genes in *C. cassiicola* (isolate CC_29) during the infection of soybean leaves (Fig. 6 and Supplementary Fig. S2). Generally, the relative expression levels of the five PME genes were low during the early stages of infection (0-4 dpi) and gradually increased from 6 dpi to 8 dpi. Although all five genes showed a similar expression trend, their relative expression levels varied considerably. Specifically, CC_29_g7533, a member of the Cc_PME2.3 clade, exhibited the highest relative expression levels, whereas the remaining four genes had relatively lower levels of expression. Notably, CC_29_g7531, a member of the Cc_PME1.2 clade, showed consistently low levels of relative expression throughout the 0-8 dpi period, with only a slight increase at 6 dpi. The relative expression levels of the remaining three PME genes were higher than that of Cc_29_g7531, but lower than CC_29_g7533.

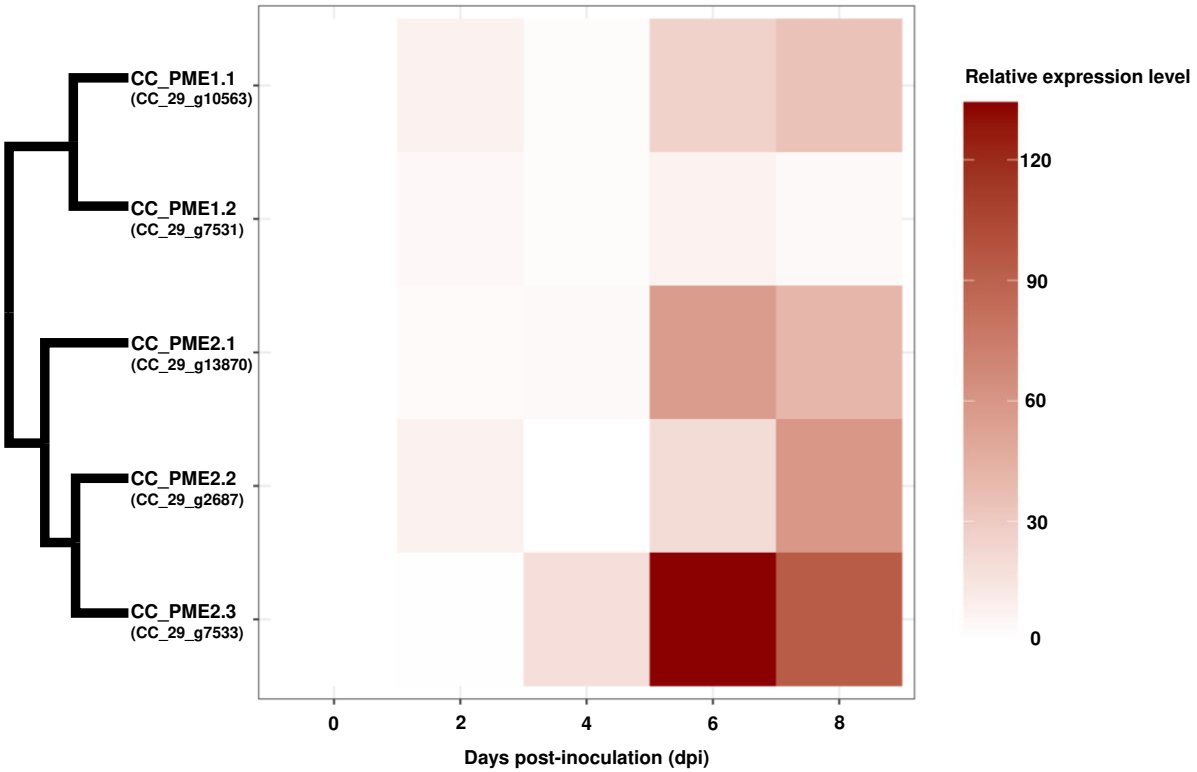

Figure 6. Heatmap showing the relative expression level of the five Pectin Methylterase (PME) genes of *Corynespora cassiicola* after spore inoculation on soybean leaves. The relative expression level was calculated using the $2^{-\Delta\Delta Ct}$ method. The constitutive β-tubulin gene of *C. cassiicola* was used as an endogenous control. The x-axis shows the five time points of the expression analyses: 0, 2, 4, 6, and 8 days post-inoculation (dpi). The y-axis shows the five PME genes: Cc_PME1.1 (CC_29_g10563), Cc_PME1.2 (CC_29_g7531), Cc_PME2.1 (CC_29_g13870), Cc_PME2.2 (CC_29_g2687), and Cc_PME2.3 (CC_29_g7533). The scheme of the phylogenetic tree came from Figure 2. Color intensity corresponds to relative expression level. Heatmap was generated according to results showed in Supplementary Figure S2.

4 DISCUSSION

4.1 The PME gene family across the Dothideomycetes

The Pectin methylesterase (PME) gene family was widespread across the Dothideomycetes class of fungi. Overall, it was a small gene family, with up to five members per genome. Interestingly, the genomes of plant pathogenic fungi that infect a wide range of hosts tend to contain more PME members than the genomes of non-pathogenic fungi. For example, *C. cassiicola* (Pleosporales) and *Neofusicoccum parvum* (Botryophaeriales) have five members of the PME gene family in their respective genomes.

Plant pathogenic fungi generally possess sets of genes that code for cell wall-degrading enzymes (CWDEs), which include PMEs (Zhao et al., 2013). These CWDEs are believed to facilitate fungal penetration and migration into the plant tissue (Zhao et al., 2013; Lo Presti et al., 2015). PMEs, in particular, have been associated with pathogenicity in several fungi and oomycetes (Valete-Collet et al., 2003; Reignault et al 2008; Feng et al., 2010; Horowitz et al., 2015; Sella et al., 2016). Notably, in addition to degrading host cell wall pectin, a PME of *Phytophthora capsici* has been shown to induce necrotic lesions on pepper leaves (Feng et al., 2010)

Host specificity may explain the rare occurrence of PMEs in three species of Capnodiales (Cercospora zeae-maydis, *Pseudocercospora eumusae*, and *Zymoseptoria tritici*) that infect monocotyledons exclusively. The cell walls of monocotyledons have a lower pectin content compared to dicotyledons (Caffal and Mohnen, 2004), which may result in lower selective pressure to increase PME family size in monocots. A previous study also noted that pathogenic fungi that infect monocots only have a low number of pectinases, including PMEs (Zhao et al., 2013).

4.2 Putative-effector PMEs

In our study, all putative effector PMEs contained a signal peptide. Effector proteins are crucial for suppressing plant immunity and establishing successful pathogen infections (Sánchez-Vallet et al., 2018). The presence of an N-terminal signal peptide is a major trait of effector proteins for their secretion (Wang et al., 2022). Therefore, our findings suggest that putative effector PMEs can be directed

for secretion outside the fungal cell, where they may reach the pectin in host cell walls.

In addition to a conserved PME domain, putative effector PMEs contained amino acid residues in the active site that are also conserved (Supplementary Table S6). These amino acid residues are likely to play a functional role during enzyme activity. While putative effector PMEs were ubiquitous across the Dothideomycetes, putative non-effector PMEs occurred with low frequency. In addition to the rarity, genes that coded for putative non-effector PMEs harbored indels that disrupted the reading frame of their DNA sequences and resulted in the loss of the signal peptide from their respective proteins. These findings suggest that genes coding for putative non-effector PMEs may be nonfunctional paralogs.

4.3 Evolutionary patterns of the PME gene family in the Dothideomycetes

Our study suggested that both gene loss and gene retention have contributed to the evolution of the PME gene family in the Dothideomycetes. When a gene duplication event occurs, one copy of the duplicated gene may become nonfunctional due to accumulating deleterious mutations and may be eliminated under strong purifying selection (Lynch and Conery, 2000). Alternatively, the duplicated copy may acquire a new trait that confers some functional advantage, thus being more likely to be retained (Kuzmin et al., 2022). Under relaxing selection, redundant copies of the duplicated gene can also be kept in the genome (Lynch and Conery, 2000). These alternative fates have been observed throughout the evolutionary history of other gene families in the Dothideomycetes (Dal'Sasso et al., 2023). Similarly, gene loss and retention have also played important roles in shaping the evolution of gene families in land plants (Rody and Oliveira, 2018).

Our findings suggest that biased gene retention and gene loss events have contributed to shaping the evolutionary patterns we uncovered for the PME gene family of the Dothideomycetes. Biased gene retention events, following gene duplication events, have led to the diversification of the PME family over time, and the extant members of this gene family grouped into three major clades (PME1, PME2, and PME3, respectively). Our results suggest that the PME1 (Fig. 1B) and PME2 clades (Fig. 1C) had their evolutionary patterns largely shaped by repeated gene retention events. Over time, members of either the PME1 clade or the PME2 clade were maintained in most of the extant species of Dothideomycetes. Notably,

the genomes of many species within the orders Botryosphaeriales and Pleosporales retained up to three copies of the PME genes, all of which clustered together within the PME2 clade. The retention of PME genes across both clades, PME1 and PME2, may confer a functional advantage that is crucial for the success of Dothideomycetes. Interestingly, members of either the PME1 clade or the PME2 clade contain distinct amino acid residues in the active sites (Supplementary Table S6), suggesting that the genes of each clade may code for proteins that may exhibit distinct (but complementary) biochemical properties, such as different substrate specificities.

Ancient gene duplications followed by gene retentions seem to have occurred in the order Botryosphaeriales, in which some species exhibited duplicated genes within the PME2 clade (Fig. 1C). Meanwhile, biased gene loss events were predominant in shaping the current evolutionary pattern we uncovered for the PME3 clade (Fig. 1D) and may explain the rarity of members of the PME3 clade among the Dothideomycetes. The DNA sequences of the few remaining members that belong to the PME3 clade have accumulated a high rate of mutations along regions that code for motifs associated with the active site of the enzyme. We hypothesize that the lack of genes that belong to the PME3 clade may result from gene loss due to pseudogenization processes that occurred throughout the evolutionary history of the PME gene family across the Dothideomycetes.

4.4 Evolution of the PME gene family in *Corynespora*

The presence of a large repertoire of PME genes (five members) in *C. cassiicola* suggests that this species may have evolved a specialized mechanism for degrading the cell walls of host plants during plant-pathogen interactions. The congruence between independent phylogenies for each PME clade in *C. cassiicola* (Fig. 2) and previous intraspecific phylogenomic reconstructions of the fungus (Lopez et al,. 2018; Dal'Sasso, 2021) indicates an ancient origin of the PME gene family in *C. cassiicola*, with early gene duplications leading to the retention of multiple PME genes over time. This suggests that PME genes may play an important role in the evolutionary success of *C. cassiicola* as a polyphagous plant pathogen. Similarly, other plant pathogenic fungi such as *Botrytis cinerea* and *Sclerotinia sclerotiorum* also possess a high number of PME genes in their genomes, indicating the

importance of PME genes in the evolution of these fungi as well (Amselem et al., 2011; Zhao et al., 2013).

Effector genes are known to evolve rapidly and accumulate high genetic diversity due to various factors such as gene duplications and subsequent sequence modifications (Sánchez-Vallet et al., 2018; Dal'Sasso et al., 2022). In *C. cassiicola*, the haplogroups Cc_PME1.1 and Cc_PME1.2 exhibited an accelerated rate of evolution, with numerous mutations among members of each haplogroup. This rapid evolution could be due to either relaxed selective constraints or an adaptive mechanism to avoid recognition by the plant immune system. On the other hand, the three remaining haplogroups (Cc_PME2.1, Cc_PME2.2, and Cc_PME2.3) appeared to be under purifying selective constraints, preventing the accumulation of polymorphisms.

To overcome host immune system resistance, fungal effectors often undergo adaptive changes fixed by positive selection (Derbyshire, 2020). Our study provides evidence that positive selection has acted on members of the haplogroup Cc_PME1.1 in *C. cassiicola*. Additionally, two putative amino acid residues (388N and 391W) were identified under positive selection (Fig. 5), which could be associated with a novel functional adaptation of PME genes in *C. cassiicola*.

4.5 A recent origin for the putative non-effector PMEs of *Corynespora*

The PME genes that we identified as putative non-effector PMEs were rare in the *C. cassiicola* genome, but they were found in all four haplogroups. This suggests that they arose from several independent diversification events within each haplogroup. The placement of the putative non-effector PMEs in various tip positions within the networks (Fig. 3) suggested that they had recently evolved, a prediction that derives from the Coalescent Theory (Crandall and Templeton, 1993). Furthermore, the network topology indicated that the haplotypes containing putative non-effector PMEs originated from nearby haplotypes that had putative effector PMEs. This finding suggests that recent duplication events led to the accumulation of mutations in a daughter copy, resulting in the loss of essential motifs such as the peptide signal. While one of the paralogs retained its original properties, the other paralog underwent relaxed selective pressures and evolved more rapidly.

4.6 Gene expression of PMEs in *Corynespora*

All five putative effector PME genes were found to be expressed during *C. cassiicola* CC_29 infection of soybean leaves, with the highest levels observed during the late stages of infection, at six dpi. This finding is consistent with the upregulation of PME genes in the plant pathogen oomycete *P. capsici*, which were found to be upregulated at 5 dpi in cucumber and 7 dpi in tomato and pepper (Li et al., 2011). The varying levels of expression among the putative effector PMEs of *C. cassiicola* may represent a coordinated functional response depending on the host specificity, as seen in other plant pathogens like *P. capsici* (Li et al., 2011) and *B. cinerea* (Blanco-Ulate et al., 2014). Despite their lower expression during the early stages of infection, PMEs may work in coordination with other pectinases, such as pectin lyases (PLs) for degrading the host cell walls. Two PLs were found to be significant differentially expressed during the early stages of infection (1-2 dpi) on rubber tree leaves infected with *C. cassiicola* (Lopez et al., 2018). The five putative effector PME genes of *C. cassiicola* are likely functional and exhibited no signs of pseudogenization, such as frameshift mutations or premature stop codons.

ACKNOWLEDGEMENTS

We thank Dr. Elizabeth P. B. Fontes for generously provide her 7500 Real-Time PCR System. This study was supported by Minas Gerais State Foundation of Research Aid – FAPEMIG (APQ-00150-17) and by The National Council of Scientific and Technological Development – CNPq to LOO (fellowship number PQ 302336/2019-2). VDR also received a student fellowship from CNPq (GD 143393/2019-7).

CONFLICT OF INTEREST

We declare no conflicting interest.

DATA AVAILABILITY

This study analyzed genomic data that is publicly available at https://mycocosm.jgi.doe.gov/mycocosm/home and https://www.ncbi.nlm.nih.gov/genbank/. Additional information that supports the findings of this study can be found in the supplementary material.

5. REFERENCES

Amselem, J., Cuomo, C.A., van Kan, J.A.L., Viaud, M., Benito, E.P., Couloux, A., Coutinho, P.M., de Vries, R.P., Dyer, P.S., Fillinger, S., Fournier, E., Gout, L., Hahn, M., Kohn, L., Lapalu, N., Plummer, K.M., Pradier, J.-M., Quévillon, E., Sharon, A., Simon, A., ten Have, A., Tudzynski, B., Tudzynski, P., Wincker, P., Andrew, M., Anthouard, V., Beever, R.E., Beffa, R., Benoit, I., Bouzid, O., Brault, B., Chen, Z., Choquer, M., Collémare, J., Cotton, P., Danchin, E.G., Da Silva, C., Gautier, A., Giraud, C., Giraud, T., Gonzalez, C., Grossetete, S., Güldener, U., Henrissat, B., Howlett, B.J., Kodira, C., Kretschmer, M., Lappartient, A., Leroch, M., Levis, C., Mauceli, E., Neuvéglise, C., Oeser, B., Pearson, M., Poulain, J., Poussereau, N., Quesneville, H., Rascle, C., Schumacher, J., Ségurens, B., Sexton, A., Silva, E., Sirven, C., Soanes, D.M., Talbot, N.J., Templeton, M., Yandava, C., Yarden, O., Zeng, Q., Rollins, J.A., Lebrun, M.-H., Dickman, M., 2011. Genomic Analysis of the Necrotrophic Fungal Pathogens *Sclerotinia sclerotiorum* and *Botrytis cinerea*. PLoS Genet 7, e1002230. https://doi.org/10.1371/journal.pgen.1002230

Bailey, T.L., Boden, M., Buske, F.A., Frith, M., Grant, C.E., Clementi, L., Ren, J., Li, W.W., Noble, W.S., 2009. MEME SUITE: tools for motif discovery and searching. Nucleic Acids Res 37, W202–W208. https://doi.org/10.1093/nar/gkp335

Bandelt, H.J., Forster, P., Rohl, A., 1999. Median-joining networks for inferring intraspecific phylogenies. Mol Biol Evol 16, 37–48. https://doi.org/10.1093/oxfordjournals.molbev.a026036

Blanco-Ulate, B., Morales-Cruz, A., Amrine, K.C.H., Labavitch, J.M., Powell, A.L.T., Cantu, D., 2014. Genome-wide transcriptional profiling of *Botrytis cinerea* genes targeting plant cell walls during infections of different hosts. Front Plant Sci 5, 435. https://doi.org/10.3389/fpls.2014.00435

Caffall, K.H., Mohnen, D., 2009. The structure, function, and biosynthesis of plant cell wall pectic polysaccharides. Carbohydr Res 344, 1879–1900. https://doi.org/10.1016/j.carres.2009.05.021

Crandall, K.A., Templeton, A.R., 1993. Empirical tests of some predictions from coalescent theory with applications to intraspecific phylogeny reconstruction. Genetics 134, 959–969. https://doi.org/10.1093/genetics/134.3.959

Dal'Sasso, T.C.S., 2021. Evolutionary history of the necrosis-and ethylene-inducing like protein superfamily across the Dothideomycetes (Ascomycota). Ph.D. Thesis, Federal University of Viçosa.

Dal'Sasso, T.C.S., Rocha, V.D., Rody, H.V.S., Costa, M.D.B.L., Oliveira, L.O., 2022. The necrosis-and ethylene-inducing peptide 1-like protein (NLP) gene family of the plant pathogen *Corynespora cassiicola*. Curr Genet 68, 645–659. https://doi.org/10.1007/s00294-022-01252-0

Dal'Sasso, T.C.S., Rody, H.V.S., Grijalba, P.E., Oliveira, L.O., 2021. Genome sequences and in silico effector mining of *Corynespora cassiicola* CC_29 and *Corynespora olivacea* CBS 114450. Arch Microbiol 203, 5257–5265. https://doi.org/10.1007/s00203-021-02456-7

Dal'Sasso, T.C.S., Rody, H.V.S., Oliveira, L.O., 2023. Genome-Wide Analysis and Evolutionary History of the Necrosis- and Ethylene-Inducing Peptide 1-Like Protein (NLP) Superfamily Across the Dothideomycetes Class of Fungi. Curr Microbiol 80, 44. https://doi.org/10.1007/s00284-022-03125-8

Déon, M., Fumanal, B., Gimenez, S., Bieysse, D., Oliveira, R.R., Shuib, S.S., Breton, F., Elumalai, S., Vida, J.B., Seguin, M., Leroy, T., Roeckel-Drevet, P., Pujade-Renaud, V., 2014. Diversity of the cassiicolin gene in *Corynespora cassiicola* and relation with the pathogenicity in *Hevea brasiliensis*. Fungal Biol 118, 32–47. https://doi.org/10.1016/j.funbio.2013.10.011

Déon, M., Scomparin, A., Tixier, A., Mattos, C.R.R., Leroy, T., Seguin, M., Roeckel-Drevet, P., Pujade-Renaud, V., 2012. First characterization of endophytic *Corynespora cassiicola* isolates with variant cassiicolin genes recovered from rubber trees in Brazil. Fungal Divers 54, 87–99. https://doi.org/10.1007/s13225-012-0169-6

Derbyshire, M.C., 2020. Bioinformatic Detection of Positive Selection Pressure in Plant Pathogens: The Neutral Theory of Molecular Sequence Evolution in Action. Front Microbiol 11, 644. https://doi.org/10.3389/fmicb.2020.00644

Drula, E., Garron, M.-L., Dogan, S., Lombard, V., Henrissat, B., Terrapon, N., 2022. The carbohydrate-active enzyme database: functions and literature. Nucleic Acids Res 50, D571–D577. https://doi.org/10.1093/nar/gkab1045

Emanuelsson, O., Nielsen, H., Brunak, S., von Heijne, G., 2000. Predicting Subcellular Localization of Proteins Based on their N-terminal Amino Acid Sequence. J Mol Biol 300, 1005–1016. https://doi.org/10.1006/jmbi.2000.3903

Feng, B., Li, P., Wang, H., Zhang, X., 2010. Functional analysis of Pcpme6 from oomycete plant pathogen *Phytophthora capsici*. Microb Pathog 49, 23–31. https://doi.org/10.1016/j.micpath.2010.03.004

Grigoriev, I. V., Nikitin, R., Haridas, S., Kuo, A., Ohm, R., Otillar, R., Riley, R., Salamov, A., Zhao, X., Korzeniewski, F., Smirnova, T., Nordberg, H., Dubchak, I., Shabalov, I., 2014. MycoCosm portal: gearing up for 1000 fungal genomes. Nucleic Acids Res 42, D699–D704. https://doi.org/10.1093/nar/gkt1183

Haridas, S., Albert, R., Binder, M., Bloem, J., LaButti, K., Salamov, A., Andreopoulos, B., Baker, S.E., Barry, K., Bills, G., Bluhm, B.H., Cannon, C., Castanera, R., Culley, D.E., Daum, C., Ezra, D., González, J.B., Henrissat, B., Kuo, A., Liang, C., Lipzen, A., Lutzoni, F., Magnuson, J., Mondo, S.J., Nolan, M., Ohm, R.A., Pangilinan, J., Park, H.J., Ramírez, L., Alfaro, M., Sun, H., Tritt, A., Yoshinaga, Y., Zwiers, L.H., Turgeon, B.G., Goodwin, S.B., Spatafora, J.W., Crous, P.W., Grigoriev, I.V., 2020. 101 Dothideomycetes genomes: A test case for predicting lifestyles and emergence of pathogens. Stud Mycol 96, 141–153. https://doi.org/10.1016/j.simyco.2020.01.003

Hoang, D.T., Chernomor, O., von Haeseler, A., Minh, B.Q., Vinh, L.S., 2018. UFBoot2: Improving the Ultrafast Bootstrap Approximation. Mol Biol Evol 35, 518–522. https://doi.org/10.1093/molbev/msx281

Horowitz, B.B., Ospina-Giraldo, M.D., 2015. The Pectin Methylesterase Gene Complement of *Phytophthora sojae*: Structural and Functional Analyses, and the

Evolutionary Relationships with Its Oomycete Homologs. PLoS One 10, e0142096. https://doi.org/10.1371/journal.pone.0142096

Hückelhoven, R., 2007. Cell Wall–Associated Mechanisms of Disease Resistance and Susceptibility. Annu Rev Phytopathol 45, 101–127. https://doi.org/10.1146/annurev.phyto.45.062806.094325

Hurst, L.D., 2002. The Ka/Ks ratio: diagnosing the form of sequence evolution. Trends in Genetics 18, 486–487. https://doi.org/10.1016/S0168-9525(02)02722-1

Hyde, K.D., Jones, E.B.G., Liu, J.K., Ariyawansa, H., Boehm, E., Boonmee, S., Braun, U., Chomnunti, P., Crous, P.W., Dai, D.-Q., Diederich, P., Dissanayake, A., Doilom, M., Doveri, F., Hongsanan, S., Jayawardena, R., Lawrey, J.D., Li, Y.M., Liu, Y.X., Lücking, R., Monkai, J., Muggia, L., Nelsen, M.P., Pang, K.L., Phookamsak, R., Senanayake, I.C., Shearer, C.A., Suetrong, S., Tanaka, K., Thambugala, K.M., Wijayawardene, N.N., Wikee, S., Wu, H.X., Zhang, Y., Aguirre-Hudson, B., Alias, S.A., Aptroot, A., Bahkali, A.H., Bezerra, J.L., Bhat, D.J., Camporesi, E., Chukeatirote, E., Gueidan, C., Hawksworth, D.L., Hirayama, K., De Hoog, S., Kang, J.C., Knudsen, K., Li, W.J., Li, X.H., Liu, Z.Y., Mapook, A., McKenzie, E.H.C., Miller, A.N., Mortimer, P.E., Phillips, A.J.L., Raja, H.A., Scheuer, C., Schumm, F., Taylor, J.E., Tian, Q., Tibpromma, S., Wanasinghe, D.N., Wang, Y., Xu, J.C., Yacharoen, S., Yan, J.Y., Zhang, M., 2013. Families of Dothideomycetes. Fungal Divers 63, 1–313. https://doi.org/10.1007/s13225-013-0263-4

Jolie, R.P., Duvetter, T., Van Loey, A.M., Hendrickx, M.E., 2010. Pectin methylesterase and its proteinaceous inhibitor: a review. Carbohydr Res 345, 2583–2595. https://doi.org/10.1016/j.carres.2010.10.002

Jones, P., Binns, D., Chang, H.Y., Fraser, M., Li, W., McAnulla, C., McWilliam, H., Maslen, J., Mitchell, A., Nuka, G., Pesseat, S., Quinn, A.F., Sangrador-Vegas, A., Scheremetjew, M., Yong, S.Y., Lopez, R., Hunter, S., 2014. InterProScan 5: genome-scale protein function classification. Bioinformatics 30, 1236–1240. https://doi.org/10.1093/bioinformatics/btu031

Kalyaanamoorthy, S., Minh, B.Q., Wong, T.K.F., Von Haeseler, A., Jermiin, L.S., 2017. ModelFinder: Fast model selection for accurate phylogenetic estimates. Nat Methods 14, 587–589. https://doi.org/10.1038/nmeth.4285

Katoh, K., Standley, D.M., 2013. MAFFT Multiple Sequence Alignment Software Version 7: Improvements in Performance and Usability. Mol Biol Evol 30, 772–780. https://doi.org/10.1093/molbev/mst010

Kent, L.M., Loo, T.S., Melton, L.D., Mercadante, D., Williams, M.A.K., Jameson, G.B., 2016. Structure and Properties of a Non-processive, Salt-requiring, and Acidophilic Pectin Methylesterase from *Aspergillus niger* Provide Insights into the Key Determinants of Processivity Control. Journal of Biological Chemistry 291, 1289–1306. https://doi.org/10.1074/jbc.M115.673152

Kirk, P.M., Cannon, P.F., Minter, D.W. and Stalpers, J.A., 2008. Dictionary of the Fungi. 10th Edition, Wallingford.

Krogh, A., Larsson, B., von Heijne, G., Sonnhammer, E.L.L., 2001. Predicting transmembrane protein topology with a hidden markov model: application to

complete genomes. J Mol Biol 305, 567–580. https://doi.org/10.1006/jmbi.2000.4315

Kuzmin, E., Taylor, J.S., Boone, C., 2022. Retention of duplicated genes in evolution. Trends in Genetics 38, 59–72. https://doi.org/10.1016/j.tig.2021.06.016

Li, P., Feng, B., Wang, H., Tooley, P.W., Zhang, X., 2011. Isolation of nine *Phytophthora capsici* pectin methylesterase genes which are differentially expressed in various plant species. J Basic Microbiol 51, 61–70. https://doi.org/10.1002/jobm.201000317

Lionetti, V., Cervone, F., Bellincampi, D., 2012. Methyl esterification of pectin plays a role during plant–pathogen interactions and affects plant resistance to diseases. J Plant Physiol 169, 1623–1630. https://doi.org/10.1016/j.jplph.2012.05.006

Liu, J.-K., Hyde, K.D., Jeewon, R., Phillips, A.J.L., Maharachchikumbura, S.S.N., Ryberg, M., Liu, Z.-Y., Zhao, Q., 2017. Ranking higher taxa using divergence times: a case study in Dothideomycetes. Fungal Divers 84, 75–99. https://doi.org/10.1007/s13225-017-0385-1

Livak, K.J., Schmittgen, T.D., 2001. Analysis of Relative Gene Expression Data Using Real-Time Quantitative PCR and the 2−ΔΔCT Method. Methods 25, 402–408. https://doi.org/10.1006/meth.2001.1262

Lo Presti, L., Lanver, D., Schweizer, G., Tanaka, S., Liang, L., Tollot, M., Zuccaro, A., Reissmann, S., Kahmann, R., 2015. Fungal Effectors and Plant Susceptibility. Annu Rev Plant Biol 66, 513–545. https://doi.org/10.1146/annurev-arplant-043014-114623

Looi, H.K., Toh, Y.F., Yew, S.M., Na, S.L., Tan, Y.-C., Chong, P.-S., Khoo, J.-S., Yee, W.-Y., Ng, K.P., Kuan, C.S., 2017. Genomic insight into pathogenicity of dematiaceous fungus *Corynespora cassiicola*. PeerJ 5, e2841. https://doi.org/10.7717/peerj.2841

Lopez, D., Ribeiro, S., Label, P., Fumanal, B., Venisse, J.-S., Kohler, A., de Oliveira, R.R., Labutti, K., Lipzen, A., Lail, K., Bauer, D., Ohm, R.A., Barry, K.W., Spatafora, J., Grigoriev, I. V., Martin, F.M., Pujade-Renaud, V., 2018. Genome-Wide Analysis of *Corynespora cassiicola* Leaf Fall Disease Putative Effectors. Front Microbiol 9, 276. https://doi.org/10.3389/fmicb.2018.00276

Lynch, M., Conery, J.S., 2000. The Evolutionary Fate and Consequences of Duplicate Genes. Science 290, 1151–1155. https://doi.org/10.1126/science.290.5494.1151

MacKenzie, K.J., Sumabat, L.G., Xavier, K. V., Vallad, G.E., 2018. A Review of *Corynespora cassiicola* and Its Increasing Relevance to Tomato in Florida. Plant Health Prog 19, 303–309. https://doi.org/10.1094/PHP-05-18-0023-RV

Markovič, O., Janeček, Š., 2004. Pectin methylesterases: sequence-structural features and phylogenetic relationships. Carbohydr Res 339, 2281–2295. https://doi.org/10.1016/j.carres.2004.06.023

Miedes, E., Vanholme, R., Boerjan, W., Molina, A., 2014. The role of the secondary cell wall in plant resistance to pathogens. Front Plant Sci 5. https://doi.org/10.3389/fpls.2014.00358

Mingora, C., Ewer, J., Ospina-Giraldo, M., 2014. Comparative structural and functional analysis of genes encoding pectin methylesterases in *Phytophthora* spp. Gene 538, 74–83. https://doi.org/10.1016/j.gene.2014.01.016

Mistry, J., Chuguransky, S., Williams, L., Qureshi, M., Salazar, G.A., Sonnhammer, E.L.L., Tosatto, S.C.E., Paladin, L., Raj, S., Richardson, L.J., Finn, R.D., Bateman, A., 2021. Pfam: The protein families database in 2021. Nucleic Acids Res 49, D412–D419. https://doi.org/10.1093/nar/gkaa913

Mohnen, D., 2008. Pectin structure and biosynthesis. Curr Opin Plant Biol 11, 266–277. https://doi.org/10.1016/j.pbi.2008.03.006

Nguyen, L.T., Schmidt, H.A., von Haeseler, A., Minh, B.Q., 2015. IQ-TREE: A Fast and Effective Stochastic Algorithm for Estimating Maximum-Likelihood Phylogenies. Mol Biol Evol 32, 268–274. https://doi.org/10.1093/molbev/msu300

Ohm, R.A., Feau, N., Henrissat, B., Schoch, C.L., Horwitz, B.A., Barry, K.W., Condon, B.J., Copeland, A.C., Dhillon, B., Glaser, F., Hesse, C.N., Kosti, I., LaButti, K., Lindquist, E.A., Lucas, S., Salamov, A.A., Bradshaw, R.E., Ciuffetti, L., Hamelin, R.C., Kema, G.H.J., Lawrence, C., Scott, J.A., Spatafora, J.W., Turgeon, B.G., de Wit, P.J.G.M., Zhong, S., Goodwin, S.B., Grigoriev, I. V., 2012. Diverse Lifestyles and Strategies of Plant Pathogenesis Encoded in the Genomes of Eighteen Dothideomycetes Fungi. PLoS Pathog 8, e1003037. https://doi.org/10.1371/journal.ppat.1003037

Panstruga, R., Parker, J.E., Schulze-Lefert, P., 2009. SnapShot: Plant Immune Response Pathways. Cell 136, 978.e1-978.e3. https://doi.org/10.1016/j.cell.2009.02.020

Pelloux, J., Rusterucci, C., Mellerowicz, E., 2007. New insights into pectin methylesterase structure and function. Trends Plant Sci 12, 267–277. https://doi.org/10.1016/j.tplants.2007.04.001

Petersen, T.N., Brunak, S., von Heijne, G., Nielsen, H., 2011. SignalP 4.0: discriminating signal peptides from transmembrane regions. Nat Methods 8, 785–786. https://doi.org/10.1038/nmeth.1701

Rambaut, A., 2009. FigTree v1. 3.1. http://tree. bio. ed. ac. uk/software/figtree/.

Reignault, Ph., Valette-Collet, O., Boccara, M., 2007. The importance of fungal pectinolytic enzymes in plant invasion, host adaptability and symptom type. Eur J Plant Pathol 120, 1–11. https://doi.org/10.1007/s10658-007-9184-y

Rody, H.V.S., Oliveira, L.O. de, 2018. Evolutionary history of the cobalamin-independent methionine synthase gene family across the land plants. Mol Phylogenet Evol 120, 33–42. https://doi.org/10.1016/j.ympev.2017.12.003

Rondon, MN., Lawrence, K., 2021. The fungal pathogen *Corynespora cassiicola*: A review and insights for target spot management on cotton and Soya bean. Journal of Phytopathology 169, 329–338. https://doi.org/10.1111/jph.12992

Rozas, J., Ferrer-Mata, A., Sánchez-DelBarrio, J.C., Guirao-Rico, S., Librado, P., Ramos-Onsins, S.E., Sánchez-Gracia, A., 2017. DnaSP 6: DNA Sequence Polymorphism Analysis of Large Data Sets. Mol Biol Evol 34, 3299–3302. https://doi.org/10.1093/molbev/msx248

Sánchez-Vallet, A., Fouché, S., Fudal, I., Hartmann, F.E., Soyer, J.L., Tellier, A., Croll, D., 2018. The Genome Biology of Effector Gene Evolution in Filamentous Plant Pathogens. Annu Rev Phytopathol 56, 21–40. https://doi.org/10.1146/annurev-phyto-080516-035303

Schoch, C.L., Crous, P.W., Groenewald, J.Z., Boehm, E.W.A., Burgess, T.I., de Gruyter, J., de Hoog, G.S., Dixon, L.J., Grube, M., Gueidan, C., Harada, Y., Hatakeyama, S., Hirayama, K., Hosoya, T., Huhndorf, S.M., Hyde, K.D., Jones, E.B.G., Kohlmeyer, J., Kruys, Å., Li, Y.M., Lücking, R., Lumbsch, H.T., Marvanová, L., Mbatchou, J.S., McVay, A.H., Miller, A.N., Mugambi, G.K., Muggia, L., Nelsen, M.P., Nelson, P., Owensby, C.A., Phillips, A.J.L., Phongpaichit, S., Pointing, S.B., Pujade-Renaud, V., Raja, H.A., Plata, E.R., Robbertse, B., Ruibal, C., Sakayaroj, J., Sano, T., Selbmann, L., Shearer, C.A., Shirouzu, T., Slippers, B., Suetrong, S., Tanaka, K., Volkmann-Kohlmeyer, B., Wingfield, M.J., Wood, A.R., Woudenberg, J.H.C., Yonezawa, H., Zhang, Y., Spatafora, J.W., 2009. A class-wide phylogenetic assessment of Dothideomycetes. Stud Mycol 64, 1–15. https://doi.org/10.3114/sim.2009.64.01

Sella, L., Castiglioni, C., Paccanaro, M.C., Janni, M., Schäfer, W., D'Ovidio, R., Favaron, F., 2016. Involvement of Fungal Pectin Methylesterase Activity in the Interaction Between *Fusarium graminearum* and Wheat. Molecular Plant-Microbe Interactions® 29, 258–267. https://doi.org/10.1094/MPMI-07-15-0174-R

Stanke, M., Morgenstern, B., 2005. AUGUSTUS: a web server for gene prediction in eukaryotes that allows user-defined constraints. Nucleic Acids Res 33, W465–W467. https://doi.org/10.1093/nar/gki458

Sumabat, L.G., Kemerait, R.C., Kim, D.K., Mehta, Y.R., Brewer, M.T., 2018. Clonality and geographic structure of host-specialized populations of *Corynespora cassiicola* causing emerging target spot epidemics in the southeastern United States. PLoS One 13, e0205849. https://doi.org/10.1371/journal.pone.0205849

Valette-Collet, O., Cimerman, A., Reignault, P., Levis, C., Boccara, M., 2003. Disruption of *Botrytis cinerea* Pectin Methylesterase Gene Bcpme1 Reduces Virulence on Several Host Plants. Molecular Plant-Microbe Interactions® 16, 360–367. https://doi.org/10.1094/MPMI.2003.16.4.360

Vicente, C.S.L., Nemchinov, L.G., Mota, M., Eisenback, J.D., Kamo, K., Vieira, P., 2019. Identification and characterization of the first pectin methylesterase gene discovered in the root lesion nematode *Pratylenchus penetrans*. PLoS One 14, e0212540. https://doi.org/10.1371/journal.pone.0212540

Voglmayr, H., Jaklitsch, W.M., 2017. *Corynespora*, *Exosporium* and *Helminthosporium* revisited - New species and generic reclassification. Stud Mycol 87, 43–76. https://doi.org/10.1016/j.simyco.2017.05.001

Wang, Y., Wu, J., Yan, J., Guo, M., Xu, L., Hou, L., Zou, Q., 2022. Comparative genome analysis of plant ascomycete fungal pathogens with different lifestyles reveals distinctive virulence strategies. BMC Genomics 23, 34. https://doi.org/10.1186/s12864-021-08165-1

Wijayawardene, N.N., Hyde, K.D., Rajeshkumar, K.C., Hawksworth, D.L., Madrid, H., Kirk, P.M., Braun, U., Singh, R. V., Crous, P.W., Kukwa, M., Lücking, R., Kurtzman, C.P., Yurkov, A., Haelewaters, D., Aptroot, A., Lumbsch, H.T., Timdal,

E., Ertz, D., Etayo, J., Phillips, A.J.L., Groenewald, J.Z., Papizadeh, M., Selbmann, L., Dayarathne, M.C., Weerakoon, G., Jones, E.B.G., Suetrong, S., Tian, Q., Castañeda-Ruiz, R.F., Bahkali, A.H., Pang, K.-L., Tanaka, K., Dai, D.Q., Sakayaroj, J., Hujslová, M., Lombard, L., Shenoy, B.D., Suija, A., Maharachchikumbura, S.S.N., Thambugala, K.M., Wanasinghe, D.N., Sharma, B.O., Gaikwad, S., Pandit, G., Zucconi, L., Onofri, S., Egidi, E., Raja, H.A., Kodsueb, R., Cáceres, M.E.S., Pérez-Ortega, S., Fiuza, P.O., Monteiro, J.S., Vasilyeva, L.N., Shivas, R.G., Prieto, M., Wedin, M., Olariaga, I., Lateef, A.A., Agrawal, Y., Fazeli, S.A.S., Amoozegar, M.A., Zhao, G.Z., Pfliegler, W.P., Sharma, G., Oset, M., Abdel-Wahab, M.A., Takamatsu, S., Bensch, K., de Silva, N.I., De Kesel, A., Karunarathna, A., Boonmee, S., Pfister, D.H., Lu, Y.-Z., Luo, Z.-L., Boonyuen, N., Daranagama, D.A., Senanayake, I.C., Jayasiri, S.C., Samarakoon, M.C., Zeng, X.-Y., Doilom, M., Quijada, L., Rampadarath, S., Heredia, G., Dissanayake, A.J., Jayawardana, R.S., Perera, R.H., Tang, L.Z., Phukhamsakda, C., Hernández-Restrepo, M., Ma, X., Tibpromma, S., Gusmao, L.F.P., Weerahewa, D., Karunarathna, S.C., 2017. Notes for genera: Ascomycota. Fungal Divers 86, 1–594. https://doi.org/10.1007/s13225-017-0386-0

Wolf, S., Mouille, G., Pelloux, J., 2009. Homogalacturonan Methyl-Esterification and Plant Development. Mol Plant 2, 851–860. https://doi.org/10.1093/mp/ssp066

Yang, Z., 2007. PAML 4: Phylogenetic Analysis by Maximum Likelihood. Mol Biol Evol 24, 1586–1591. https://doi.org/10.1093/molbev/msm088

Yang, Z., Nielsen, R., Goldman, N., Pedersen, A.-M.K., 2000. Codon-Substitution Models for Heterogeneous Selection Pressure at Amino Acid Sites. Genetics 155, 431–449. https://doi.org/10.1093/genetics/155.1.431

Zhang, H., Yohe, T., Huang, L., Entwistle, S., Wu, P., Yang, Z., Busk, P.K., Xu, Y., Yin, Y., 2018. dbCAN2: a meta server for automated carbohydrate-active enzyme annotation. Nucleic Acids Res 46, W95–W101. https://doi.org/10.1093/nar/gky418

Zhang, Y., Crous, P.W., Schoch, C.L., Hyde, K.D., 2012. Pleosporales. Fungal Divers 53, 1–221. https://doi.org/10.1007/s13225-011-0117-x

Zhao, Z., Liu, H., Wang, C., Xu, J.-R., 2013. Comparative analysis of fungal genomes reveals different plant cell wall degrading capacity in fungi. BMC Genomics 14, 274. https://doi.org/10.1186/1471-2164-14-274

SUPPLEMENTARY MATERIAL

Unveiling the evolutionary history of the Pectin methylesterase (PME) gene family in the Dothideomycetes class of fungi

Table S1. List of fungal species, with assembled genome size (GZ), number of predicted genes (PG) in each genome, number of predicted Pectin Methylesterase (PME) genes, number of PMEs (putative effectors and putative non-effectors), and number of PMEs for each clade.

							Prediction from this study			Clades		
Species (Isolate)	**Alias**	**Class**	**Order**	**GZ (Mb)**	**#PG**	**Reference**	**#PME genes**	**# putative effector PMEs**	**# putative non-effector PMEs**	**#PME1**	**#PME2**	**#PME3**
Aaosphaeria arxii (CBS 175.79)	Aaoar	Dothideomycetes	Pleosporales	38.9	14,203	Haridas et al., 2020	1	0	1	1	2	0
Acidomyces richmondensis (BFW)	Aciri	Dothideomycetes	Capnodiales	29.9	11,202	Mosier et al., 2016	3	1	2	1	2	0
Alternaria alternata (BMP0270)	Altal	Dothideomycetes	Pleosporales	33.0	13,469	Dang et al., 2015	4	4	0	1	1	0
Amniculicola lignicola (CBS 123094)	Amnli	Dothideomycetes	Pleosporales	49.6	15,590	Haridas et al., 2020	4	3	1	1	2	0
Aplosporella prunicola (CBS 121.167)	Aplpr	Dothideomycetes	Botryosphaeriales	32.8	12,579	Haridas et al., 2020	5	4	1	1	1	0
Ascochyta rabiei (ArDII)	Ascra	Dothideomycetes	Pleosporales	34.7	10,596	Verma et al., 2016	3	2	1	1	2	1
Aulographum hederae	Aulhe	Dothideomycetes	Aulographales	32.0	12,127	Haridas et al., 2020	3	2	1	1	2	0
Baudoinia compniacensis (UAMH 10762 (4089826))	Bauco	Dothideomycetes	Capnodiales	21.9	10,513	Ohm et al., 2012	1	1	0	1	2	1
Bimuria novae-zelandiae (CBS 107.79)	Bimnz	Dothideomycetes	Pleosporales	78.2	16,681	Haridas et al., 2020	3	3	0	1	2	0
Botryosphaeria dothidea	Botdo	Dothideomycetes	Botryosphaeriales	43.5	14,998	Marsberg et al., 2017	3	0	3	1	1	0
Byssothecium circinans (CBS 675.92)	Bysci	Dothideomycetes	Pleosporales	49.3	15,785	Haridas et al., 2020	4	4	0	1	1	0
Cenococcum geophilum (1.58)	Cenge	Dothideomycetes	Mytilinidiales	177.6	14,748	Peter et al., 2016	2	2	0	1	2	0
Cercospora zeae-maydis	Cerzm	Dothideomycetes	Capnodiales	46.6	12,020	Haridas et al., 2020	1	1	0	1	2	0
Cladosporium fulvum	Clafu	Dothideomycetes	Capnodiales	61.1	14,127	de Wit et al., 2012	2	2	0	1	2	0
Clathrospora elynae (CBS 161.51)	Clael	Dothideomycetes	Pleosporales	37.4	13,617	Haridas et al., 2020	3	1	2	1	2	0
Clohesyomyces aquaticus	Cloaq	Dothideomycetes	Pleosporales	49.7	15,810	Mondo et al., 2017	1	1	0	1	2	0
Cochliobolus heterostrophus (C5)	Coche	Dothideomycetes	Pleosporales	36.5	13,336	Ohm et al., 2012	3	3	0	1	2	0
Corynespora cassiicola (CCP)	Corca	Dothideomycetes	Pleosporales	44.8	17,166	Lopez et al., 2018	5	3	2	1	1	1
Cucurbitaria berberidis (CBS 394.84)	Cucbe	Dothideomycetes	Pleosporales	32.9	12,439	Haridas et al., 2020	5	2	3	1	2	1
Delitschia confertaspora (ATCC 74209)	Delco	Dothideomycetes	Pleosporales	31.2	10,171	Haridas et al., 2020	2	2	0	1	2	0
Delphinella strobiligena (CBS 735.71)	Delst	Dothideomycetes	Dothideales	29.2	10,337	Haridas et al., 2020	4	3	1	0	1	0
Didymella exigua (CBS 183.55)	Didex	Dothideomycetes	Pleosporales	34.4	12,394	Haridas et al., 2020	4	3	1	1	1	0
Diplodia seriata (DS831)	Dipse	Dothideomycetes	Botryosphaeriales	37.1	9,343	Morales-Cruz et al., 2015	5	2	3	1	2	0
Dissoconium aciculare	Disac	Dothideomycetes	Capnodiales	26.5	10,299	Haridas et al., 2020	0	0	0	2	3	0
Dothidotthia symphoricarpi	Dotsy	Dothideomycetes	Pleosporales	34.4	11,790	Haridas et al., 2020	3	3	0	0	1	0
Dothistroma septosporum (NZE10)	Dotse	Dothideomycetes	Capnodiales	30.2	12,580	De Wit et al., 2012	2	2	0	1	2	0
Elsinoe ampelina (CECT 20119)	Elsam	Dothideomycetes	Myriangiales	28.3	10,209	Haridas et al., 2020	4	2	2	1	2	0
Eremomyces bilateralis (CBS 781.70)	Erebi	Dothideomycetes	Eremomycetales	26.9	9,881	Haridas et al., 2020	2	2	0	1	2	0
Glonium stellatum (CBS 207.34)	Glost	Dothideomycetes	Mytilinidiales	40.5	14,362	Peter et al., 2016	2	1	1	0	1	0
Hysterium pulicare	Hyspu	Dothideomycetes	Hysteriales	38.4	12,352	Ohm et al., 2012	3	0	3	0	1	0
Karstenula rhodostoma (CBS 690.94)	Karrh	Dothideomycetes	Pleosporales	44.9	12,469	Haridas et al., 2020	3	2	1	1	3	0
Lentithecium fluviatile	Lenfl	Dothideomycetes	Pleosporales	54.7	16,742	Haridas et al., 2020	2	2	0	0	2	0
Lepidopterella palustris	Leppa	Dothideomycetes	Mytilinidiales	45.7	13,870	Peter et al., 2016	2	2	0	0	1	0

Continued Table S1

Leptosphaeria maculans	Lepma	Dothideomycetes	Pleosporales	44.9	12,469	Rouxel et al 2011	3	3	0	1	2	0
Lindgomyces ingoldianus (ATCC 200398)	Linin	Dothideomycetes	Pleosporales	69.0	15,956	Haridas et al., 2020	2	2	0	1	1	0
Lineolata rhizophorae (ATCC 16933)	Linrh	Dothideomycetes	Lineolatales	31.1	10,230	Haridas et al., 2020	0	0	0	0	1	0
Lizonia empirigonia (CBS 542.76)	Lizem	Dothideomycetes	Pleosporales	51.5	12,467	Haridas et al., 2020	4	3	1	1	2	0
Lophiostoma macrostomum	Lopma	Dothideomycetes	Pleosporales	42.6	16,160	Haridas et al., 2020	4	2	2	1	1	0
Lophiotrema nucula (CBS 627.86)	Lopnu	Dothideomycetes	Pleosporales	48.6	18,117	Haridas et al., 2020	5	4	1	1	1	0
Lophium mytilinum (CBS 269.34)	Lopmy	Dothideomycetes	Mytilinidiales	43.4	15,153	Haridas et al., 2020	1	1	0	1	2	1
Macrophomina phaseolina (MS6)	Macph	Dothideomycetes	Botryosphaeriales	48.9	13,806	Islam et al., 2012	3	2	1	1	1	0
Macroventuria anomochaeta (CBS 525.71)	Macan	Dothideomycetes	Pleosporales	33.3	12,954	Haridas et al., 2020	4	4	0	1	1	0
Massarina eburnea (CBS 473.64)	Maseb	Dothideomycetes	Pleosporales	38.2	12,935	Haridas et al., 2020	3	3	0	1	1	0
Massariosphaeria phaeospora (CBS 611.86)	Masph	Dothideomycetes	Pleosporales	42.1	14,021	Haridas et al., 2020	1	1	0	0	0	0
Melanomma pulvis-pyrius	Melpu	Dothideomycetes	Pleosporales	42.1	15,881	Haridas et al., 2020	4	4	0	0	1	0
Microthyrium microscopicum (CBS 115976)	Micmi	Dothideomycetes	Microthyriales	37.1	12,494	Haridas et al., 2020	3	2	1	1	2	0
Myriangium duriaei (CBS 260.36)	Myrdu	Dothideomycetes	Myriangiales	25.7	10,685	Haridas et al., 2020	3	1	2	0	2	0
Mytilinidion resinicola (CBS 304.34)	Mytre	Dothideomycetes	Mytilinidiales	47.3	16,794	Haridas et al., 2020	0	0	0	1	1	0
Neofusicoccum parvum (UCRNP2)	Neopa	Dothideomycetes	Botryosphaeriales	42.6	10,366	Blanco-Ulate et al., 2013	5	4	1	1	3	0
Paraconiothyrium sporulosum (AP3s5-JAC2a)	Parsp	Dothideomycetes	Pleosporales	38.5	14,745	Zeiner et al., 2016	4	3	1	1	3	0
Patellaria atrata	Patat	Dothideomycetes	Patellariales	28.7	9,794	Haridas et al., 2020	0	0	0	1	2	0
Periconia macrospinosa (DSE2036)	Perma	Dothideomycetes	Pleosporales	55.0	18,750	Knapp et al., 2018	1	0	1	1	4	0
Phoma tracheiphila (IPT5)	Photr	Dothideomycetes	Pleosporales	34.2	13,209	Haridas et al., 2020	5	3	2	1	1	0
Phyllosticta citricarpa (CBS 127454)	Phyci	Dothideomycetes	Botryosphaeriales	29.0	11,088	Guarnaccia et al., 2019	3	1	2	0	0	0
Piedraia hortae (CBS 480.64)	Pieho	Dothideomycetes	Capnodiales	16.9	7,572	Haridas et al., 2020	0	0	0	0	0	0
Pleomassaria siparia	Plesi	Dothideomycetes	Pleosporales	43.2	13,486	Haridas et al., 2020	3	2	1	1	0	0
Polychaeton citri	Polci	Dothideomycetes	Capnodiales	27.2	10,582	Haridas et al., 2020	0	0	0	1	1	1
Polyplosphaeria fusca (CBS 125425)	Polfu	Dothideomycetes	Pleosporales	37.0	15,194	Haridas et al., 2020	2	1	1	1	2	1
Pseudocercospora eumusae (CBS 114824)	Pseeu	Dothideomycetes	Capnodiales	47.1	12,632	Chang et al., 2016	1	1	0	1	1	1
Pseudovirgaria hyperparasitica (CBS 121739)	Psehy	Dothideomycetes	Acrospermales	35.4	11,232	Haridas et al., 2020	3	2	1	1	0	0
Pyrenophora tritici-repentis	Pyrtr	Dothideomycetes	Pleosporales	37.8	12,141	Manning et al., 2013	2	1	1	0	1	1
Rhizodiscina lignyota (CBS 133067)	Rhili	Dothideomycetes	Aulographales	33.4	12,801	Haridas et al., 2020	2	1	1	0	1	1
Rhytidhysteron rufulum	Rhyru	Dothideomycetes	Hysteriales	40.2	12,117	Ohm et al., 2012	4	0	4	0	1	0
Saccharata proteae (CBS 121410)	Sacpr	Dothideomycetes	Botryosphaeriales	31.4	9,234	Haridas et al., 2020	2	2	0	0	0	0
Septoria musiva (SO2202)	Sepmu	Dothideomycetes	Capnodiales	29.4	10,233	Ohm et al., 2012	0	0	0	0	1	0
Setomelanomma holmii (CBS 110217)	Setho	Dothideomycetes	Pleosporales	39.2	14,389	Haridas et al., 2020	4	4	0	1	1	0
Setosphaeria turcica (Et28A)	Settu	Dothideomycetes	Pleosporales	43.0	12,028	Ohm et al., 2012	3	3	0	1	1	0
Stagonospora nodorum (SN15)	Stano	Dothideomycetes	Pleosporales	37.2	12,380	Hane et al., 2007	3	3	0	1	0	0
Teratosphaeria nubilosa (CBS 116005)	Ternu	Dothideomycetes	Capnodiales	28.4	10,998	Haridas et al., 2020	2	1	1	1	0	0
Tothia fuscella (CBS 130266)	Totfu	Dothideomycetes	Venturiales	36.8	13,685	Haridas et al., 2020	4	3	1	0	0	0
Trematosphaeria pertusa (CBS 122368)	Trepe	Dothideomycetes	Pleosporales	47.7	17,306	Haridas et al., 2020	3	3	0	1	2	0

Continued Table S1

Venturia inaequalis	Venin	Dothideomycetes	Venturiales	55.1	13,233	Deng et al., 2017	3	3	0	0	0	0
Verruconis gallopava	Verga	Dothideomycetes	Venturiales	31.8	11,357	Teixeira et al., 2017	1	1	0	1	1	0
Verruculina enalia (CBS 304.66)	Veren	Dothideomycetes	Pleosporales	61.2	13,748	Haridas et al., 2020	1	0	1	0	1	0
Viridothelium virens	Virvi	Dothideomycetes	Trypetheliales	32.2	11,858	Haridas et al., 2020	1	1	0	0	0	0
Westerdykella ornata (CBS 379.55)	Wesor	Dothideomycetes	Pleosporales	27.0	10,410	Haridas et al., 2020	1	1	0	1	1	0
Zasmidium cellare (ATCC 36951)	Zasce	Dothideomycetes	Capnodiales	38.2	16,015	Haridas et al., 2020	1	1	0	1	2	0
Zopfia rhizophila	Zoprh	Dothideomycetes	Pleosporales	152.8	21,730	Haridas et al., 2020	3	2	1	1	2	0
Zymoseptoria tritici	Zymtr	Dothideomycetes	Capnodiales	39.7	10,933	Goodwin et al., 2011	1	1	0	0	1	0
Aspergillus fumigatus (A1163)	Aspfu	Eurotiomycetes	Eurotiales	29.2	9,916	Fedorova et al., 2008	4	4	0	1	1	0
Aspergillus nidulans	Aspni	Eurotiomycetes	Eurotiales	30.5	10,608	Arnaud et al., 2012	3	2	1	2	1	0
						Total	209	151	58	61	111	10

Table S2. List of *Corynespora* isolates, with host species, country of origin, assembled genome size (GZ), number of predicted genes (PG) in each genome, number of predicted Pectin Methylesterase (PME) genes, number of PMEs (putative effectors and putative non-effectors).

								Prediction from this study		
Species (isolate)	**BioSample**	**BioProject**	**Assembly**	**Host species**	**Country**	**GZ (Mb) – [Reference]**	**#PG – [Reference]**	**# PME genes**	**# putative effector PMEs**	**# putative non-effector PMEs**
Corynespora cassiicola (777AA)	SAMN08330686	PRJNA428435	GCA_002976175.1	*Glycine max*	Brazil	41.7 [Lopez et al., 2018]	14,873 [Dal'Sasso et al., 2022]	5	5	0
Corynespora cassiicola (ATI11)	SAMN08330687	PRJNA428435	GCA_002976025.1	*Cucumis sativus*	Brazil	41.1 [[Lopez et al., 2018]]	14,497 [Dal'Sasso et al., 2022]	5	5	0
Corynespora cassiicola (C7_L008)	SAMEA103891068	PRJEB19843	GCA_900169545.1	-	-	42.5 [-]	14,569 [Dal'Sasso et al., 2022]	5	5	0
Corynespora cassiicola (CAL-4)	SAMN12086008	PRJNA549429	GCA_006523515.1	*Gossypium hirsutum*	USA	47.5 [-]	19,239 [Dal'Sasso et al., 2022]	5	4	1
Corynespora cassiicola (CBS12925)	SAMN08330688	PRJNA428435	GCA_002976015.1	*Cucumis sativus*	Brazil	40.8 [Lopez et al., 2018]	14,403 [Dal'Sasso et al., 2022]	5	4	1
Corynespora cassiicola (CCAM1)	SAMN08330689	PRJNA428435	GCA_002975975.1	*Hevea brasiliensis*	Cameroon	42.3 [Lopez et al., 2018]	14,634 [Dal'Sasso et al., 2022]	5	5	0
Corynespora cassiicola (CCAM2)	SAMN08330690	PRJNA428435	GCA_002976125.1	*Hevea brasiliensis*	Cameroon	41.9 [Lopez et al., 2018]	14,785 [Dal'Sasso et al., 2022]	5	5	0
Corynespora cassiicola (CCAM3)	SAMN08330691	PRJNA428435	GCA_002975935.1	*Hevea brasiliensis*	Cameroon	42.7 [Lopez et al., 2018]	15,022 [Dal'Sasso et al., 2022]	5	5	0
Corynespora cassiicola (CCAM4)	SAMN08330692	PRJNA428435	GCA_002975955.1	*Hevea brasiliensis*	Cameroon	42.3 [Lopez et al., 2018]	14,545 [Dal'Sasso et al., 2022]	5	5	0
Corynespora cassiicola (CCI13)	SAMN08330693	PRJNA428435	GCA_002975895.1	*Hevea brasiliensis*	Côte d'Ivoire	41.9 [Lopez et al., 2018]	14,847 [Dal'Sasso et al., 2022]	5	4	1
Corynespora cassiicola (CCI6)	SAMN08330694	PRJNA428435	GCA_002975915.1	*Hevea brasiliensis*	Côte d'Ivoire	42.0 [Lopez et al., 2018]	14,905 [Dal'Sasso et al., 2022]	5	4	1
Corynespora cassiicola (CGAB1)	SAMN08330695	PRJNA428435	GCA_002975825.1	*Hevea brasiliensis*	Gabon	41.2 [Lopez et al., 2018]	14,635 [Dal'Sasso et al., 2022]	5	5	0
Corynespora cassiicola (CGAB2)	SAMN08330696	PRJNA428435	GCA_002975875.1	*Hevea brasiliensis*	Gabon	41.2 [Lopez et al., 2018]	14,638 [Dal'Sasso et al., 2022]	5	5	0
Corynespora cassiicola (CIND3)	SAMN08330697	PRJNA428435	GCA_002975845.1	*Hevea brasiliensis*	India	41.7[Lopez et al., 2018]	14,733 [Dal'Sasso et al., 2022]	5	5	0
Corynespora cassiicola (CLN16)	SAMN08330698	PRJNA428435	GCA_002975795.1	*Hevea brasiliensis*	Malaysia	41.7 [Lopez et al., 2018]	14,803 [Dal'Sasso et al., 2022]	5	5	0
Corynespora cassiicola (CSB16)	SAMN08330699	PRJNA428435	GCA_002976145.1	*Hevea brasiliensis*	Malaysia	40.7 [Lopez et al., 2018]	14,489 [Dal'Sasso et al., 2022]	5	4	1
Corynespora cassiicola (CSRI1)	SAMN08330700	PRJNA428435	GCA_002975815.1	*Hevea brasiliensis*	Sri Lanka	40.6 [Lopez et al., 2018]	14,327 [Dal'Sasso et al., 2022]	5	4	1
Corynespora cassiicola (CSRI2)	SAMN08330701	PRJNA428435	GCA_002975775.1	*Hevea brasiliensis*	Sri Lanka	40.8 [Lopez et al., 2018]	14,391 [Dal'Sasso et al., 2022]	5	4	1
Corynespora cassiicola (CSRI5)	SAMN08330702	PRJNA428435	GCA_002975755.1	*Hevea brasiliensis*	Sri Lanka	41.7 [Lopez et al., 2018]	14,736 [Dal'Sasso et al., 2022]	5	5	0
Corynespora cassiicola (CTHA1)	SAMN08330703	PRJNA428435	GCA_002975725.1	*Hevea brasiliensis*	Thailand	41.3 [Lopez et al., 2018]	14,432 [Dal'Sasso et al., 2022]	5	5	0
Corynespora cassiicola (CTHA2)	SAMN08330704	PRJNA428435	GCA_002976105.1	*Hevea brasiliensis*	Thailand	40.8 [Lopez et al., 2018]	14,424 [Dal'Sasso et al., 2022]	5	4	1
Corynespora cassiicola (CTHA3)	SAMN08330705	PRJNA428435	GCA_002975705.1	*Hevea brasiliensis*	Thailand	40.4 [Lopez et al., 2018]	14,616 [Dal'Sasso et al., 2022]	5	5	0
Corynespora cassiicola (CTHA4)	SAMN08330706	PRJNA428435	GCA_002975685.1	*Hevea brasiliensis*	Thailand	40.7 [Lopez et al., 2018]	14,410 [Dal'Sasso et al., 2022]	5	5	0
Corynespora cassiicola (CTHA5)	SAMN08330707	PRJNA428435	GCA_002975655.1	*Hevea brasiliensis*	Thailand	40.9 [Lopez et al., 2018]	14,461 [Dal'Sasso et al., 2022]	5	4	1
Corynespora cassiicola (CTHA6)	SAMN08330708	PRJNA428435	GCA_002976085.1	*Hevea brasiliensis*	Thailand	40.9 [Lopez et al., 2018]	14,444 [Dal'Sasso et al., 2022]	5	4	1
Corynespora cassiicola (CVa5)	SAMN12086010	PRJNA549429	GCA_006523535.1	*Gossypium hirsutum*	USA	45.3 [-]	15,347 [Dal'Sasso et al., 2022]	5	5	0
Corynespora cassiicola (E139)	SAMN08330709	PRJNA428435	GCA_002975665.1	*Hevea brasiliensis*	Brazil	42.8 [Lopez et al., 2018]	14,648 [Dal'Sasso et al., 2022]	5	5	0
Corynespora cassiicola (E55)	SAMN08330710	PRJNA428435	GCA_002976075.1	*Hevea brasiliensis*	Brazil	40.5 [Lopez et al., 2018]	14,352 [Dal'Sasso et al., 2022]	5	5	0
Corynespora cassiicola (E79)	SAMN08330711	PRJNA428435	GCA_002976045.1	*Hevea brasiliensis*	Brazil	42.5 [Lopez et al., 2018]	14,373 [Dal'Sasso et al., 2022]	5	5	0
Corynespora cassiicola (EDIG)	SAMN08330712	PRJNA428435	GCA_002975615.1	*Cucumis sativus*	Brazil	41.2 [Lopez et al., 2018]	14,743 [Dal'Sasso et al., 2022]			0
Corynespora cassiicola (GSO2)	SAMN08330713	PRJNA428435	GCA_002975635.1	*Vernonia cinerea*	Brazil	41.8 [Lopez et al., 2018]	15,072 [Dal'Sasso et al., 2022]	5	4	1
Corynespora cassiicola (IA)	SAMN08330714	PRJNA428435	GCA_002975535.1	*Cucumis sativus*	Brazil	41.6 [Lopez et al., 2018]	14,793 [Dal'Sasso et al., 2022]	5	5	0
Corynespora cassiicola (India_Hevea)	SAMN10434155	PRJNA505742	SRR8196886	*Hevea brasiliensis*	India	42.9 [Dal'Sasso et al., 2022]	14,404 [Dal'Sasso et al., 2022]	5	4	1

Continued Table S2

Corynespora cassiicola (JQ)	SAMN08330715	PRJNA428435	GCA_002975595.1	*Cucumis sativus*	Brazil	41.6 [Lopez et al., 2018]	14,815 [Dal'Sasso et al., 2022]	5	4	1
Corynespora cassiicola (LPO7)	SAMN08330716	PRJNA428435	GCA_002975495.1	*Piper hispidinervum*	Brazil	42.2 [Lopez et al., 2018]	14,535 [Dal'Sasso et al., 2022]	5	5	0
Corynespora cassiicola (PB)	SAMN08330717	PRJNA428435	GCA_002975575.1	*Cucumis sativus*	Brazil	41.6 [Lopez et al., 2018]	14,801 [Dal'Sasso et al., 2022]	5	4	1
Corynespora cassiicola (RUD)	SAMN08330718	PRJNA428435	GCA_002975505.1	*Glycine max*	Brazil	41.6 [Lopez et al., 2018]	14,858 [Dal'Sasso et al., 2022]	5	4	1
Corynespora cassiicola (SS1)	SAMN08330719	PRJNA428435	GCA_002975995.1	*Hevea brasiliensis*	Malaysia	40.7 [Lopez et al., 2018]	14,378 [Dal'Sasso et al., 2022]	5	4	1
Corynespora cassiicola (TCl3)	SAMN12086019	PRJNA549429	GCA_006519745.1	*Solanum lycospersium*	USA	46.0 [-]	14,986 [Dal'Sasso et al., 2022]	5	5	0
Corynespora cassiicola (TSB1)	SAMN08330720	PRJNA428435	GCA_002975555.1	*Hevea brasiliensis*	Malaysia	40.9 [Lopez et al., 2018]	14,435 [Dal'Sasso et al., 2022]	5	4	1
Corynespora cassiicola (Tscotton1)	SAMN06706475	PRJNA382361	SRR5435235	*Gossypium hirsutum*	USA	42.1 [Dal'Sasso et al., 2022]	14,988 [Dal'Sasso et al., 2022]	5	4	1
Corynespora cassiicola (UM591)	SAMN02981578	PRJNA236064	GCA_000603925.1	*Homo sapiens*	Malaysia	41.3 [Looi et al., 2016]	14,695 [Dal'Sasso et al., 2022]	5	5	0
Corynespora cassiicola (CCP)	SAMN05660679	PRJNA234811	GCA_003016335.1	*Hevea brasiliensis*	Philippines	44.8 [Lopez et al., 2018]	17,166 [Lopez et al., 2018]	5	3	2
Corynespora cassiicola (CC_29)	SAMN18718492	PRJNA721456	GCA_019202905.1	*Glycine max*	Brazil	44.7 [Dal'Sasso et al., 2021]	18,487 [Dal'Sasso et al., 2021]	5	5	0
Corynespora cassiicola (CC01)	SAMN17150876	PRJNA687613	GCA_016906425.1	*Hevea brasiliensis*	China	47.1 [Li et al., 2021]	15,606 [this study]	5	5	0
Corynespora cassiicola (YN49)	SAMN17150874	PRJNA687612	GCA_016906405.1	*Hevea brasiliensis*	China	45.1 [Li et al., 2021]	15,005 [this study]	5	4	1
Corynespora cassiicola (ZM170522)	SAMN17573700	PRJNA694745	GCA_022059125.1	*Hevea brasiliensis*	China	44.4 [Xu et al., 2021]	14,467 [this study]	5	4	1
Corynespora cassiicola (ZM160181)	SAMN17573614	PRJNA694745	GCA_022496115.1	*Fragaria x ananassa*	China	44.9 [-]	15,257 [this study]	5	5	0
Corynespora cassiicola (HG20101029)	SAMN09258516	PRJNA473037	GCA_023647615.1	*Cucumis sativus*	China	42.7 [Gao et al., 2020]	14,599 [this study]	5	5	0
Corynespora cassiicola (SAR-9)	SAMN12086012	PRJNA549429	GCA_023653695.1	*Glycine max*	USA	47.6 [-]	20,522 [this study]	5	5	0
Corynespora cassiicola (SMR2)	SAMN12086013	PRJNA549429	GCA_023653595.1	*Glycine max*	USA	48.4 [-]	21,607 [this study]	5	5	0
Corynespora cassiicola (FIM4)	SAMN12086011	PRJNA549429	GCA_023653765.1	*Gossypium hirsutum*	USA	49.1 [-]	22,414 [this study]	5	5	0
Corynespora cassiicola (CC1551)	SAMN12086017	PRJNA549429	GCA_023653545.1	*Solanum lycospersium*	USA	50.1 [-]	22,587 [this study]	5	5	0
Corynespora cassiicola (TCf2)	SAMN12086018	PRJNA549429	GCA_023653535.1	*Solanum lycospersium*	USA	50.8 [-]	22,751 [this study]	5	5	0
Corynespora cassiicola (Ssta1)	SAMN12086014	PRJNA549429	GCA_023653575.1	*Glycine max*	USA	45.0 [-]	15,596 [this study]	5	4	1
Corynespora cassiicola (CM13)	SAMN12086009	PRJNA549429	GCA_024500335.1	*Gossypium hirsutum*	USA	53.3 [-]	18,721 [this study]	5	5	0
Corynespora cassiicola (STNa-1)	SAMN12086015	PRJNA549429	GCA_024500205.1	*Glycine max*	USA	50.9 [-]	25,819 [this study]	5	4	1
Corynespora cassiicola (CC1343)	SAMN12086016	PRJNA549429	GCA_024500185.1	*Solanum lycospersium*	USA	54.1 [-]	20,620 [this study]	5	5	0
Corynespora cassiicola (CC_08)	-	-	-	*Commelina benghalensis*	Brazil	Dal'Sasso et al., (unpublished)	Dal'Sasso et al., (unpublished)	5	5	0
Corynespora cassiicola (CC_10)	-	-	-	*Lantana camara*	Brazil	Dal'Sasso et al., (unpublished)	Dal'Sasso et al., (unpublished)	5	5	0
Corynespora cassiicola (CC_28)	-	-	-	*Plectranthus barbatus*	Brazil	Dal'Sasso et al., (unpublished)	Dal'Sasso et al., (unpublished)	5	5	0
Corynespora smithii (CBS139925)	-	-	-	-	-	Dal'Sasso et al., (unpublished)	Dal'Sasso et al., (unpublished)	3	3	0
							Total	308	282	26

Table S3. Description of primer sequences used for RT-qPCR analysis of Pectin Methylesterase (PME) genes in *Corynespora cassiicola* (isolate CC_29).

Gene name	Gene ID (CC_29)	Sequences 5'- 3'	References
Cc_PME1.1	CC_29_g10563	F: AGGGCACAAACACGACCTAC R: ACACTTTCCGTCAATGGCGA	This study
Cc_PME1.2	CC_29_g7531	F: TGTTACAGTCACTTGGGCGT R: TCGGTGCGATAGTGATGACG	This study
Cc_PME2.1	CC_29_g13870	F: AGCAGAGCCTCTTTAACCGT R: ACCCGGATATTTCTCAGAAGCA	This study
Cc_PME2.2	CC_29_g2687	F: AAGCTGAGCACCAGCAGTAG R: CCAGCCAGTGCCTTGATGTA	This study
Cc_PME2.3	CC_29_g7533	F: GCTGCCAATGCAACACCTAC R: TAGCCGTCAACCACTTCCTG	This study
β-tubulin	CC_29_g4872	F: CAGACCGGTCAATGCGGTAA R: GCCATTGTAGACGCCGGATC	Dal'Sasso et al., 2022

Table S4. Details about Pectin Methylesterase (PME) proteins containing multiple PME domains.

Protein ID	Species/isolate	Ordem	Classification	Number of PME domains
Altal_115003	*Alternaria alternata* BMP0270	Pleosporales	Putative effector	4
Clael_294950	*Clathrospora elynae* CBS 161.51	Pleosporales	Putative non-effector	4
Photr_528851	*Phoma tracheiphila* IPT5	Pleosporales	Putative effector	4
Cucbe_379106	*Cucurbitaria berberidis* CBS 394.84 v1.0	Pleosporales	Putative effector	3
Setho_117982	*Setomelanomma holmii* CBS 110217 v1.0	Pleosporales	Putative effector	3
Stano_11857	*Stagonospora nodorum* SN15 v2.0	Pleosporales	Putative effector	4
Ascra_8129	*Ascochyta rabiei ArDII*	Pleosporales	Putative non-effector	3
Lizem_26709	*Lizonia empirigonia* CBS 542.76 v1.0	Pleosporales	Putative non-effector	4
Macan_19039	*Macroventuria anomochaeta* CBS 525.71 v1.0	Pleosporales	Putative effector	3
Didex_92474	*Didymella exigua* CBS 183.55	Pleosporales	Putative effector	4
Parsp_965437	*Paraconiothyrium sporulosum* AP3s5-JAC2a	Pleosporales	Putative effector	5
Melpu_306641	*Melanomma pulvis-pyrius* v1.0	Pleosporales	Putative effector	4
Lopnu_594842	*Lophiotrema nucula* CBS 627.86 v1.0	Pleosporales	Putative effector	4
Amnli_601992	*Amniculicola lignicola* CBS 123094 v1.0	Pleosporales	Putative effector	4
Hyspu_122423	*Hysterium pulicare*	Hysteriales	Putative non-effector	5
Macph_4586	*Macrophomina phaseolina* MS6	Botryosphaeriales	Putative non-effector	4
Dipse_4877	*Diplodia seriata* DS834	Botryosphaeriales	Putative non-effector	5
Neopa_995	*Neofusicoccum parvum* UCRNP2	Botryosphaeriales	Putative non-effector	4
Micmi_153697	*Microthyrium microscopicum* CBS 115976 v1.0	Microthyriales	Putative effector	2
Myrdu_262084	*Myriangium duriaei* CBS 260.36 v1.0	Myriangiales	Putative non-effector	3
Elsamp_263318	*Elsinoe ampelina* CECT 20119 v1.0	Myriangiales	Putative non-effector	3
Delst_419985	*Delphinella strobiligena* CBS 735.71 v1.3	Dothideales	Putative effector	2
Aspfu_107433	*Aspergillus fumigatus* A1163	Eurotiales	Putative effector	4

Table S5. Details about Pectin Methylesterase (PME) proteins containing other domains in addition to a PME domain.

Protein ID	Species/isolate	Ordem	Classifcation	Domains
Botdo_287534	*Lophiostoma macrostomum* v1.0	Pleosporales	Putative non-effector	PF01095 (Pectin methylesterase), PF13205 (Big_5: Bacterial Ig-like)
Lopma_782105	*Botryosphaeria dothidea*	Botryosphaeriales	Putative non-effector	PF01095 (Pectin methylesterase), PF00067 (cytochrome P450)
Rhili_78039	*Rhizodiscina lignyota* CBS 133067	Aulographales	Putative effector	PF01095 (Pectin methylesterase), PF13205 (Big_5: Bacterial Ig-like)
Aspnid_1389	*Aspergillus nidulans*	Eurotiales	Putative non-effector	PF01095 (Pectin methylesterase), PF00295 (Glyco_hydro_28)

Table S6. Amino acid sequence alignment of five conserved segments for 182 Pectin Methylesterase (PME) proteins across the clades PME1, PME2, and PME3. The alignment was generated by MAFFT v7.453. Arrows indicate amino acid positions, using the protein Aspnid_267 of *Aspergilus nidulans* as a reference sequence. Code-color: blue, highly conservated amino acid residues; yellow, sites containing putative amino acid residues involved in active site of the enzyme. Protein ID with highlight in red: a putative non-effector PME.

		Segments				
Clade	**Protein ID**	**I**	**II**	**III**	**IV**	**V**
		76	180	202	225	289
PME1	Aspnid_267	GTYTE	PAHAL	QDTV	DFIYG	LGRPW
	Aspfu_103215	GNYTE	PAHAL	QDTV	DFLYG	LGRPW
	Rhili_66085	GSYFE	PSHAV	QDTV	DFLYG	LGRPW
	Verga_121510	GNYTE	PALTV	QDTV	DFLYG	LGRPW
	Aspfu_106988	GTYVE	PAHAV	QDTL	DFLYG	LGRPW
	Coche_1087744	GNYTE	PSLAI	QDTL	DFLYG	LGRPW
	Settu_31057	GNYTE	PSLAV	QDTV	DFFYG	LGRPW
	Altal_115721	GNYTE	PALAV	QDTV	DFFYG	LGRPW
	Photr_420235	GNYTE	PSLAV	QDTV	DFFYG	LGRPW
	Cucbe_417360	GNYTE	PALAV	QDTV	DFFYG	LGRPW
	Dotsy_302074	GNYTE	PALAV	QDTV	DFFYG	LGRPW
	Ascra_1917	GNYTE	PSLAV	QDTV	DFFYG	LGRPW
	Lizem_162071	GNYTE	PALAV	QDTV	DFFYG	LGRPW
	Macan_401247	GNYTE	PALAV	QDTV	DFFYG	LGRPW
	Didex_418780	GNYTE	PSLAV	QDTV	DFFYG	LGRPW
	Setho_101090	GNYTE	PALAV	QDTV	DFFYG	LGRPW
	Pytr_10681	GNYTE	PALAI	QDTV	DFFYG	LGRPW
	Stano_22	GNYTE	PALAV	QDTV	DFLYG	LGRPW
	Clael_73600	GIYTE	PALAV	QDTV	DFLYG	LGRPW
	Lepmu_10971	GNYTE	PSLAV	QDTV	DFLYG	LGRPW
	Hyspu_116211	GTYTE	PSLAL	QDTI	DFLYG	LGRPW
	Cenge_708901	GNYTE	PSLAL	QDTI	DFLYG	LGRPW
	Glost_284495	GNYTE	PSLAL	QDTI	DFLYG	LGRPW
	Leppa_300809	GNYTE	PSLAL	QDTI	DFLYG	LGRPW
	Sacpr_47908	GTYIE	PSLAL	QDTI	DFLYG	LGRPW
	Myrdu_304953	GNYTE	PSLAL	QDTI	DFLYG	LGRPW
	Elsamp_47975	GNYTE	PALAL	QDTV	DFFYG	LGRPW
	Virvi_575863	GNYTE	PSLAL	QDTV	DFFYG	LGRPW
	Macph_2734	GTYVE	PALAI	QDTV	DFLYG	LGRPW
	Neopa_6229	GTYTE	PALAI	QDTV	DFLYG	LGRPW
	Dipse_2103	GTYTE	PALAI	QDTI	DFLYG	LGRPW
	Aplpr_354418	GTYTE	PALAL	QDTV	DFLYG	LGRPW
	Psehy_473941	GNYTE	PSLAV	QDTV	DFLYG	LGRPW
	Delst_377613	GNYTE	PSLAI	QDTV	DFLYG	LGRPW
	Clafu_194088	GDYTE	PSLAL	QDTV	DFFYG	LGRPW
	Dotse_134632	GDYTE	PSLAL	QDTV	DFFYG	LGRPW
	Aciri_148029	GNYTE	PSLAV	QDTV	DFFYG	LGRPW
	Bauco_568892	GNYTE	PSLAV	QDTV	DFVYG	LGRPW
	Karrh_431734	GQYTE	PSLAL	QDTI	DFLYG	LGRPW
	Parsp_536334	GQYTE	PSLAL	QDTI	DFLYG	LGRPW
	Bimnz_588933	GQYTE	PSLAL	QDTI	DFLYG	LGRPW
	Lenfl_361857	GQYTE	PSLAL	QDTI	DFLYG	LGRPW
	Trepe_97564	GQYTE	PSLAL	QDTV	DFLYG	LGRPW
	Lopnu_606153	GQYTE	PSLAL	QDTI	DFLYG	LGRPW
	Amnli_599375	GIYTE	PSLAL	QDTI	DFLYG	LGRPW
	Linin_380480	GTYTE	PSLAV	QDTI	DFLYG	LGRPW

Continued Table S6

	Zoprh_720438	GQYTE	PSLAL	QDTI	DFLYG	LGRPW
	Delco_476930	GQYTE	PSLAL	QDTI	DFLYG	LGRPW
	Corca_371920	GLYTE	PSLAL	QDTV	DFLYG	LGRPW
	Lopma_692510	GLYPE	PSLAL	QDTV	DFLYG	LGRPW
	Maseb_504458	GQYNE	PSLAL	QDTV	DFLYG	LGRPW
	Bysci_467202	GLYRE	PSLAL	QDTV	DFLYG	LGRPW
	Ternu_311880	GDYKE	PSLAV	QDTV	DFLYG	LGRPW
	Rhyru_114074	GVYYG	PALAL	QDTI	DFLYG	LGRPW
	Phyci_610752	GIYEE	PSLAL	QDTV	DFLYG	LGRPW
	Totfu_116681	GTYRE	PSLAV	QDTV	DFFYG	LGRPW
	Venin_22176	GLYTE	PSLAV	QDTV	DYLYG	LGRPW
	Melpu_252400	GNYTE	PSLAL	QDTI	DFFYG	LGRPW
	Corca_486221	GDYRE	PSLAV	QDTV	DFLYG	LGRPW
	Aulhe_462886	GVYTE	PSLAV	QDTV	DFLYG	LGRPW
	Plesi_463730	GTYIE	PSLAV	QDTV	DFFYG	LGRPW
PME2	Aspnid_8703	GTYKE	QAVAL	QDTL	DYIFG	LGRPW
	Aspfu_107026	GTYQE	QAVTL	QDTL	DYIFG	LGRPW
	Dipse_6825	GTYAE	QAVAL	QDTL	DYIFG	LGRPW
	Karrh_495632	GTYTE	QAVAL	QDTL	DYIFG	LGRPW
	Parsp_1238408	GTYTE	QAVAL	QDTL	DYIFG	LGRPW
	Bysci_398890	GTYKE	QAVAV	QDTL	DYIFG	LGRPW
	Maseb_455864	GTYKE	QAVAV	QDTL	DYIFG	LGRPW
	Trepe_587606	GTYNE	QAVAV	QDTL	DYIFG	LGRPW
	Lopnu_547721	GTYKE	QAVAV	QDTL	DYIFG	LGRPW
	Amnli_546045	GTYAE	QAVAV	QDTL	DYIFG	LGRPW
	Rhyru_111187	GTYKE	QAVAV	QDTL	DYVFG	LGRPW
	Psehy_433061	GTYKE	QAVAV	QDTL	DYIFG	LGRPW
	Plesi_528821	GTYTE	QAVAL	QDTL	DYIFG	LGRPW
	Phyci_616728	GTYKE	QAVAL	QDTL	DYIFG	LGRPW
	Aplpr_302427	GTYTE	QAVAL	QDTL	DYVFG	LGRPW
	Zoprh_614260	GTYNE	QAVAL	QDTL	DYIFG	LGRPW
	Corca_630853	GTYTE	QAVAL	QDTL	DFIFG	LGRPW
	Totfu_231905	GTYQE	QAVAF	QDTL	DFIFG	LGRPW
	Coche_1144206	GTYTE	QALAV	QDTV	DFIFG	LGRPW
	Photr_471381	GTYKE	QALAL	QDTV	DFIFG	LGRPW
	Settu_155226	GTYKE	QALAL	QDTV	DFIFG	LGRPW
	Altal_121121	GTYKE	QALAL	QDTI	DFIFG	LGRPW
	Cucbe_368391	GTYKE	QALAL	QDTI	DFIFG	LGRPW
	Clael_456728	GTYKE	QALAL	QDTI	DFIFG	LGRPW
	Stano_5956	GTYKE	QALAL	QDTI	DFIFG	LGRPW
	Setho_97039	GTYKE	QALAL	QDTI	DFIFG	LGRPW
	Dotsy_389786	GTYSE	QALAV	QDTI	DFIFG	LGRPW
	Ascra_6731	GTYQE	QALAI	QDTI	DFIFG	LGRPW
	Lizem_164713	GTYKE	QALAL	QDTI	DFIFG	LGRPW
	Macan_400465	GTYKE	QALAL	QDTI	DFIFG	LGRPW
	Didex_67544	GTYKE	QALAL	QDTL	DFIFG	LGRPW
	Bysci_523018	GTYKE	QAVAV	QDTL	DFIFG	LGRPW
	Maseb_434462	GTYKE	QALAV	QDTI	DFIFG	LGRPW
	Lenfl_366978	GTYKE	QALAV	QDTI	DFIFG	LGRPW
	Trepe_161134	GTYKE	QALAV	QDTV	DFIFG	LGRPW
	Masph_625394	GTYTE	QALAV	QDTI	DFIFG	LGRPW
	Wesor_192944	GTYNE	QALAL	QDTV	DFIFG	LGRPW
	Aaoar_379326	GTYNE	QALAV	QDTI	DFIFG	LGRPW
	Melpu_248730	GTYSE	QALAV	QDTI	DFIFG	LGRPW
	Plesi_426225	GTYSE	QALAV	QDTI	DFIFG	LGRPW
	Lopnu_562124	GTYSE	QALAI	QDTI	DFIFG	LGRPW

Continued Table S6

Amnli_495707	GTYSE	QALAV	QDTI	DFIFG	LGRPW
Polfu_501840	GTYNE	QALAV	QDTI	DFIFG	LGRPW
Corca_647558	GTYNE	QALAV	QDTI	DFIFG	LGRPW
Veren_530935	GTYSE	QALAI	QDTV	DFIFG	LGRPW
Perma_610601	GTYKE	QAVAV	QDTL	DFIFG	LGRPW
Karrh_526723	GTYKE	QAVAV	QDTL	DFIFG	LGRPW
Parsp_1166222	GTYKE	QAVAV	QDTL	DFIFG	LGRPW
Bimnz_443851	GTYKE	QAVAV	QDTL	DFIFG	LGRPW
Lopma_658054	GTYKE	QAVAL	QDTV	DFIFG	LGRPW
Psehy_241757	GTYKE	QALAI	QDTV	DFIFG	LGRPW
Lopma_684549	GSYDE	QALAL	QDTI	DFIFG	LGRPW
Linin_340215	GTYDE	QALAL	QDTI	DFIFG	LGRPW
Zoprh_611865	GTYDE	QALAL	QDTI	DFIFG	LGRPW
Cloaq_497631	GTYDE	QALAL	QDTV	DFIFG	LGRPW
Lopnu_693925	GTYDE	QALAL	QDTI	DFIFG	LGRPW
Delco_381130	GTYDE	QALAL	QDTL	DFIFG	LGRPW
Hyspu_121475	GTYQE	QALAL	QDTL	DFIFG	LGRPW
Cenge_699144	GTYTE	QALAI	QDTV	DFIFG	LGRPW
Glost_415638	GTYNE	QALAI	QDTV	DFIFG	LGRPW
Leppa_361043	GTYTE	QAVAI	QDTV	DFIFG	LGRPW
Lopmy_575895	GTYNE	QALAL	QDTL	DFIFG	LGRPW
Rhyru_114494	GTYDE	QALAL	QDTI	DFIFG	LGRPW
Polfu_544726	GTYNE	QALAL	QDTI	DFIFG	LGRPW
Pytr_11212	GTYKE	QALAV	QDTV	DFIFG	LGRPW
Myrdu_284737	GTYSE	QALAL	QDTI	DFIFG	LGRPW
Elsamp_198435	GTYKE	QALAL	QDTI	DFIFG	LGRPW
Myceu_6468	GTYRE	QALAL	QDTI	DFIFG	LGRPW
Zasce_69576	GTYKE	QALAL	QDTI	DFIFG	LGRPW
Mycgr_66866	GTYKE	QALAL	QDTV	DFIFG	LGRPW
Clafu_187043	GTCKE	QAVAV	QDTL	DFIFG	LGRPW
Dotse_137384	GTYEE	QALAV	QDTL	DFIFG	LGRSW
Cerzm_87436	GTYNE	QAVAV	QDTL	DFIFG	LGRPW
Botdo_290297	GTYEE	QAVAL	QDTL	DFIFG	LGRPW
Macph_9957	GTYKE	QAVAL	QDTL	DFIFG	LGRPW
Neopa_6290	GTYKE	QAVAL	QDTL	DFIFG	LGRPW
Dipse_1389	GTYSE	QAVAL	QDTL	DFIFG	LGRPW
Aplpr_225563	GTYKE	QAVAI	QDTV	DFIFG	LGRPW
Aplpr_321605	GTYKE	QAIAL	QDTV	DFIFG	LGRPW
Phyci_589369	GKYEE	QAVAL	QDTV	DFIFG	LGRPW
Aplpr_292209	GTYKE	QAVAL	QDTL	DFIFG	LGRPW
Sacpr_50339	GTYDE	QALAL	QDTI	DFIFG	LGRPW
Delst_374577	GTYSE	IALAL	QDTV	DFIFG	LGRPW
Aciri_105619	GTYDE	QALAV	QDTI	DFIFG	LGRPW
Ternu_259438	GTYKE	QALAL	QDTV	DFIFG	LGRPW
Lepmu_11590	GKYQE	QALAV	QDTV	DFIFG	LGRPW
Botdo_285589	GTYEE	QAVAV	QDTL	DFIFG	LGRPW
Neopa_2308	GTYEE	QAVAV	QDTL	DFIFG	LGRPW
Dipse_3509	GTYEE	QAVAV	QDTL	DFIFG	LGRPW
Erebi_504401	GKYNE	QALAL	QDTV	DFIFG	LGRPW
Melpu_386551	GTYAE	QAVAL	QDTV	DFVFG	LGRPW
Venin_24092	GTYKE	QALAL	QDTV	DFIFG	LGRPW
Micmi_433574	GTYKE	QALAL	QDTV	DFIFG	LGRPW
Aulhe_372178	GTYNE	QALAL	QDTV	DFIFG	LGRPW
Neopa_789	GNYTE	QAVAL	VDTV	DFIFG	LGRPW
Aciri_89457	GLYKE	QNLAL	QDTL	DFIFG	LGRPW
Delst_343653	GVYSE	QALAL	QDTL	DFIFG	LGRPW
Coche_1189533	GTYTE	QALAL	QDTI	DFIFG	LGRPW

Continued Table S6

	Settu_170878	GTYTE	QALAL	QDTI	DFIFG	LGRPW
	Aalte_122217	GVYNE	QALAI	QDTI	DFIFG	LGRPW
	Photr_500138	GVYEE	QALAL	QDTI	DFIFG	LGRPW
	Lepmu_10589	GVYEE	QALAL	QDTI	DFIFG	LGRPW
	Cucbe_272673	GTYTE	QALAL	QDTI	DFIFG	LGRPW
	Setho_116805	GTYTE	QALAL	QDTI	DFIFG	LGRPW
	Lizem_123319	GTYTE	QALAL	QDTV	DFIFG	LGRPW
	Macan_345552	GVYTE	QALAL	QDTV	DFIFG	LGRPW
	Didex_68406	GTYTE	QALAL	QDTI	DFIFG	LGRPW
	Elsamp_199465	GVYRE	QALAL	QDTI	DFIFG	LGRPW
	Corca_604944	GKYVE	QALAL	QDTI	DFIFG	LGRPW
	Dotsy_67493	GTYNE	QALAL	QDTI	DFIFG	LGRPW
	Totfu_588964	GKYKG	QALAV	QDTL	DFIFG	LGRPW
PME3	Photr_508183	GEYKE	QAEAL	GDAL	DTILG	FARPN
	Cucbe_367788	GNYEE	QAEAL	GDAL	DTILG	FARAN
	Rhyru_115434	GNYEE	QAEAL	GDAL	DTILG	FARAN
	Bysci_534408	GTYTE	QAEAL	GDAL	DTILG	LARPN
	Bimnz_204356	GTYEE	QAEAL	GDAL	DTILG	FARDN
	Aulhe_4169	GNYTE	QAEGL	GDAF	DTVLG	FSRAN
	Venin_16528	GWYEE	QAEAL	GDAF	DTVLG	FARQN
	Micmi_428082	GNYEE	QAEAI	GDAF	DTVLG	FARSN
	Erebi_301971	GNYEE	QAEAL	GDAF	DTVLG	YGRAN
	Totfu_104879	GDYEE	QAEAV	GDAF	DTILG	FARCN

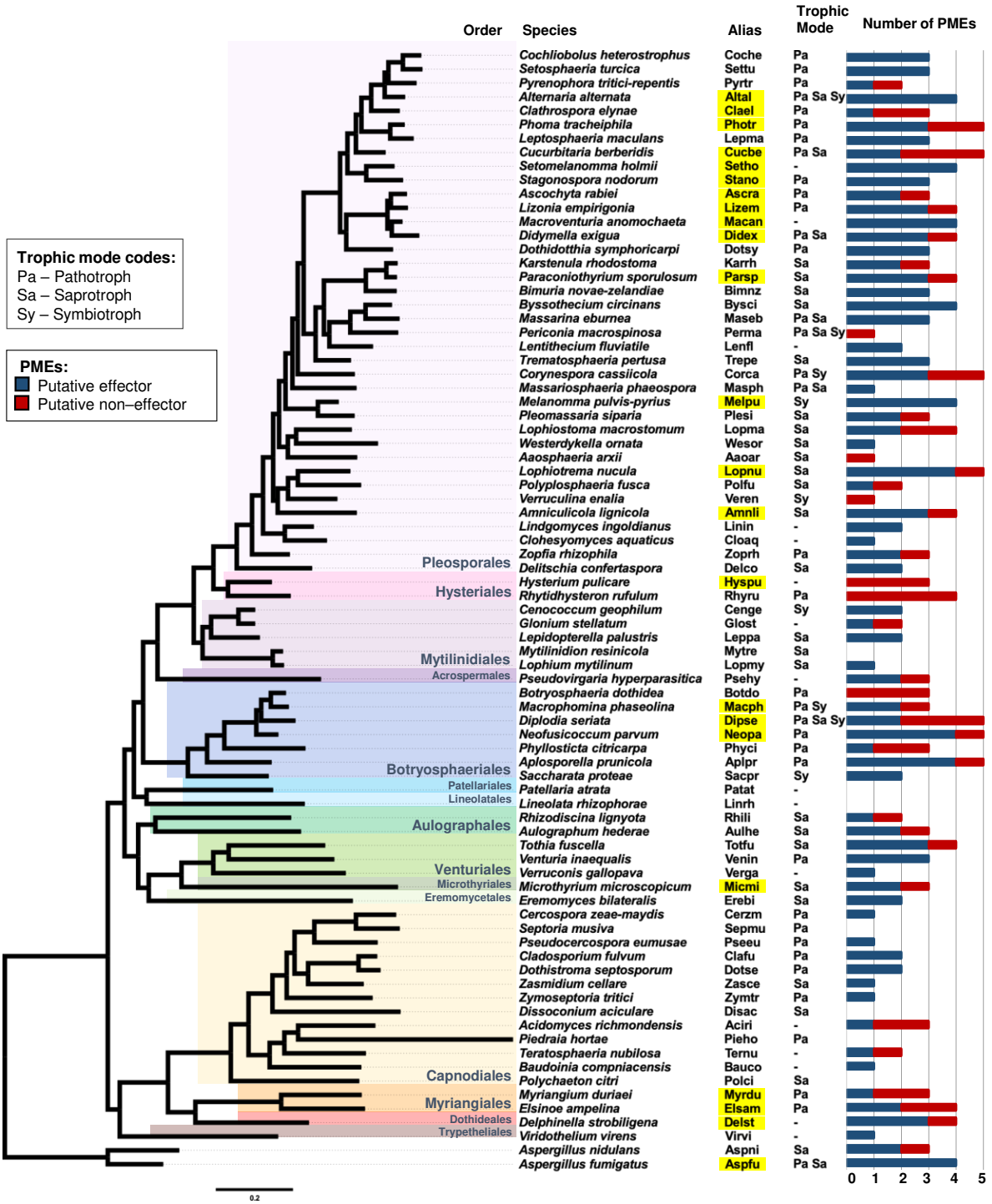

Figure S1. Phylogenomic distributions of Pectin Methylterase (PME) gene family among 79 species of Dothideomycetes, with two *Aspergillus* species (Eurotiomycetes) as outgroup. Branch lengths are drawn to scale. All nodes were fully supported (100 local bootstraps). Scale bars correspond to the expected number of substitutions per site. Clades are color-coded according to the orders of Dothideomycetes, as indicated. Alias (five-letter codes) represents species name. Alias with yellow highlight: a species that harbors PME genes that contained multiple PME domains. Bars on the far right site: the number of PMEs (putative effector and putative non-effector genes) uncovered per species. Both the phylogenomic reconstruction and the trophic modes were obtained during a previous study (Dal Sasso et al., 2023).

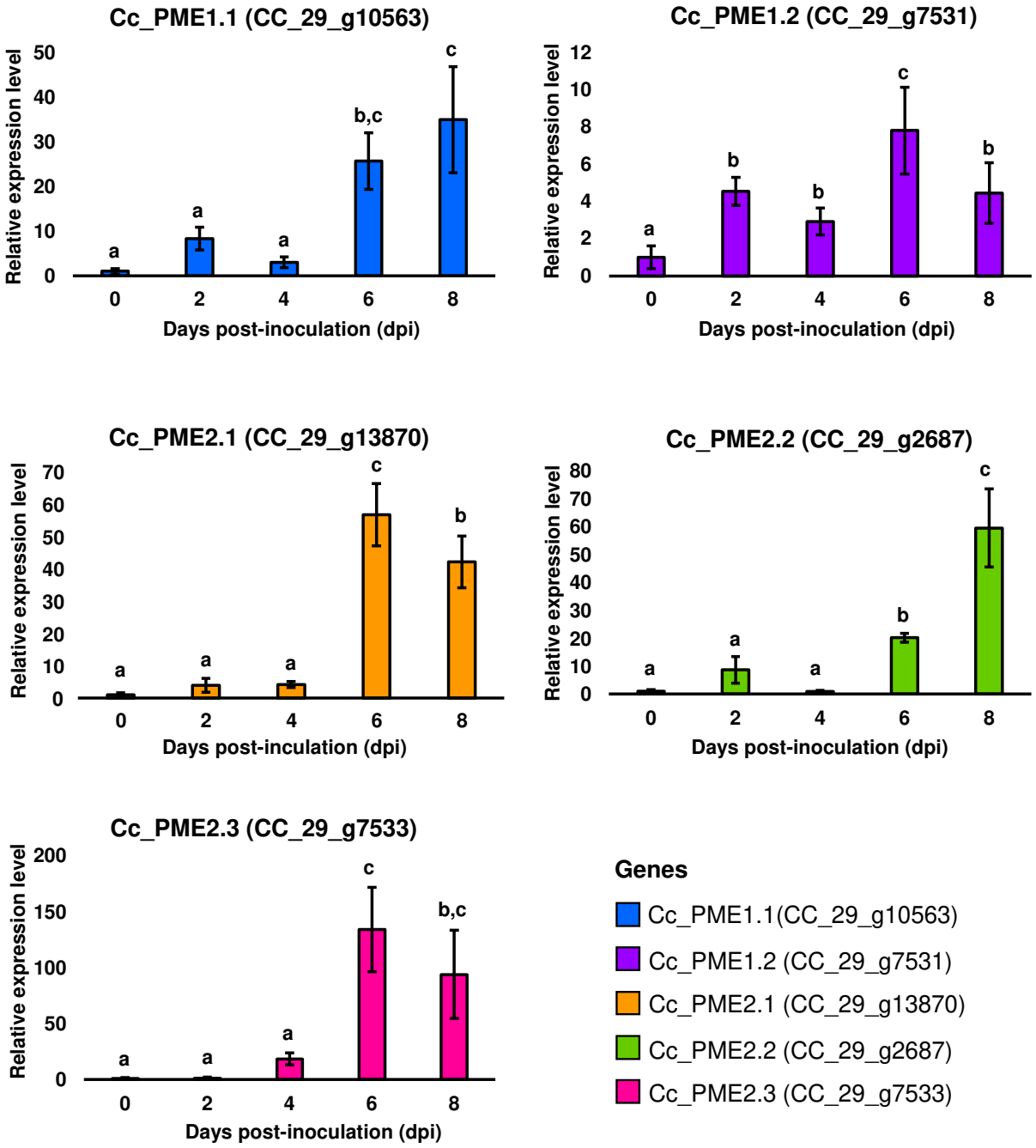

Figure S2. Relative expression levels of five Pectin Methylterase (PME) genes of *Corynespora cassiicola* on soybean leaves, during 0, 2, 4, 6, and 8 days post-inoculation (dpi), respectively. Data were obtained from the RT-qPCR analyses. The relative expression levels were calculated using the$2^{-\Delta\Delta Ct}$ method, with four biological replicates for each time point. The constitutive β-tubulin gene of *C. cassiicola* was used an endogenous control. The relative expression level was calibrated and set as 1 at 0 dpi. Letters above bars indicate statistically significant differences according to Tukey's test (p-value < 0.05). Error bars show standard error of the mean. Levels of expression were color-coded according to the five PME genes, as indicated.

REFERENCES

Arnaud, M.B., Cerqueira, G.C., Inglis, D.O., Skrzypek, M.S., Binkley, J., Chibucos, M.C., Crabtree, J., Howarth, C., Orvis, J., Shah, P., Wymore, F., Binkley, G., Miyasato, S.R., Simison, M., Sherlock, G., Wortman, J.R., 2012. The *Aspergillus* Genome Database (AspGD): recent developments in comprehensive multispecies curation, comparative genomics and community resources. Nucleic Acids Res 40, D653–D659. https://doi.org/10.1093/nar/gkr875

Blanco-Ulate, B., Rolshausen, P., Cantu, D., 2013. Draft Genome Sequence of *Neofusicoccum parvum* Isolate UCR-NP2, a Fungal Vascular Pathogen Associated with Grapevine Cankers. Genome Announc 1, e00339-13. https://doi.org/10.1128/genomeA.00339-13

Chang, T.-C., Salvucci, A., Crous, P.W., Stergiopoulos, I., 2016. Comparative Genomics of the Sigatoka Disease Complex on Banana Suggests a Link between Parallel Evolutionary Changes in *Pseudocercospora fijiensis* and *Pseudocercospora eumusae* and Increased Virulence on the Banana Host. PLoS Genet 12, e1005904. https://doi.org/10.1371/journal.pgen.1005904

Dal'Sasso, T.C.S., Rocha, V.D., Rody, H.V.S., Costa, M.D.B.L., Oliveira, L.O., 2022. The necrosis- and ethylene-inducing peptide 1-like protein (NLP) gene family of the plant pathogen *Corynespora cassiicola*. Curr Genet 68, 645–659. https://doi.org/10.1007/s00294-022-01252-0

Dal'Sasso, T.C.S., Rody, H.V.S., Grijalba, P.E., Oliveira, L.O., 2021. Genome sequences and in silico effector mining of *Corynespora cassiicola* CC_29 and *Corynespora olivacea* CBS 114450. Arch Microbiol 203, 5257–5265. https://doi.org/10.1007/s00203-021-02456-7

Dang, H.X., Pryor, B., Peever, T., Lawrence, C.B., 2015. The *Alternaria* genomes database: a comprehensive resource for a fungal genus comprised of saprophytes, plant pathogens, and allergenic species. BMC Genomics 16, 239. https://doi.org/10.1186/s12864-015-1430-7

De Wit, P.J.G.M., van der Burgt, A., Ökmen, B., Stergiopoulos, I., Abd-Elsalam, K.A., Aerts, A.L., Bahkali, A.H., Beenen, H.G., Chettri, P., Cox, M.P., Datema, E., de Vries, R.P., Dhillon, B., Ganley, A.R., Griffiths, S.A., Guo, Y., Hamelin, R.C., Henrissat, B., Kabir, M.S., Jashni, M.K., Kema, G., Klaubauf, S., Lapidus, A., Levasseur, A., Lindquist, E., Mehrabi, R., Ohm, R.A., Owen, T.J., Salamov, A., Schwelm, A., Schijlen, E., Sun, H., van den Burg, H.A., van Ham, R.C.H.J., Zhang, S., Goodwin, S.B., Grigoriev, I. V., Collemare, J., Bradshaw, R.E., 2012. The Genomes of the Fungal Plant Pathogens *Cladosporium fulvum* and *Dothistroma septosporum* Reveal Adaptation to Different Hosts and Lifestyles But Also Signatures of Common Ancestry. PLoS Genet 8, e1003088. https://doi.org/10.1371/journal.pgen.1003088

Deng, C.H., Plummer, K.M., Jones, D.A.B., Mesarich, C.H., Shiller, J., Taranto, A.P., Robinson, A.J., Kastner, P., Hall, N.E., Templeton, M.D., Bowen, J.K., 2017. Comparative analysis of the predicted secretomes of Rosaceae scab pathogens *Venturia inaequalis* and *V. pirina* reveals expanded effector families and putative determinants of host range. BMC Genomics 18, 339. https://doi.org/10.1186/s12864-017-3699-1

Fedorova, N.D., Khaldi, N., Joardar, V.S., Maiti, R., Amedeo, P., Anderson, M.J., Crabtree, J., Silva, J.C., Badger, J.H., Albarraq, A., Angiuoli, S., Bussey, H., Bowyer, P., Cotty, P.J., Dyer, P.S., Egan, A., Galens, K., Fraser-Liggett, C.M., Haas, B.J., Inman, J.M., Kent, R., Lemieux, S., Malavazi, I., Orvis, J., Roemer, T., Ronning, C.M., Sundaram, J.P., Sutton, G., Turner, G., Venter, J.C., White, O.R., Whitty, B.R., Youngman, P., Wolfe, K.H., Goldman, G.H., Wortman, J.R., Jiang, B., Denning, D.W., Nierman, W.C., 2008. Genomic Islands in the Pathogenic Filamentous Fungus *Aspergillus fumigatus*. PLoS Genet 4, e1000046. https://doi.org/10.1371/journal.pgen.1000046

Gao, S., Zeng, R., Xu, L., Song, Z., Gao, P., Dai, F., 2020. Genome sequence and spore germination-associated transcriptome analysis of *Corynespora cassiicola* from cucumber. BMC Microbiol 20, 199. https://doi.org/10.1186/s12866-020-01873-w

Goodwin, S.B., Ben M'Barek, S., Dhillon, B., Wittenberg, A.H.J., Crane, C.F., Hane, J.K., Foster, A.J., Van der Lee, T.A.J., Grimwood, J., Aerts, A., Antoniw, J., Bailey, A., Bluhm, B., Bowler, J., Bristow, J., van der Burgt, A., Canto-Canché, B., Churchill, A.C.L., Conde-Ferràez, L., Cools, H.J., Coutinho, P.M., Csukai, M., Dehal, P., De Wit, P., Donzelli, B., van de Geest, H.C., van Ham, R.C.H.J., Hammond-Kosack, K.E., Henrissat, B., Kilian, A., Kobayashi, A.K., Koopmann, E., Kourmpetis, Y., Kuzniar, A., Lindquist, E., Lombard, V., Maliepaard, C., Martins, N., Mehrabi, R., Nap, J.P.H., Ponomarenko, A., Rudd, J.J., Salamov, A., Schmutz, J., Schouten, H.J., Shapiro, H., Stergiopoulos, I., Torriani, S.F.F., Tu, H., de Vries, R.P., Waalwijk, C., Ware, S.B., Wiebenga, A., Zwiers, L.-H., Oliver, R.P., Grigoriev, I. V., Kema, G.H.J., 2011. Finished Genome of the Fungal Wheat Pathogen *Mycosphaerella graminicola* Reveals Dispensome Structure, Chromosome Plasticity, and Stealth Pathogenesis. PLoS Genet 7, e1002070. https://doi.org/10.1371/journal.pgen.1002070

Guarnaccia, V., Gehrmann, T., Silva-Junior, G.J., Fourie, P.H., Haridas, S., Vu, D., Spatafora, J., Martin, F.M., Robert, V., Grigoriev, I. V., Groenewald, J.Z., Crous, P.W., 2019. *Phyllosticta citricarpa* and sister species of global importance to *Citrus*. Mol Plant Pathol 20, 1619–1635. https://doi.org/10.1111/mpp.12861

Hane, J.K., Lowe, R.G.T., Solomon, P.S., Tan, K.-C., Schoch, C.L., Spatafora, J.W., Crous, P.W., Kodira, C., Birren, B.W., Galagan, J.E., Torriani, S.F.F., McDonald, B.A., Oliver, R.P., 2007. Dothideomycete–Plant Interactions Illuminated by Genome Sequencing and EST Analysis of the Wheat Pathogen *Stagonospora nodorum*. Plant Cell 19, 3347–3368. https://doi.org/10.1105/tpc.107.052829

Haridas, S., Albert, R., Binder, M., Bloem, J., LaButti, K., Salamov, A., Andreopoulos, B., Baker, S.E., Barry, K., Bills, G., Bluhm, B.H., Cannon, C., Castanera, R., Culley, D.E., Daum, C., Ezra, D., González, J.B., Henrissat, B., Kuo, A., Liang, C., Lipzen, A., Lutzoni, F., Magnuson, J., Mondo, S.J., Nolan, M., Ohm, R.A., Pangilinan, J., Park, H.-J., Ramírez, L., Alfaro, M., Sun, H., Tritt, A., Yoshinaga, Y., Zwiers, L.-H., Turgeon, B.G., Goodwin, S.B., Spatafora, J.W., Crous, P.W., Grigoriev, I.V., 2020. 101 Dothideomycetes genomes: A test case for predicting lifestyles and emergence of pathogens. Stud Mycol 96, 141–153. https://doi.org/10.1016/j.simyco.2020.01.003

Islam, M.S., Haque, M.S., Islam, M.M., Emdad, E.M., Halim, A., Hossen, Q.M.M., Hossain, M.Z., Ahmed, B., Rahim, S., Rahman, M.S., Alam, M.M., Hou, S., Wan,

X., Saito, J.A., Alam, M., 2012. Tools to kill: Genome of one of the most destructive plant pathogenic fungi *Macrophomina phaseolina*. BMC Genomics 13, 493. https://doi.org/10.1186/1471-2164-13-493

Knapp, D.G., Németh, J.B., Barry, K., Hainaut, M., Henrissat, B., Johnson, J., Kuo, A., Lim, J.H.P., Lipzen, A., Nolan, M., Ohm, R.A., Tamás, L., Grigoriev, I. V., Spatafora, J.W., Nagy, L.G., Kovács, G.M., 2018. Comparative genomics provides insights into the lifestyle and reveals functional heterogeneity of dark septate endophytic fungi. Sci Rep 8, 6321. https://doi.org/10.1038/s41598-018-24686-4

Li, B., Yang, Y., Cai, J., Liu, X., Shi, T., Li, C., Chen, Y., Xu, P., Huang, G., 2021. Genomic Characteristics and Comparative Genomics Analysis of Two Chinese *Corynespora cassiicola* Strains Causing Corynespora Leaf Fall (CLF) Disease. Journal of Fungi 7, 485. https://doi.org/10.3390/jof7060485

Looi, H.K., Toh, Y.F., Yew, S.M., Na, S.L., Tan, Y.C., Chong, P.-S., Khoo, J.-S., Yee, W.-Y., Ng, K.P., Kuan, C.S., 2017. Genomic insight into pathogenicity of dematiaceous fungus *Corynespora cassiicola*. PeerJ 5, e2841. https://doi.org/10.7717/peerj.2841

Lopez, D., Ribeiro, S., Label, P., Fumanal, B., Venisse, J.S., Kohler, A., de Oliveira, R.R., Labutti, K., Lipzen, A., Lail, K., Bauer, D., Ohm, R.A., Barry, K.W., Spatafora, J., Grigoriev, I. V., Martin, F.M., Pujade-Renaud, V., 2018. Genome-Wide Analysis of *Corynespora cassiicola* Leaf Fall Disease Putative Effectors. Front Microbiol 9, 276. https://doi.org/10.3389/fmicb.2018.00276

Manning, V.A., Pandelova, I., Dhillon, B., Wilhelm, L.J., Goodwin, S.B., Berlin, A.M., Figueroa, M., Freitag, M., Hane, J.K., Henrissat, B., Holman, W.H., Kodira, C.D., Martin, J., Oliver, R.P., Robbertse, B., Schackwitz, W., Schwartz, D.C., Spatafora, J.W., Turgeon, B.G., Yandava, C., Young, S., Zhou, S., Zeng, Q., Grigoriev, I. V, Ma, L.-J., Ciuffetti, L.M., 2013. Comparative Genomics of a Plant-Pathogenic Fungus, *Pyrenophora tritici-repentis*, Reveals Transduplication and the Impact of Repeat Elements on Pathogenicity and Population Divergence. G3 Genes|Genomes|Genetics 3, 41–63. https://doi.org/10.1534/g3.112.004044

Marsberg, A., Kemler, M., Jami, F., Nagel, J.H., Postma-Smidt, A., Naidoo, S., Wingfield, M.J., Crous, P.W., Spatafora, J.W., Hesse, C.N., Robbertse, B., Slippers, B., 2017. *Botryosphaeria dothidea*: a latent pathogen of global importance to woody plant health. Mol Plant Pathol 18, 477–488. https://doi.org/10.1111/mpp.12495

Mondo, S.J., Dannebaum, R.O., Kuo, R.C., Louie, K.B., Bewick, A.J., LaButti, K., Haridas, S., Kuo, A., Salamov, A., Ahrendt, S.R., Lau, R., Bowen, B.P., Lipzen, A., Sullivan, W., Andreopoulos, B.B., Clum, A., Lindquist, E., Daum, C., Northen, T.R., Kunde-Ramamoorthy, G., Schmitz, R.J., Gryganskyi, A., Culley, D., Magnuson, J., James, T.Y., O'Malley, M.A., Stajich, J.E., Spatafora, J.W., Visel, A., Grigoriev, I. V, 2017. Widespread adenine N6-methylation of active genes in fungi. Nat Genet 49, 964–968. https://doi.org/10.1038/ng.3859

Morales-Cruz, A., Amrine, K.C.H., Blanco-Ulate, B., Lawrence, D.P., Travadon, R., Rolshausen, P.E., Baumgartner, K., Cantu, D., 2015. Distinctive expansion of gene families associated with plant cell wall degradation, secondary metabolism,

and nutrient uptake in the genomes of grapevine trunk pathogens. BMC Genomics 16, 469. https://doi.org/10.1186/s12864-015-1624-z

Mosier, A.C., Miller, C.S., Frischkorn, K.R., Ohm, R.A., Li, Z., LaButti, K., Lapidus, A., Lipzen, A., Chen, C., Johnson, J., Lindquist, E.A., Pan, C., Hettich, R.L., Grigoriev, I. V., Singer, S.W., Banfield, J.F., 2016. Fungi Contribute Critical but Spatially Varying Roles in Nitrogen and Carbon Cycling in Acid Mine Drainage. Front Microbiol 7. https://doi.org/10.3389/fmicb.2016.00238

Ohm, R.A., Feau, N., Henrissat, B., Schoch, C.L., Horwitz, B.A., Barry, K.W., Condon, B.J., Copeland, A.C., Dhillon, B., Glaser, F., Hesse, C.N., Kosti, I., LaButti, K., Lindquist, E.A., Lucas, S., Salamov, A.A., Bradshaw, R.E., Ciuffetti, L., Hamelin, R.C., Kema, G.H.J., Lawrence, C., Scott, J.A., Spatafora, J.W., Turgeon, B.G., de Wit, P.J.G.M., Zhong, S., Goodwin, S.B., Grigoriev, I. V., 2012. Diverse Lifestyles and Strategies of Plant Pathogenesis Encoded in the Genomes of Eighteen Dothideomycetes Fungi. PLoS Pathog 8, e1003037. https://doi.org/10.1371/journal.ppat.1003037

Peter, M., Kohler, A., Ohm, R.A., Kuo, A., Krützmann, J., Morin, E., Arend, M., Barry, K.W., Binder, M., Choi, C., Clum, A., Copeland, A., Grisel, N., Haridas, S., Kipfer, T., LaButti, K., Lindquist, E., Lipzen, A., Maire, R., Meier, B., Mihaltcheva, S., Molinier, V., Murat, C., Pöggeler, S., Quandt, C.A., Sperisen, C., Tritt, A., Tisserant, E., Crous, P.W., Henrissat, B., Nehls, U., Egli, S., Spatafora, J.W., Grigoriev, I. V., Martin, F.M., 2016. Ectomycorrhizal ecology is imprinted in the genome of the dominant symbiotic fungus *Cenococcum geophilum*. Nat Commun 7, 12662. https://doi.org/10.1038/ncomms12662

Rouxel, T., Grandaubert, J., Hane, J.K., Hoede, C., Van De Wouw, A.P., Couloux, A., Dominguez, V., Anthouard, V., Bally, P., Bourras, S., Cozijnsen, A.J., Ciuffetti, L.M., Degrave, A., Dilmaghani, A., Duret, L., Fudal, I., Goodwin, S.B., Gout, L., Glaser, N., Linglin, J., Kema, G.H.J., Lapalu, N., Lawrence, C.B., May, K., Meyer, M., Ollivier, B., Poulain, J., Schoch, C.L., Simon, A., Spatafora, J.W., Stachowiak, A., Turgeon, B.G., Tyler, B.M., Vincent, D., Weissenbach, J., Amselem, J., Quesneville, H., Oliver, R.P., Wincker, P., Balesdent, M.H., Howlett, B.J., 2011. Effector diversification within compartments of the *Leptosphaeria maculans* genome affected by repeat-induced point mutations. Nat Commun 2. https://doi.org/10.1038/ncomms1189

Teixeira, M.M., Moreno, L.F., Stielow, B.J., Muszewska, A., Hainaut, M., Gonzaga, L., Abouelleil, A., Patané, J.S.L., Priest, M., Souza, R., Young, S., Ferreira, K.S., Zeng, Q., da Cunha, M.M.L., Gladki, A., Barker, B., Vicente, V.A., de Souza, E.M., Almeida, S., Henrissat, B., Vasconcelos, A.T.R., Deng, S., Voglmayr, H., Moussa, T.A.A., Gorbushina, A., Felipe, M.S.S., Cuomo, C.A., de Hoog, G.S., 2017. Exploring the genomic diversity of black yeasts and relatives (*Chaetothyriales*, *Ascomycota*). Stud Mycol 86, 1–28. https://doi.org/10.1016/j.simyco.2017.01.001

Verma, S., Gazara, R.K., Nizam, S., Parween, S., Chattopadhyay, D., Verma, P.K., 2016. Draft genome sequencing and secretome analysis of fungal phytopathogen *Ascochyta rabiei* provides insight into the necrotrophic effector repertoire. Sci Rep 6, 24638. https://doi.org/10.1038/srep24638

Xu, C., Xue, C., Hou, M., Geng, Y., Zang, R., Wu, H., Zhang, M., 2021. Nanopore/Illumina Hybrid Genome Sequence Resource for *Corynespora cassiicola* Strain XJ Infecting Rubber Tree in China. Plant Dis 105, 3727–3731. https://doi.org/10.1094/PDIS-03-21-0458-A

Zeiner, C.A., Purvine, S.O., Zink, E.M., Paša-Tolić, L., Chaput, D.L., Haridas, S., Wu, S., LaButti, K., Grigoriev, I. V., Henrissat, B., Santelli, C.M., Hansel, C.M., 2016. Comparative Analysis of Secretome Profiles of Manganese(II)-Oxidizing Ascomycete Fungi. PLoS One 11, e0157844. https://doi.org/10.1371/journal.pone.0157844

CHAPTER II

Genome-wide survey and molecular evolution of the Deuterolysin metalloprotease (M35) gene family in the Dothideomycetes class of fungi

Genome-wide survey and molecular evolution of the Deuterolysin metalloprotease (M35) gene family in the Dothideomycetes class of fungi

Vinicius Delgado da Rocha[a], Thaís Carolina da Silva Dal'Sasso[b], Maximiller Dal-Bianco Lamas Costa[a], Luiz Orlando de Oliveira[a]

[a]Departamento de Bioquímica e Biologia Molecular, Universidade Federal de Viçosa, Viçosa, Brazil.
[b]Departamento de Genética, Universidade de São Paulo/Escola Superior de Agricultura "Luiz de Queiroz", Piracicaba, Brazil

Corresponding author: :Luiz Orlando de Oliveira
Email: luiz.ufv@hotmail.com

Abstract

Deuterolysin metalloproteases (M35s) are a gene family of proteolytic enzymes depending on a metal ion zinc for their catalysis. M35s have been identified as virulence factors in bacteria and fungi. Plant pathogenetic fungi can secrete M35s to induce cell death and inhibit plant chitinases, thus preventing the degradation of fungal cell walls and avoiding the release of chitin oligomers capable of inducing plant immune responses. We explored the evolutionary history of M35s in the Dothideomycetes class of fungi using genome data from 79 Dothideomycetes species (15 orders) and 61 isolates of *Corynespora cassiicola*. Phylogenetic analyses and gene genealogies were used to investigate the evolutionary patterns of M35s. The gene expression profiles of M35s were also evaluated in *C. cassiicola* during the infection of soybean leaves. Among the Dothideomycetes, we predicted a total of 146 M35 genes (107 putative effector M35s and 39 putative non-effector M35s). The M35 family size varied largely, ranging from zero to seven members per genome. The plant pathogenic fungi (*Botryosphaeria dothidea* and *Diplodia seriata*) displayed the highest number of M35 genes. Mostly, *C. cassiicola* isolates contained three M35 genes per genome. The M35 family in *C. cassiicola* consists of four sub-clades. Exhibiting a high number of members, sub-clades (Cc_M35_1.1 and Cc_M35_2.1) likely evolved under duplications and sequent gene retentions. Meanwhile, the sub-clades (Cc_M35_1.2 and Cc_M35_2.2) contained a low number of members among *C. cassiicola* isolates and likely experienced gene loss events. Putative effector M35s within the sub-clade Cc_M35_2.2 was observed exclusively in *C. cassiicola* isolates obtained from cotton, suggesting that these putative effectors may play a specific role in the *C. cassiicola*-cotton interaction. Although all three M35 genes were expressed throughout the soybean infection, the gene CC_29_g9669 (Cc_M35_1.1) exhibited the highest expression level at eight days post-inoculation when compared to the other two genes.

Keywords: *Corynespora*, effectors, genomics, molecular phylogeny, pathogenicity, soybean

1. INTRODUCTION

Deuterolysin metalloproteases (M35s) are zinc-dependent proteolytic enzymes and belong to the M35 family according to the current classification of peptidase as described in the MEROPS database (Rawlings et al., 2018). The first characterized enzyme within the M35 family was deuterolysin (EC:3.4.24.39) also known as Neutral proteinase II from *Aspergillus oryzae* (Nakadai et al., 1973; Tatsumi et al., 1991). The deuterolysin structure consisted of a putative signal peptide preceding an N-terminal extension (pro region) and a mature region (Tatsumi et al., 1991). The pro region contains a full-length of 175 amino acid residues and is cleaved to form a mature protein, which has 177 amino acid residues and a molecular mass of about 19 kDa (Tatsumi et al., 1991). Specifically, deuterolysin exhibits high proteolytic on nuclear proteins that are rich in basic amino acids, such as histones and protamines (Sekine, 1973), but the functional role of deuterolysin is not yet known.

Although the catalytic mechanisms of M35s are still unclear, a divalent zinc metal ion (Zn^{2+}) is essential for their catalytic activity. Within the active site of M35s, three conserved amino acid residues (two histidines and one acid aspartic) are bounded to the ion zinc (Rawlings et al., 2018). Structurally, M35s exhibit a conserved Peptidase_M35 domain (PF02102; IPR001384), including two typical amino acid motifs: HEXXH and GTXDXXYG (Rawlings et al., 2018). The first motif harbors two zinc-binding histidine (H) residues and catalytic glutamate residue (E), while the second motif contains a third zinc-binding acid aspartic (D) residue (Hori et al., 2001; Rawlings et al., 2018). Notably, the crystallographic structure of members of the M35 family, such as deuterolysin from *Aspergillus oryzae* (McAuley et al., 2011) and *Gf*MEP from the edible mushroom *Grifola frondolosa* (Hori et al., 2001), exhibit four conserved beta strands, but the number of alpha helices varies. Specifically, deuterolysin from *Aspergillus oryzae* has eight alpha helices, while *Gf*MEP from *Grifola frondolosa* exhibits six alpha helices.

Notably, M35s are found in fungi (Li and Zhang et al., 2014) and bacteria (Arnadottir et al., 2009). It is believed that M35s play functional roles in pathogenicity in both bacteria and fungi. For example, *Aeromonas salmonicida* subsp. *Achromogenes*, a fish-pathogenic bacterium, secretes an M35 protein (AsaP1) that is highly cytotoxic to fish (Arnadottir et al., 2009), but the mechanism of toxicity of AsaP1 is unknown yet. Molecular analyses showed that a mutant strain of

Aeromonas salmonicida subsp. *Achromogenes* lacking the M35 gene that encoded for AsaP1 exhibited reduced virulence compared to the wild-type strain (Arnadottir et al., 2009). In the plant-pathogenic fungus *Verticillium dahliae*, two genes (VdM35-1 and VdASPF2) encode for M35 proteins that trigger plant immune mechanisms, such as hypersensitive response associated with cell death (Lv et al., 2022). In addition, the knockout of each of these two genes from *Verticillium dahliae* caused a reduction in virulence, production of spores, and mycelial growth (Lv et al., 2022). Interestingly, the genome of the entomopathogenic fungus *Metarhizium robertsii* displays seven M35 genes, but only a single gene, MrM35-4, plays a crucial role in fungal virulence (Huang et al., 2020). Bioassays showed that deletion of the gene MrM35-4 from *Metarhizium robertsii* resulted in a decreased ability for penetration into insect cuticles (Huang et al., 2020). Furthermore, the gene MrM35-4 from *Metarhizium robertsii* encodes an M35 protein that induces host cell apoptosis and suppresses the insect immune system through cleavage of prophenoloxidase enzymes (PPO1 and PPO2) (Huang et al., 2020). Curiously, M35s may also play important roles in mycoparasitic fungi during interactions with their host or prey. For example, in the mycoparasite fungus *Trichoderma guizhouense*, the disruption of an M35 gene (NMP1) led to a loss of ability to inhibit the *in vitro* growth of plant-pathogenic fungi, such as *Atheria rolfsii*, *Fusarium oxysporum*, and *Sclerotinia sclerotiorum* (Zhang et al., 2016)

A body of evidence suggests that M35s act as crucial virulence factors during plant-pathogen interaction, specifically in the suppression of plant chitinases that may degrade fungal cell walls through hydrolysis of chitin (Pan et al., 2020; Zhang et al., 2021). For example, the necrotrophic fungi *Fusarium oxysporum* f. sp. *cubense* secretes an M35 virulence effector (FocM35_1) that inhibits *in vitro* the activity of banana chitinases and it also interacts specifically with the MaChiA chitinase (Zhang et al., 2021). Moreover, transient expression assays showed that FocM35_1 is secreted into the apoplast and triggers cell death in *Nicotiana benthamiana* leaves (Zhang et al., 2021). Another M35 protein, RcMEP2 from the polyphagous fungus *Rhizoctonia cerealis* induces cell death and inhibits the expression of host chitinases when infiltrated into wheat leaves (Pan et al., 2020). The inhibition of plant chitinases represents a fungal strategy to establish successful infections, preserving the integrity of their cell walls and preventing the release of chitin oligomers that trigger the host's immune responses (Sánchez-Vallet et al., 2015). Chitin oligomers are

recognized through pattern recognition receptors (PRRs) located on the surface of plant cells, leading to the activation of a defense line called chitin-triggered immunity (Zipfel, 2014). The chitin-triggered immunity initiates intracellular immune responses, such as specific activation of defense-related MAPK (mitogen-activated protein kinases) cascades and accumulation of reactive oxygen species (Kawasaki et al., 2017). In addition to M35, other metalloproteases also suppress plant chitinases, for example, M36 metalloproteases (fungalysins) that are capable of cleaving chitinases from both *Arabidopsis* (Naumann and Price, 2012) and *Zea mays* (Ökmen et al., 2018).

A previous study showed that the M35 gene family has experienced intense gene duplications and subsequent positive selection, particularly in two vertebrate-pathogenic fungi: *Coccidioides posadasii* and *Coccidioides immitis* (Li et al., 2012). Using genome sequences of 50 species from the Ascomycota phylum of fungi, another study revealed large variations in the number of M35 genes across species (ranging from zero to seven M35 genes per species) and detected that several gene duplication and loss events occurred in the M35 gene family intensively in vertebrate-pathogenic fungi within order Onygeneales belonging to class Eurotiomycetes (Li and Zhang et al., 2014), however, the biological function of M35s have not been elucidated in vertebrate-pathogenic fungi so far. The presence of M35 genes in fungi and their functional importance in pathogenicity have received our attention, raising intriguing questions regarding the evolution of M35s in these fungi. Understanding the evolutionary history of the M35 gene family may reveal how evolutionary forces contribute to the current distribution patterns of M35 genes and to their functional roles.

Recently, we have studied the interesting Dothideomycetes class of fungi, which encompasses a diverse array of plant-pathogenic species (Dal'Sasso et al., 2023, Rocha et al., 2023). The Dothideomycetes is a species-rich class within the phylum Ascomycota. It comprises over 19,000 species that are distributed across 23 orders (Wijayawardene et al., 2017; Haridas et al., 2020). Most Dothideomycetes species are globally distributed and exhibit a notable ability to occupy a broad range of trophic modes, such as pathogenic, endophytic, mycorrhizal, saprobic, and lichenized (Schoch et 2009; Haridas et al., 2020). The evolutionary history of class Dothideomycetes is complex. Likely, the saprophytic style is an ancestral trait in this class and there were four major ecological transitions from saprophytic style to plant-

pathogen during the evolutionary history of Dothideomycetes (Haridas et al. 2020). Within the class Dothideomycetes, three orders (Capnodiales, Botryosphaeriales, and Pleosporales) particularly contain a large number of plant-pathogenic species that cause serious diseases in agronomically important crops (Ohm et al., 2012). Notably, Pleosporales stands out as the largest order within Dothideomycetes, containing approximately 25% of all Dothideomycetes species (Kirk et al., 2008; Zhang et al., 2012).

One striking plant-pathogenic species within the order Pleosporales is *Corynespora cassiicola* (Corynesporascaceae), which has the ability to infect at least 400 distinct plant species, including commercial crops (Rondon and Lawrence, 2021). In addition, *C. cassiicola* infections have been documented in nematodes (Carris et al., 1986) and humans (Looi et al., 2017). Across the Americas, *C. cassiicola* has affected the production of several crops (soybean, cotton, and tomato), causing the 'target spot' disease that results in intense defoliation (MacKenzie et al., 2018; Sumabat et al., 2018; Rondon and Lawrence, 2021). Target spot symptoms are lesions on leaves with a yellowish-green halo (Rondon and Lawrence, 2021). *Corynespora cassiicola* also causes Corynespora Leaf Fall (CLF), a severe disease that induces necrotic lesions on the leaves of rubber trees (*Hevea brasiliensis*) in Asia and Africa (Déon et al., 2012). Previously, we have obtained genomic data from many *C. cassiicola* isolates (Dal'Sasso et al., 2022; Rocha et al., 2023) and have successfully completed the genome sequencing of *Corynespora smithii* isolate CBS 139925 (Dal'Sasso et al., unpublished), which is a species closely related to *C. cassiicola* (Voglmayr and Jaklitsch, 2017). These data may provide new insights into the evolution of fungal gene families, such as M35.

Herein**,** we investigated the evolutionary history of the M35 gene family in both Dothideomycetes and *C. cassiicola*. Firstly, we retrieved high-quality genomic data from 79 Dothideomycetes species and used an array of genomic tools to predict members of the M35 gene family among these species. Examining the occurrence of M35 genes across Dothideomycetes, we determined if the size of the M35 gene family could have experienced expansions or contractions over time. We also employed different software tools to classify the predicted M35s as putative effectors or putative non-effectors. Phylogenetic analyses were used to reveal relationships among M35s in Dothideomycetes and Pleosporales.

To explore the evolution of M35 specifically within *C. cassiicola*, we conducted phylogenetic analyses using M35 genes from 61 *C. cassiicola* isolates, including *C. smithii*. These analyses allow us to uncover if biased gene retention and loss have played a role in shaping the evolutionary patterns of the M35 gene family in *C. cassiicola*. We also examined the evolutionary relationship of M35 genes between *C. cassiicola* and *C. smithii*. Finally, we utilized gene expression analyses through RT-qPCR to investigate the expression patterns of M35 genes from *C. cassiicola* during the infection process of soybean leaves. Our study shed light on the evolutionary mechanisms that have driven the diversification of fungal M35s across Dothideomycetes.

2. MATERIAL AND METHODS

2.1 Data assembly and gene prediction

For a comprehensive phylogenetic investigation into the evolutionary history of the M35 gene family within the Dothideomycetes class of fungi, we obtained protein sequence data from 79 species, representing 15 orders, through the MycoCosm database (Grigoriev et al., 2013) (Supplementary Table S1). This protein dataset has been previously utilized in phylogenetic studies (Dal'Sasso et al., 2023; Rocha et al., 2023). As outgroup, we included protein sequences from two related species belonging to the Eurotiomycetes class of fungi, namely *Aspergillus nidulans* and *Aspergillus fumigatus*.

For a more focused investigation of within-species phylogeny, we analyzed a total of 61 isolates of *Corynespora cassiicola*, a globally distributed phytopathogenic fungus known to infect a wide range of plant hosts, including humans (Dal'Sasso et al., 2022). We retrieved genome sequences for 14 isolates from GenBank. Additionally, we utilized predicted coding-DNA sequences (CDSs) and protein sequences from a set of 44 isolates analyzed in a previous study (Dal'Sasso et al., 2022) (Supplementary Table S2). Furthermore, we included CDSs and protein data from three additional isolates of *C. cassiicola*: CC_08, CC_10, and CC_28 (Dal'Sasso et al., unpublished data). Finally, we incorporated CDSs and protein data from the closely related species *Corynespora smithii* isolate CBS 139925, for which genomic data is available (Dal'Sasso et al., unpublished data).

To predict genes in the genomic data obtained from GenBank, we utilized Augustus v3.2.2 (Stanke and Morgenstern, 2005) with a method described in a previous study (Dal'Sasso et al., 2022). The *C. cassiicola* isolate CCP was used as a pre-trained 'species model' for the "--species" parameter.

2.2 Protein annotation and secretome prediction

Both protein annotation and secretome prediction were carried out using a custom pipeline, as previously described (Dal'Sasso et al., 2022). The predicted proteins were annotated using two software tools: PfamScan with Pfam database v33.0 (Mistry et al., 2021), and InterProScan v5.30.69 (Jones et al., 2014). The InterProScan analysis included eight parameters, namely SMART-7.1,

SUPERFAMILY-1.75, ProDom-2006.1, CDD-3.16, TIGRFAM-15.0, Pfam v31.0, Coils-2.2.1, and Gene3D-4.2.0.

To be classified as a putative secreted protein, a sequence had to possess a signal peptide, as determined by SignalP v4.1 (Petersen et al., 2011), and it must not contain any transmembrane domains, as assessed by TMHMM v2.0c (Krogh et al., 2001). For each sequence identified as a potential secreted protein, its subcellular localization was predicted using TargetP v.1.1b (Emanuelsson et al., 2000).

2.3 Identification of M35s

To identify members of the M35 gene family, we performed local BLASTp searches (using a cutoff e-value of $1e^{-4}$) against the MEROPS database v12.4 (Rawlings et al., 2018) using fungal proteomes as queries.

Additionally, we utilized HMMER v3.3.2 (http://hmmer.org/) to predict M35 homologues (with an e-value < 0.001). We employed profile Hidden Markov Models (HMMs) for the Peptidase_M35 domain (PF02102) downloaded from Pfam database v33.0 (Mistry et al., 2021). A protein was considered a member of the M35 family when it exhibited two key characteristics: firstly, it was identified as part of the M35 family from MEROPS (MER0001394), and secondly, it possessed the Peptidase_M35 domain (PF02102) as identified by at least two out of three software tools (PfamScan, InterproScan, and HMMER).

Furthermore, each predicted M35 protein was classified as either a putative effector or a putative non-effector. To determine if an M35 protein was a putative effector, we established three criteria: (1) the presence of a signal peptide as predicted by SignalP software, (2) the absence of transmembrane domains as determined by TMHMM software, and (3) localization within the secretory pathway as predicted by TargetP software. An M35 protein was classified as a putative effector only if it satisfied all three criteria. Proteins that did not meet these criteria were classified as putative non-effector M35 proteins.

2.4 Datasets and alignments

We assembled a total of five distinct datasets containing M35 sequences. Firstly, dataset ‘A’ was specifically prepared for Dothideomycetes and consisted of 146 full-length protein sequences (1536 amino acid residues each) from 65 Dothideomycetes species (out of a total of 79 species) and two *Aspergillus* spp.

Subsequently, we created dataset ‘B’ exclusively for the order Pleosporales. Dataset B comprised 63 full-length protein sequences (830 amino acid residues) from a total of 31 species within this order. Furthermore, we assembled three additional datasets specifically for *Corynespora* species. Dataset ‘C’ (2602 base pairs) consisted of 165 coding DNA sequences (CDSs) obtained from 61 isolates of *C. cassiicola* and two CDSs from *C. smithii*. Dataset ‘D’ (165 CDSs; 2594 base pairs) and dataset ‘E' (165 protein sequences; 675 amino acids) were derived solely from the 61 isolates of *C. cassiicola*. Alignments for each dataset were generated using the L-INS-i algorithm implemented in MAFFT v7.453 (Katoh and Standley, 2013), with default parameters.

2.5 Phylogenetic reconstructions

We performed separate maximum likelihood (ML) analyses to elucidate the phylogenetic relationships among members of the M35 gene family across Dothideomycetes, Pleosporales, and isolates of *C. cassiicola*. Dataset A and dataset B were used to reconstruct the broad phylogenetic relationships of M35 genes across Dothideomycetes and Pleosporales, respectively. Dataset C enabled us to investigate the relationships among M35 genes within *C. cassiicola* and the closely-related species *C. smithii*.

To determine the best evolutionary models for each dataset, we employed ModelFinder 2 (Kalyaanamoorthy et al., 2017) implemented in IQ-TREE v1.6.12 (Nguyen et al., 2015). The Bayesian Information Criterion (BIC) was used to select the best-fit models for each dataset, resulting in the following models: LG+R6 (dataset A), LG+I+G4 (dataset B), and HKY+F+G4 (dataset C). Subsequently, ML phylogenies were estimated using IQ-TREE v1.6.12 (Nguyen et al., 2015) with the respective datasets and best-fit models. Each ML analysis consisted of ten independent runs and 1000 ultrafast bootstrap replicates, with a bootstrap convergence criterion of a minimum correlation coefficient of 0.99 (Hoang et al., 2018). A consensus tree was obtained for each analysis, and the phylogenetic trees were visualized using FigTree v1.2.4 (Rambaut, 2009).

2.6 Gene genealogies and nucleotide diversity analyses

Gene genealogies for the M35-encoding genes (CDSs) recovered from the genomes of *C. cassiicola* were inferred using Network v.5.0.03 (Fluxus Technology Ltd) with the median-joining network method (Bandelt et al., 1999) and default

parameters. Indels were not considered as a source of information during these analyses. To investigate the genealogical relationships among the M35s, we utilized the full dataset D. Subsequently, dataset D was divided into sub-datasets based on the haplogroups identified in the previous analysis, and genealogical relationships within each haplogroup were inferred separately.

For each haplogroup, DNAsp v6 (Rozas et al., 2017) was used to estimate several measures of nucleotide diversity, including the number of segregating sites (S), the number of haplotypes (H), haplotype diversity (Hd), nucleotide diversity (π), and the average number of nucleotide differences (K).

2.7 Identification of conserved motifs

To identify conserved motifs in the M35 proteins of *C. cassiicola*, we utilized dataset E. Motif prediction was performed using the GLAM2 and GLAMSCAN2 tools available in MEME suite v5.0.5 (Bailey et al., 2009) with default parameters. Firstly, GLAM2 analyzed the set of M35 proteins and generated a set of motifs. Subsequently, GLAMSCAN2 searched for matches to the motifs identified by GLAM2. For each match, a score was reported, allowing us to assess the significance of the match. Finally, we selected motifs with high scores as the conserved motifs of interest.

2.8 Gene expression analyses

In our study, we performed RT-qPCR analyses to investigate the expression profiles of M35 genes in *C. cassiicola* during interactions with the soybean cultivar BR/MG Conquista, which is known to be susceptible to the pathogen. We specifically used the *C. cassiicola* isolate CC_29, which was isolated from soybean leaves in Brazil (Dal'Sasso et al., 2021). The experimental design and methodology followed a previously described protocol (Dal'Sasso et al., 2022).

The soybean plants were cultivated in a greenhouse and inoculated at the V3 development stage. To perform the inoculations, a conidia solution was prepared from isolate CC_29 at a concentration of 3.5 x 10^4 conidia/mL, supplemented with 0.01% Tween 20. Four droplets, each containing 20 µL of the conidia solution, were spotted on the abaxial face of each leaflet from a leaf. Following the inoculation, the plants were maintained in the greenhouse. Leaf disks (1.4 cm^2) were collected from the inoculation spots at five time points: 0, 2, 4, 6, and 8 days post-inoculation (dpi).

Four biological replicates, corresponding to four individual plants, were used for each time point. As a control, we included plants that were inoculated with distilled autoclaved water containing 0.01% Tween 20.

For molecular work, each infected leaf disk was macerated using liquid nitrogen, and total RNA was extracted using TRIzol Reagent (Life Technologies) according to the manufacturer's instructions. The extracted RNA was then resuspended in 25 µL of distilled autoclaved water and stored at -80°C. RNA concentrations were quantified using a NanoDrop 2000 spectrophotometer (Thermo Fisher Scientific), and RNA integrity was verified using a 1.5% (w/v) agarose gel. Prior to cDNA synthesis, 4 µg of RNA was treated with DNase I Amp Grade (Invitrogen) to eliminate any genomic DNA contamination. The cDNA synthesis was performed using the M-MLV Reverse Transcriptase kit (Invitrogen) following the manufacturer's instructions, with a total of 4 µg of RNA used for each reaction.

In our study, the primers for each M35 gene of *C. cassiicola* isolate CC_29 were designed using the Primer3Plus software (https://www.primer3plus.com/). The specificity of each primer pair was confirmed through melt curve analysis. The primer sequences used in this study can be found in Supplementary Table S3.

The RT-qPCR assays were conducted on a 7500 Real-Time PCR System (Applied Biosystems). Each assay included one reaction for each of the four biological replicates and one reaction for the bulk RNA derived from the four replicates. The reaction mixture had a final volume of 10 µL, consisting of 5 µL of PowerUp SYBR Green Master Mix (Life Technologies), 2 µL of each primer (1.5 µM), and 1 µL of 2-fold diluted cDNA. The amplification conditions were as follows: an initial step at 50 °C for 2 minutes, followed by 95 °C for 10 minutes, and then 40 cycles of 94 °C for 15 seconds and 60 °C for 1 minute.

For data normalization, the expression of the endogenous β-tubulin gene was used as a control. The expression levels of each M35 gene were calculated using the $2^{-\Delta\Delta Ct}$ method (Livak and Schmittgen, 2001). Statistical differences in gene expression for each M35 were assessed using one-way ANOVA and Tukey's test. Both analyses were performed using version 4.2.2 of the R software (https://www.r-project.org/). To visualize the relative expression values, a heatmap was generated using the ggplot package in R.

3.1 RESULTS

3.2 The M35 gene family in the Dothideomycetes

The analysis of complete genomes from 79 Dothideomycetes species revealed a total of 139 predicted M35 genes, while the two genomes of *Aspergillus spp.* contained a total of seven genes (Supplementary Table S1). Each predicted M35 gene was found to possess a single Peptidase_M35 domain (PF02102). In the Dothideomycetes, all 139 M35 genes encoded proteins that contained three zinc-binding residues (304H, 308H, 319D) and a catalytic residue (304E) (Supplementary Table S4). These residues were also present in the majority of M35s (5 out of 7) identified in *Aspergillus* spp. However, two M35s of *Aspergillus* spp. lacked the zinc-binding residue 319D.

The size of the M35 gene family varied across the Dothideomycetes, with up to seven copies per genome in the studied species (Supplementary Figure S1 and Table S1). Notably, the largest M35 gene family was observed in two plant-pathogenic species within the order Botryosphaeriales: *Botryosphaeria dothidea* (with seven members) and *Diplodia seriata* (with six members). On the other hand, the M35 gene family was absent from the genomes of 14 species across six orders, including Capnodiales (six species), Botryosphaeriales (one), Dothidiales (one), Myriangiales (two), Mytilinidiales (one), and Pleosporales (three). Among the Pleosporales, the M35 gene family comprised three members in 12 species, including *C. cassiicola* (isolate CCP).

3.3 Predicted putative effector and putative non-effector M35s

Our in-silico analyses predicted a total of 107 M35s to be putative effector M35s (Supplementary Figure S1 and Table S1). The number of putative effector M35s varied among the studied species, with a maximum of four observed, except for *Diplodia seriata* (order Botryosphaeriales), which had five putative effectors. Within the Pleosporales, *C. cassiicola* (isolate CCP) and eight additional species contained three putative effector M35s.

The occurrence of putative non-effector M35s was relatively low, with a total of 39 putative non-effector M35s identified (Supplementary Figure S1 and Table S1). There were seven species from five different orders that harbored exclusively putative non-effector M35s: one species of Aulographales, one of Botryosphaeriales,

two of Histeriales, one of Micothyriales, and two of Pleosporales. Interestingly, many of the genes encoding putative non-effector M35s exhibited large indels at the 5'-end, resulting in the absence of a signal peptide for secretion.

3.4 Phylogenetic analyses of M35s

The ML phylogenetic tree was constructed to analyze the relationships among 139 M35 proteins from 65 Dothideomycetes species, along with seven M35 proteins from *Aspergillus ssp* (Supplementary Figure S2). The tree exhibited three major clades; however, these clades received low bootstrap support values (< 70). We attributed the low reliability of the clades to the high sequence divergence among the M35 proteins, which introduced a high noise-to-signal ratio in dataset A. To address this issue, we focused our phylogenetic analysis within the Pleosporales (dataset B), which is the most species-rich order within the Dothideomycetes represented in our study and includes the genus *Corynespora*.

Using 63 M35 proteins from 31 Pleosporales species, we reconstructed a second ML phylogenetic tree (Figure 1). This tree exhibited well-supported nodes, with bootstrap values > 90 for major nodes. It consisted of two major clades, referred to as clades M35_1 and M35_2, respectively. Clade M35_1 was the most populous, with 39 members (34 putative effector M35s and 5 putative non-effector M35s). Members of M35_1 were present in 30 out of the 31 Pleosporales species included in the study (Figure 1). Among these 30 species, 22 of which contained a single member of the M35 gene family within the clade M35_1, while remaining eight species had two members. In *C. cassiicola* isolate CCP, members of the clade M35_1 were named Cc_M35_1.1 and Cc_M35_1.2, respectively. Clade M35_2 consisted of 29 members (25 putative effector M35s and 4 putative non-effector M35s) from 22 Pleosporales species (Figure 1). The third M35 gene of *C. cassiicola* (isolate CCP), named Cc_M35_2.1, was placed within the M35_2 clade.

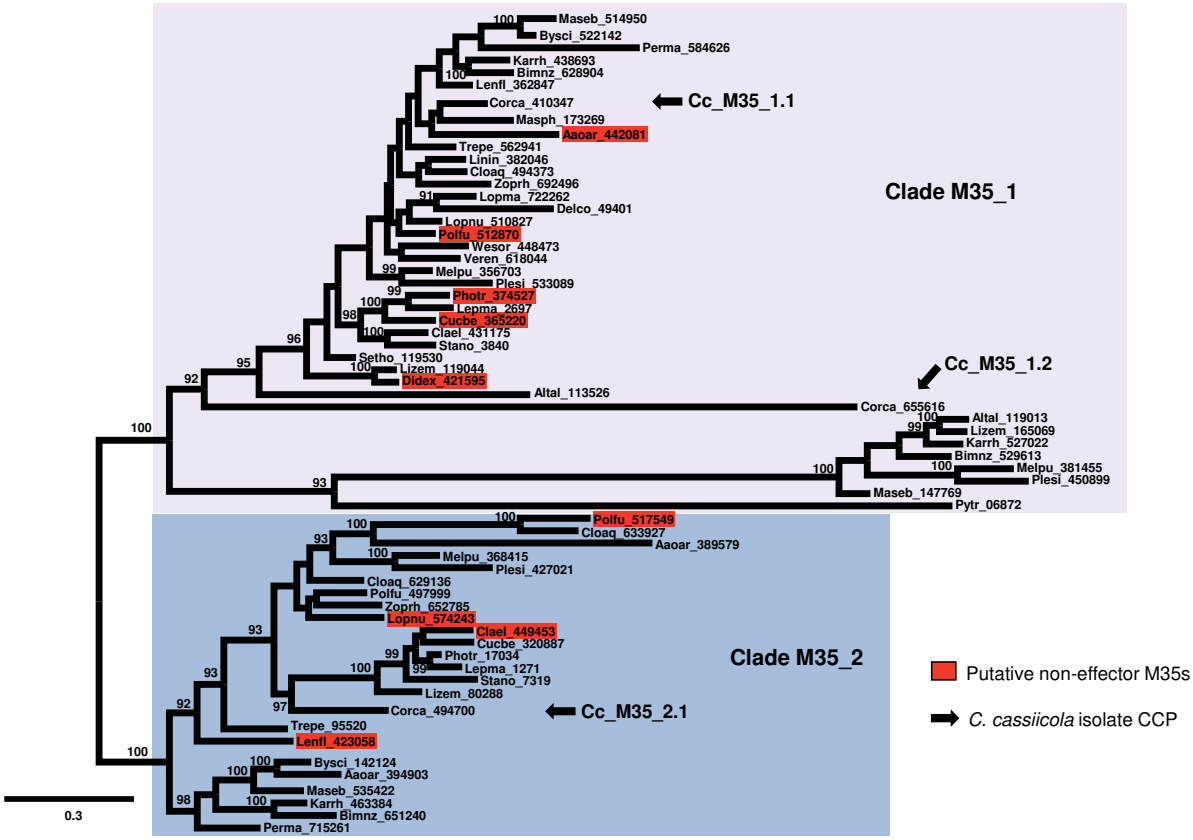

Figure 1. Maximum likelihood tree showing the two clades (M35_1 and M35_2) of the Deuterolysin Metalloprotease (M35) gene family across the Pleosporales. The unroot consensus tree was based on 63 protein sequences of members of the M35 gene family from 31 species of Pleosporales. Proteins contained 830 amino acids. Nodal support values are given as bootstrap values above the branches when > 80. Scale bar corresponds to the expected number of substitutions per site. Arrows indicate the three predicted M35 genes (Cc_M35_1.1, Cc_M35_1.2, and Cc_M35_2.1) identified in the genome of *Corynespora cassiicola* isolate CCP. Proteins were predicted to be putative effector M35s; red highlights indicate putative non-effector M35s.

3.5 The M35 gene family in *Corynespora*

Our analysis recovered a total of 165 M35 genes across 61 isolates of *C. cassiicola* (Supplementary Table S2). The number of M35 genes within each genome ranged from 1 to 4, with the majority of isolates (42 out of 61) harboring three M35 genes. Notably, isolate CC_28 stood out with four members in its M35 gene repertoire. Among the 165 M35 genes, 119 were identified as putative effectors, while 46 were classified as putative non-effectors. In addition, the genome of the closely-related congener *C. simithii* contained two M35 genes, one of which was classified as a putative effector, while the other as a putative non-effector.

The ML phylogenetic tree was constructed using the CDS sequences of the 165 M35 genes from *C. cassiicola*, along with two genes from *C. smithii*, resulting in a total of 167 sequences (Figure 2A). The ML tree exhibited two major clades, each with a bootstrap support value of 100. Interestingly, each clade contained an M35 gene from the closely-related species *C. smithii*, which showed a sister relationship to the M35 genes from *C. cassiicola*. Within each clade, the M35 genes from *C. cassiicola* formed distinct sub-clades. These sub-clades were named Cc_M35_1.1, Cc_M35_1.2, Cc_M35_2.1, and Cc_M35_2.2, representing the four clusters of M35 genes (Figure 2A).

The sub-clade Cc_M35_1.1 represented the most gene-rich cluster among the M35 gene sub-clades. It included a gene from each of the 61 *C. cassiicola* isolates used in this study (Figure 2B). Its sister sub-clade, Cc_M35_1.2, was comparatively smaller, comprising only 38 members (Figure 2C). Notably, all members of both Cc_M35_1.1 and Cc_M35_1.2 sub-clades were found to encode putative effector M35 genes exclusively.

In contrast, the more phylogenetically distant sub-clade Cc_M35_2.1 exhibited a high gene count, with 60 members. This sub-clade consisted of 15 putative effector M35 genes and 45 putative non-effector M35 genes (Figure 2D). Within Cc_M35_2.1, several second-order sub-clades contained solely putative non-effectors. Members of each of these second-order sub-clades were found in isolates sampled from a wide variety of hosts in different countries. One such second-order sub-clade comprised 23 members that possessed a premature stop codon located 189 base pairs upstream of the initiation codon. Interestingly, these 23 genes were found in fungal isolates obtained from diverse hosts (cotton, cucumber, soybean, and rubber tree) across the Americas (USA and Brazil), Africa (Côte d'Ivoire and Gabon), and Asia (China, India, Malaysia, and Sri Lanka).

The smallest sub-clade, Cc_M35_2.2, consisted of only six members (Figure 2E). Five of these members were putative effector M35 genes obtained from fungal isolates collected from cotton plants in the USA, while the sixth member was a putative non-effector M35 gene from isolate CC_28, which was obtained from coleus (*Plectranthus barbatus*) in Brazil.

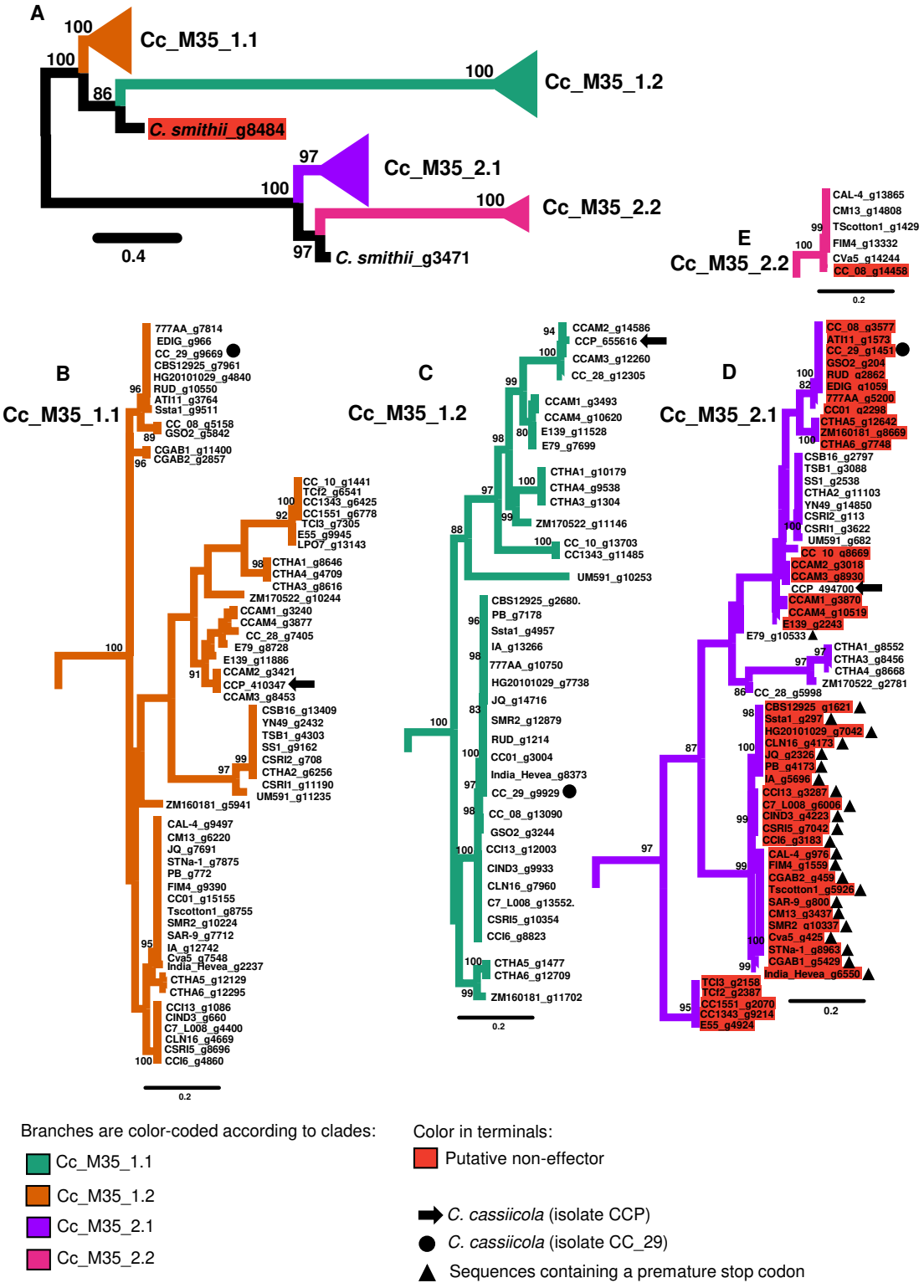

Figure 2. Phylograms of the maximum likelihood tree of Deuterolysin Metalloprotease (M35) gene family across the 61 isolates of *Corynespora cassiicola* and *Corynespora smithii* isolate CBS 139925. The analysis was based on 165 coding DNA sequences (each of which contained 2602 base pairs long) of members of the M35 gene family from 62 isolates. **A**. Overview of the full unrooted consensus tree, with four major sub-clades collapsed into triangles. **B-F**. Expanded views show the composition of each major sub-clade. **B**. Cc_M35_1.1 (orange). **C**. Cc_M35_1.2 (green). **D**. Cc_M35_2.1 (purple). **E**. Cc_M35_2.2 (pink). Nodal support values are given as bootstrap values above the branches, when > 80. Branch lengths are drawn to scale. Scale bar corresponds to the expected number of substitutions per site. Red terminals indicate putative non-effectors M35. Placements of predicted M35 family members of isolates CCP and CC_29 are as indicated.

3.6 Haplogroup diversity of M35 genes in *Corynespora*

Among the 165 M35-encoding genes recovered from the genomes of 61 *C. cassiicola* isolates, a total of 56 haplotypes were identified, forming four distinct haplogroups (Figure 3A). The haplogroup distribution closely mirrored the sub-clades identified in the previous phylogenetic analysis (Figure 2), with each haplogroup corresponding to one of the sub-clades. The haplogroups were named after their respective sub-clades: Cc_M35_1.1, Cc_M35_1.2, Cc_M35_2.1, and Cc_M35_2.2.

In the network representation, two haplogroups, Cc_M35_1.1 and Cc_M35_2.2, occupied opposite ends of the network (Figure 3A). On the other hand, the haplogroups Cc_M35_1.2 and Cc_M35_2.1 were positioned centrally within the network. The connection between the tip haplogroup Cc_M35_1.1 and the neighboring central haplogroup Cc_M35_1.2 required the largest number of mutational steps, totaling 401 steps. In contrast, the smallest number of mutational steps (331) was observed between the central haplogroup Cc_M35_2.1 and the adjacent tip haplogroup Cc_M35_2.2.

Partial networks were constructed to analyze the gene genealogies within each of the four haplogroups, providing further insights into their internal structure (Figure 3B-E). The tip haplogroup Cc_M35_1.1 was the most diverse, consisting of 20 haplotypes (Figure 3B), while the tip haplogroup Cc_M35_2.2 had only two haplotypes (Figure 3E). Within the haplogroup Cc_M35_1.2, the haplotypes displayed high levels of divergence, with mutational distances reaching up to 36 steps (Figure 3C). Notably, haplotypes containing putative effector M35 genes were predominantly found within the haplogroups Cc_M35_1.1 and Cc_M35_1.2, whereas haplotypes harboring putative non-effector M35 genes were located within the haplogroups Cc_M35_2.1 (haplotypes 9-19) and Cc_M35_2.2 (haplotype 2). The placement of haplotypes within the overall network topology did not show a clear association with host species or geographic origin of the fungal isolates (data not shown).

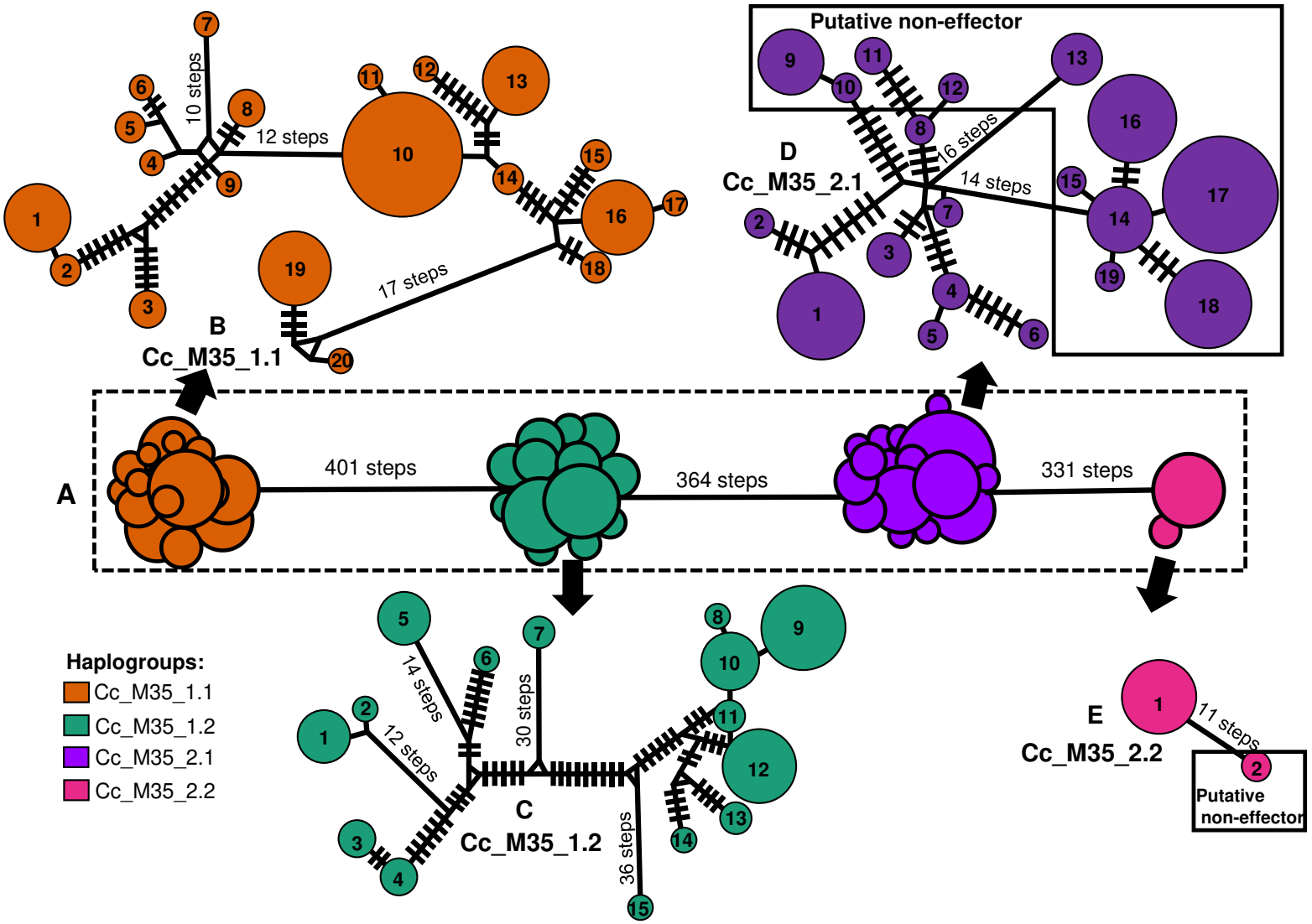

Figure 3. Genealogical relationships of the four haplogroups of the Deuterolysin Metalloprotease (M35)-encoding genes (CDS) of *Corynespora cassiicola*. **A**. The central box depicts the full median-joining network. **B-F**. Expanded views show the composition of each haplogroup. The four haplogroups are color-coded according to the predicted M35 encoding-genes: **B**. Cc_M35_1.1 (orange). **C**. Cc_M35_1.2 (green). **D**. Cc_M35_2.1 (purple). **E**. Cc_M35_2.2 (pink). A circle represents a given haplotype (coded with a number); circle size is proportional to the relative frequencies. Numbers of mutational steps are indicated with bars when more than one (unless indicated otherwise).

The analysis of molecular diversity revealed distinct levels of polymorphism among the four haplogroups (Table 1). The haplogroup Cc_M35_1.2 exhibited the highest nucleotide diversity (π = 0.03048) and average number of nucleotide differences (K ~ 16). In contrast, the haplogroup Cc_M35_2.2 displayed lower diversity, with a nucleotide diversity of π = 0.00349 and average number of nucleotide differences (K ~ 3).

Table1. Segregating sites (S), Number of haplotypes (H), haplotype diversity (Hd), Nucleotide diversity (π), and average number of nucleotide differences (K) for four metalloproteases 35 (M35) haplogroups in *Corynespora cassiicola*.

Haplogroups	**S**	**H**	**Hd**	**π**	**K**
Cc_M35_1.1	73	20	0.921	0.01528	16.18
Cc_M35_1.2	134	15	0.925	0.03048	26.64
Cc_M35_2.1	68	19	0.923	0.01415	14.86
Cc_M35_2.2	11	2	0.333	0.00349	3.66

3.7 Structural features of M35 proteins in *Corynespora*

A detailed diagram in Figure 4A illustrates the protein structure of the putative effector M35 proteins in *C. cassiicola*. On average, the full-length of the putative effector M35s was 380 amino acid residues, ranging from 349 (Cc_M35_2.2) to 420 (Cc_M35_1.2) amino acid residues. The SignalP software predicted the presence of a signal peptide in these proteins, with signal peptide lengths ranging from 18 (Cc_M35_1.1, Cc_M35_1.2, and Cc_M35_2.1) to 21 (Cc_M35_2.2) amino acid residues.

Among the putative effector M35s, HMMER analyses identified a single Peptidase_M35 domain, which varied in size from 344 (Cc_M35_1.1) to 316 (Cc_M35_2.1) amino acid residues. Towards the C-terminal region of the Peptidase_M35 domain, a conserved motif was identified (Figure 4B). This motif encompassed 50 amino acid residues and included three zinc-binding residues (30H, 34H, and 45D) as well as a catalytic residue (31E).

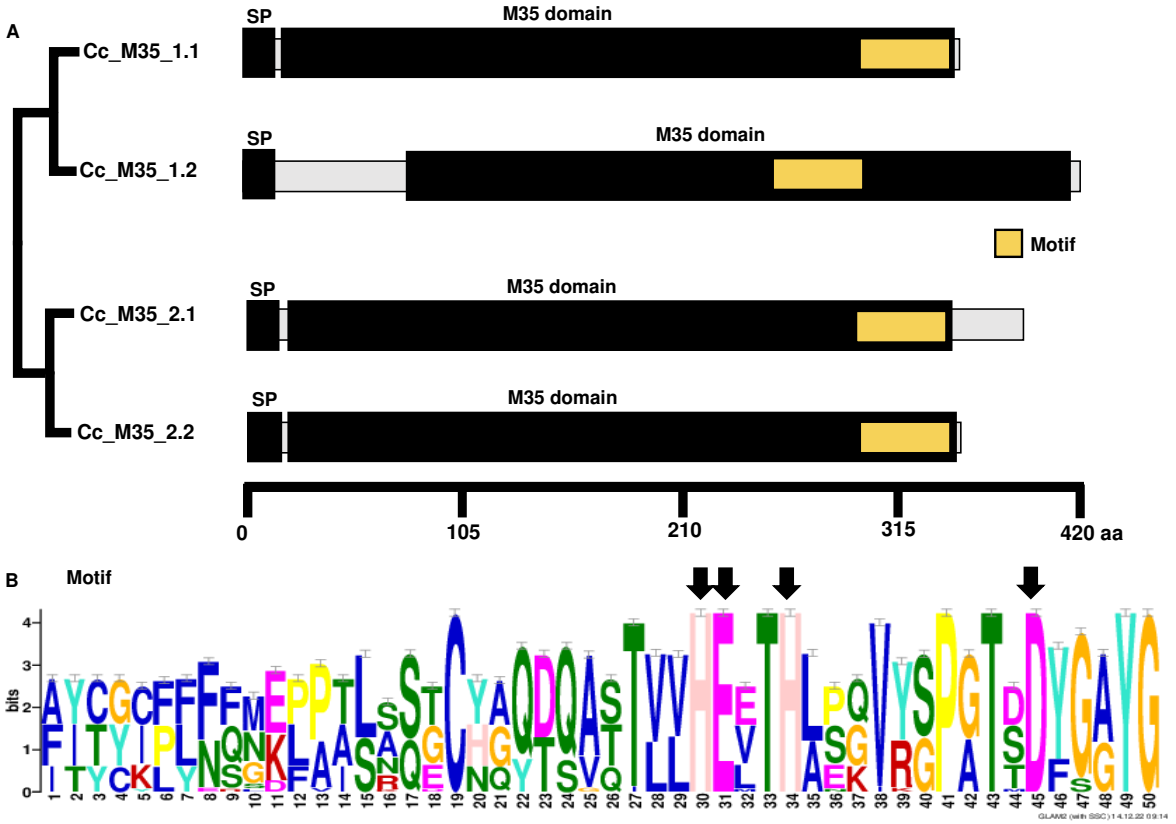

Figure 4. Structural overview of the Deuterolysin Metalloprotease (M35) family members of *Corynespora cassiicola*. **A**. Schematic diagram depicts the average length of the putative effector M35s, the signal peptide (SP), and the predicted locations for the Peptidase_M35 domain (PF01095) and its structural motif. Protein lengths were drawn to scale. Scale bar indicates the number of amino acid residues. Schematic view of the phylogenetic tree according to Figure 2. **B**. Consensus pattern for predicted M35 motif. Arrows indicate amino acid residues involved in the active site.

3.8 Expression patterns of M35 genes in *Corynespora*

We performed RT-qPCR assays to analyze the temporal expression patterns of the three M35 genes in *C. cassiicola* isolate CC_29 during its interaction with susceptible soybean plants. All three M35 genes showed expression during the infection process, but their expression levels varied (Figure 5 and Supplementary S3). Notably, gene CC_29_g9669, which belongs to the Cc_M35_1.1 haplogroup/sub-clade, exhibited the highest relative expression levels among the M35 family members. The expression of CC_29_g9669 (Cc_M35_1.1) progressively increased from 2 dpi (days post-infection) and reached its peak at 8 dpi. In contrast, the other two genes, CC_29_g9929 (Cc_M35_1.2) and CC_29_g1451

(Cc_M35_2.1), displayed low relative expression levels throughout the infection process (0-8 dpi), with a slight increase observed at 8 dpi.

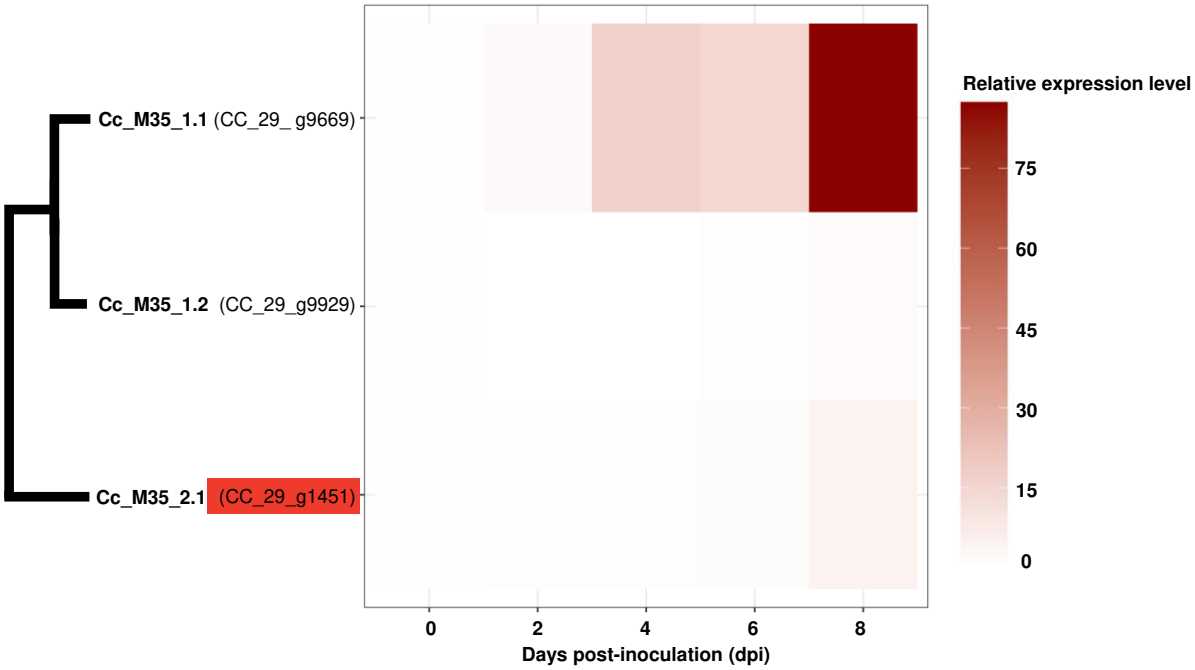

Figure 5. Heatmap showing the relative expression level of the three Deuterolysin Metalloprotease (M35) genes of *Corynespora cassiicola* after spore inoculation on soybean leaves. The relative expression level was calculated using the $2^{-\Delta\Delta Ct}$ method. The constitutive β-tubulin gene of *C. cassiicola* was used as an endogenous control. The x-axis shows the five-time points of the expression analyses: 0, 2, 4, 6, and 8 days post-inoculation (dpi). The y-axis shows the three M35 genes: Cc_M35_1.1 (CC_29_g9669). **C**. Cc_M35_1.2 (CC_29_9929). **D**. Cc_M35_2.1 (CC_29_g1451). Schematic view of the phylogenetic tree according to Figure 2. Color in terminal: red highlights indicate a putative non-effector M35. Color intensity corresponds to relative expression level. Heatmap was generated according to the results shown in Supplementary Figure S3.

4. DISCUSSION

4.1 Insights on the evolution of the M35 gene family

The size of the gene families undergoes variations over time (Demuth et al., 2006). Both gene duplication and loss events contribute to variations in the gene family size; gene duplications led to the expansion of gene family size, while gene losses result in contractions (Demuth and Hahn, 2009). Notably, the number of members of the M35 family varied substantially among Dothideomycetes species (Supplementary Figure S1). For example, *Septoria musiva* contained a single M35 gene while *Botryosphaeria dothidea* harbored seven M35 genes. This variation can be attributed to the occurrence of gene duplications and losses, which likely shaped the evolutionary dynamic of the M35 gene family over time. Indeed, gene duplication and loss events have been recognized as major driving forces in the evolution of the M35 gene family in certain fungal lineages, such as the order Onygeneales within the class Eurotiomycetes (Li and Zhang, 2014).

Interestingly, the lineage-specific expansion of the M35 gene family may have occurred within the order Botryosphaeriales, specifically in two plant-pathogenic species (*Botryosphaeria dothidea* and *Diplodia seriata*) that exhibited the largest repertoire of M35 gene. One most likely speculation is that the redundancy of M35 genes in these species may confer some adaptive advantage to manipulate the defense host and contribute to the infection. Previous findings reported that fungal M35s may interact with the plant immune system, leading to cell death and inhibition of host chitinases (Pan et al., 2020; Zhang et al., 2021; Lv et al., 2022). Curiously, Botryosphaeriales species also showed a high gene abundance in the other gene families associated with pathogenicity, such as Necrosis- and Ethylene-inducing peptide 1-like protein (NLP) superfamily (Dal'Sasso et al., 2023) and Pectin methylesterase (PME) gene family (Rocha et al., 2023).

4.2 The occurrence of putative effector M35s

The ubiquitous presence of putative effector M35 genes across the Dothideomycetes species suggests that these genes were retained within their genomes over time. The retention of putative effector M35 genes is an indicative that they may play a crucial role for fungal virulence in Dothideomycetes. Experimentally, functional analysis has demonstrated that the M35 protein (FocM35_1) from

Fusarium oxysporum f. sp. *cubense* acts as an effector to induce cell death and suppress the activity of host chitinases (Zhang et al., 2021). These chitinases degrade the chitin-rich cell wall of fungi, releasing chitin fragments that are subsequently recognized by plant receptors, leading to a cascade of events that result in the activation of plant immune responses (Sánchez-Vallet et al., 2015; Kawasaki et al., 2017). Notably, putative effector M35s we uncovered across Dothideomycetes exhibited specific features, such as an N-terminal signal peptide. Evidence from molecular assays shows that the signal peptide is essential to direct the secretion of M35s into plant apoplast (Pan et al., 2020; Zhang et al., 2021).

One of the main features that distinguished the putative non-effector M35s from the putative effector M35s was the absence of a signal peptide. The putative non-effector M35s lacked the signal peptide. Sequence modifications through the addition or deletion of nucleotides (indels) and sequent loss of peptide signal have been more likely causes for the origin of putative non-effector within the gene families in the Dothideomycetes (Dal'Sasso et al., 2023; Rocha et al., 2023). Our findings support that the occurrence of large indels at the region 5' of the putative non-effector M35 genes likely affected nucleotide sequences and caused the loss of the signal peptide in the putative non-effector M35s.

4.3 A comprehensive analysis of the M35 gene family in *Corynespora*

The size of the M35 gene family was relatively small in *C. cassiicola* (most of the isolates contained up to 3 M35 genes). This pattern is consistent with observations in other polyphagous plant-pathogenic fungi. For example, *Verticillium dahliae* has two M35 genes (Lv et al., 2022), and *Rhizoctonia cerealis* harbors four M35 genes (Pan et al., 2020) in their respective genomes. Given that M35s has identified as key virulence factors in bacteria (Arnadottir et al., 2009) and fungi during several studies (Huang et al., 2020; Pan et al., 2020; Zhang et al., 2021; Lv et al., 2022), we speculated that M35 may also contribute to pathogenicity in *C. cassiicola*.

In addition to infecting a broad host range, *C. cassiicola* stands out for its large and diverse putative effector repertoire (Lopez et al., 2018; Dal'Sasso et al., 2021). This effector repertoire is believed to be important for the adaptability and virulence of *C. cassiicola* as a polyphagous fungus (Lopez et al., 2018). Our results demonstrated that the rich effector repertoire of *C. cassiicola* likely includes members of the M35 gene family. Although putative effector M35s of *C. cassiicola* shared a

conserved Peptidase_M35 domain, they have experienced distinct diversification patterns and accumulated high levels of genetic diversity throughout their evolutionary history. The rapid evolution and accumulation of genetic variability have shaped the diversification of effector genes in plant pathogens belonging to Dothideomycetes class of fungi, such as *Leptosphaeria maculans* (Plissonneau et al., 2017) and *Zymoseptoria tritici* (Amezrou et al., 2023). Generally, effector genes undergo rapid evolution and subsequent strong selective pressure to escape from the host recognition and optimize their functions (Sánchez-Vallet et al., 2018).

Effectors are known to contribute to host specialization, they may acquire molecular adaptations to interact with a specific host species (Dong et al., 2014). Previous studies suggested that *C. cassiicola* isolates exhibited a certain degree of host specialization (Dixon et al., 2009; Sumabat et al., 2018). The host specialization in *C. cassiicola* may be associated with the presence of specialized effectors that are specifically recognized by a restricted range of compatible hosts (Lopez et al., 2018). Interestingly, within the subclade Cc_M35_2.2 (Figure 2E), the putative effector M35s were exclusively present in *C. cassiicola* isolates obtained from cotton. In addition to possessing the Peptidase_M35 domain, these putative effector M35s also displayed essential acid residues for their functional activity (Figure 4), suggesting that they are likely functional and may play a specific role in the interaction between *C. cassiicola* and cotton plants.

In contrast to the high abundance of putative effector M35s in *C. cassiicola*, the number of putative non-effector M35s was comparatively lower. Interestingly, the putative non-effector M35 genes of *C. cassiicola* were predominantly grouped into the second-order sub-clades in Cc_M35_2.1 (Figure 2D). This finding is a suggestive that these putative non-effectors shared a common evolutionary origin within each sub-clade. However, despite their common origin, putative non-effector M35s were found in isolates collected from diverse host species across several continents. The widespread occurrence of putative non-effector M35s may be due to agriculturally-mediated dispersal through recent global movements of infected material with *C. cassiicola* isolates carrying putative non-effector M35s.

The four sub-clades of the M35 gene family in *C. cassiicola* (Figure 2) have experienced distinct evolutionary patterns through biased gene retention and loss. The multiple biased gene retention and loss events have shaped the fate of paralogous genes in other gene families in the Dothideomycetes (Dal'Sasso et al.,

2023; Rocha et al., 2023). Through positive selection, functional paralogs that play advantageous role in the phenotype can be preferentially retained within the genome over time (Shiu et al., 2005). Meanwhile, nonfunctional paralogs that contain deleterious mutations undergo intense purifying selection and are purged from the genome (Lynch and Conery, 2000). Notably, the sub-clades Cc_M35_1.1 (Figure 2B) and Cc_M35_2.1(Figure 2D) likely underwent biased gene retention events. These events have contributed to preserve members of each sub-clade, Cc_M35_1.1 and Cc_M35_2.1, across most of *C. cassiicola* isolates. On the other hand, biased gene loss has shaped evolutionary patterns of the subclades Cc_M35_1.2 (Figure 2C) and Cc_M35_2.2 (Figure 2E). Gene loss events likely explain the low occurrence of M35 genes in the sub-clades Cc_M35_1.2 and Cc_M35_2.2 among *C. cassiicola* isolates.

4.4 Evolutionary relationships of M35 genes between *C. cassiicola* and *C. smithii*

Previous studies have postulated that *C. smithii* exhibits a close phylogenetic relationship to *C. cassiicola* (Shoch et al., 2009; Voglmayr and Jaklitsch, 2017). Our phylogenetic analysis in *C. cassiicola* (Figure 2A) suggested that each of the sub-clades, Cc_M35_1.2 and Cc_M35_2.2, exhibited a sister relationship to M35 genes from *C. smithii*. This indicates that each of these two sub-clades derived from an ancient gene duplication event that was shared with *C. smithii*. Notably, the sub-clades Cc_M35_1.1 and Cc_M35_2.1 lacked a sister relationship to M35 genes from *C. smithii*. Three possible scenarios could explain this result. First, our pipeline could fail to detect M35 genes from *C. smithii* that would be homologs to Cc_M35_1.1 and Cc_M35_2.1. However, this scenario is less likely because all four software tools we used (BlastP, PfamScan, InterproScan, and HMMER) yielded consistent results, and no additional M35 gene from *C. smithii* was identified apart from those two (Supplementary Table S2). The second scenario proposes that M35 genes from *C. smithii*, which shared homology to Cc_M35_1.1 and Cc_M35_2.1, were lost throughout the evolutionary history of *C. smithii*. Alternatively, the third scenario suggests that the sub-clades Cc_M35_1.1 and Cc_M35_2.1 have evolved exclusively in *C. cassiicola* and share no homology to M35 genes from *C. smithii*. At this moment, we are unable to distinguish the second scenario from the third. An extensive genome sequencing of other *C. smithii* isolates will be needed to better

understand the evolutionary dynamics of M35 genes between *C. smithii* and *C. cassiicola*.

4.5 The expression dynamics of M35 genes in *Corynespora*

The expression levels of M35 genes have been significantly induced during fungal infection (Pan et al., 2020; Zhang et al., 2021). Here, our RT-qPCR assays demonstrated that all three genes of *C. cassiicola* isolate were expressed during the infection process of soybean plants, indicating their potential role in the pathogenicity of *C. cassiicola*. Although three M35 genes of *C. cassiicola* displayed varying expression levels during the course of soybean infection (0-8 dpi), they showed a general tendency for the highest expression levels occurring at 8 dpi, which corresponds to the late stages of infection. These results differ from those reported for the plant-pathogenic fungi, *Rhizoctonia cerealis* (Pan et al., 2020) and *Fusarium oxysporum* f. sp. *cubense* (Zhang et al., 2021), in which M35 genes reached their highest expression levels during the early stages of infection. The contrasting expression patterns of M35 genes between *C. cassiicola* and the other two species indicate species-specific differences in the expression of M35 genes.

The expression of CC_29_g1451, a member of the sub-clade Cc_M35_2.1, is intriguing. It was predicted to be a putative non-effector M35 and exhibited a small but statically significant increase in expression levels at 8 dpi (Supplementary Figure S3). As a putative non-effector M35, it likely lacks the ability to be secreted outside the fungal cell due to the absence of signal peptide. The fact that CC_29_g1451 was expressed during our experiment suggests that it may play a functional role within the intracellular environment of the fungal cell. Taken together, the three M35 genes of *C. cassiicola* were upregulated during the soybean infection and they may play important functional roles to facilitate infection.

ACKNOWLEDGEMENTS

We thank Professor Elizabeth P. B. Fontes for generously provide her 7500 Real-Time PCR System. This study was supported by Minas Gerais State Foundation of Research Aid – FAPEMIG (APQ-00150-17) and by The National Council of Scientific and Technological Development – CNPq to LOO (fellowship

number PQ 302336/2019-2). VDR also received a student fellowship from CNPq (GD 143393/2019-7).

CONFLICT OF INTEREST

We declare no conflicting interest.

DATA AVAILABILITY

This study analyzed genomic data that is publicly available at https://mycocosm.jgi.doe.gov/mycocosm/home and https://www.ncbi.nlm.nih.gov/genbank/. Additional information that supports the findings of this study can be found in the supplementary material.

5. REFERENCES

Amezrou, R., Audéon, C., Compain, J., Gélisse, S., Ducasse, A., Saintenac, C., Lapalu, N., Louet, C., Orford, S., Croll, D., Amselem, J., Fillinger, S., Marcel, T.C., 2023. A secreted protease-like protein in *Zymoseptoria tritici* is responsible for avirulence on Stb9 resistance gene in wheat. PLoS Pathog 19, e1011376. https://doi.org/10.1371/journal.ppat.1011376

Arnadottir, H., Hvanndal, I., Andresdottir, V., Burr, S.E., Frey, J., Gudmundsdottir, B.K., 2009. The AsaP1 Peptidase of *Aeromonas salmonicida* subsp. *achromogenes* Is a Highly Conserved Deuterolysin Metalloprotease (Family M35) and a Major Virulence Factor. J Bacteriol 191, 403–410. https://doi.org/10.1128/JB.00847-08

Bailey, T.L., Boden, M., Buske, F.A., Frith, M., Grant, C.E., Clementi, L., Ren, J., Li, W.W., Noble, W.S., 2009. MEME SUITE: tools for motif discovery and searching. Nucleic Acids Res 37, W202–W208. https://doi.org/10.1093/nar/gkp335

Bandelt, H.J., Forster, P., Rohl, A., 1999. Median-joining networks for inferring intraspecific phylogenies. Mol Biol Evol 16, 37–48. https://doi.org/10.1093/oxfordjournals.molbev.a026036

Carris, L.M., Glawe, D.A., Gray, L.E., 1986. Isolation of the Soybean Pathogens *Corynespora cassiicola* and *Phialophora gregata* from Cysts of *Heterodera glycines* in Illinois. Mycologia 78, 503–506. https://doi.org/10.1080/00275514.1986.12025280

Dal'Sasso, T.C.S., Rocha, V.D., Rody, H.V.S., Costa, M.D.B.L., Oliveira, L.O., 2022. The necrosis- and ethylene-inducing peptide 1-like protein (NLP) gene family of the plant pathogen *Corynespora cassiicola*. Curr Genet 68, 645–659. https://doi.org/10.1007/s00294-022-01252-0

Dal'Sasso, T.C.S., Rody, H.V.S., Grijalba, P.E., Oliveira, L.O., 2021. Genome sequences and in silico effector mining of *Corynespora cassiicola* CC_29 and *Corynespora olivacea* CBS 114450. Arch Microbiol 203, 5257–5265. https://doi.org/10.1007/s00203-021-02456-7

Dal'Sasso, T.C.S., Rody, H.V.S., Oliveira, L.O., 2023. Genome-Wide Analysis and Evolutionary History of the Necrosis- and Ethylene-Inducing Peptide 1-Like Protein (NLP) Superfamily Across the Dothideomycetes Class of Fungi. Curr Microbiol 80, 44. https://doi.org/10.1007/s00284-022-03125-8

Demuth, J.P., Bie, T. De, Stajich, J.E., Cristianini, N., Hahn, M.W., 2006. The Evolution of Mammalian Gene Families. PLoS One 1, e85. https://doi.org/10.1371/journal.pone.0000085

Demuth, J.P., Hahn, M.W., 2009. The life and death of gene families. BioEssays 31, 29–39. https://doi.org/10.1002/bies.080085

Déon, M., Scomparin, A., Tixier, A., Mattos, C.R.R., Leroy, T., Seguin, M., Roeckel-Drevet, P., Pujade-Renaud, V., 2012. First characterization of endophytic *Corynespora cassiicola* isolates with variant cassiicolin genes recovered from

rubber trees in Brazil. Fungal Divers 54, 87–99. https://doi.org/10.1007/s13225-012-0169-6

Dixon, L.J., Schlub, R.L., Pernezny, K., Datnoff, L.E., 2009. Host Specialization and Phylogenetic Diversity of *Corynespora cassiicola*. Phytopathology 99, 1015–1027. https://doi.org/10.1094/PHYTO-99-9-1015

Dong, S., Stam, R., Cano, L.M., Song, J., Sklenar, J., Yoshida, K., Bozkurt, T.O., Oliva, R., Liu, Z., Tian, M., Win, J., Banfield, M.J., Jones, A.M.E., van der Hoorn, R.A.L., Kamoun, S., 2014. Effector Specialization in a Lineage of the Irish Potato Famine Pathogen. Science (1979) 343, 552–555. https://doi.org/10.1126/science.1246300

Emanuelsson, O., Nielsen, H., Brunak, S., von Heijne, G., 2000. Predicting Subcellular Localization of Proteins Based on their N-terminal Amino Acid Sequence. J Mol Biol 300, 1005–1016. https://doi.org/10.1006/jmbi.2000.3903

Grigoriev, I. V., Nikitin, R., Haridas, S., Kuo, A., Ohm, R., Otillar, R., Riley, R., Salamov, A., Zhao, X., Korzeniewski, F., Smirnova, T., Nordberg, H., Dubchak, I., Shabalov, I., 2014. MycoCosm portal: gearing up for 1000 fungal genomes. Nucleic Acids Res 42, D699–D704. https://doi.org/10.1093/nar/gkt1183

Haridas, S., Albert, R., Binder, M., Bloem, J., LaButti, K., Salamov, A., Andreopoulos, B., Baker, S.E., Barry, K., Bills, G., Bluhm, B.H., Cannon, C., Castanera, R., Culley, D.E., Daum, C., Ezra, D., González, J.B., Henrissat, B., Kuo, A., Liang, C., Lipzen, A., Lutzoni, F., Magnuson, J., Mondo, S.J., Nolan, M., Ohm, R.A., Pangilinan, J., Park, H.-J., Ramírez, L., Alfaro, M., Sun, H., Tritt, A., Yoshinaga, Y., Zwiers, L.-H., Turgeon, B.G., Goodwin, S.B., Spatafora, J.W., Crous, P.W., Grigoriev, I.V., 2020. 101 Dothideomycetes genomes: A test case for predicting lifestyles and emergence of pathogens. Stud Mycol 96, 141–153. https://doi.org/10.1016/j.simyco.2020.01.003

Hoang, D.T., Chernomor, O., von Haeseler, A., Minh, B.Q., Vinh, L.S., 2018. UFBoot2: Improving the Ultrafast Bootstrap Approximation. Mol Biol Evol 35, 518–522. https://doi.org/10.1093/molbev/msx281

Hori, T., Kumasaka, T., Yamamoto, M., Nonaka, T., Tanaka, N., Hashimoto, Y., Ueki, T., Takio, K., 2001. Structure of a new “aspzincin” metalloendopeptidase from *Grifola frondosa*: implications for the catalytic mechanism and substrate specificity based on several different crystal forms. Acta Crystallogr D Biol Crystallogr 57, 361–368. https://doi.org/10.1107/S0907444900019740

Huang, A., Lu, M., Ling, E., Li, P., Wang, C., 2020. A M35 family metalloprotease is required for fungal virulence against insects by inactivating host prophenoloxidases and beyond. Virulence 11, 222–237. https://doi.org/10.1080/21505594.2020.1731126

Jones, P., Binns, D., Chang, H.Y., Fraser, M., Li, W., McAnulla, C., McWilliam, H., Maslen, J., Mitchell, A., Nuka, G., Pesseat, S., Quinn, A.F., Sangrador-Vegas, A., Scheremetjew, M., Yong, S.-Y., Lopez, R., Hunter, S., 2014. InterProScan 5: genome-scale protein function classification. Bioinformatics 30, 1236–1240. https://doi.org/10.1093/bioinformatics/btu031

Kalyaanamoorthy, S., Minh, B.Q., Wong, T.K.F., Von Haeseler, A., Jermiin, L.S., 2017. ModelFinder: Fast model selection for accurate phylogenetic estimates. Nat Methods 14, 587–589. https://doi.org/10.1038/nmeth.4285

Katoh, K., Standley, D.M., 2013. MAFFT Multiple Sequence Alignment Software Version 7: Improvements in Performance and Usability. Mol Biol Evol 30, 772–780. https://doi.org/10.1093/molbev/mst010

Kawasaki, T., Yamada, K., Yoshimura, S., Yamaguchi, K., 2017. Chitin receptor-mediated activation of MAP kinases and ROS production in rice and *Arabidopsis*. Plant Signal Behav 12, e1361076. https://doi.org/10.1080/15592324.2017.1361076

Kirk, P.M., Cannon, P.F., Minter, D.W. and Stalpers, J.A., 2008. Dictionary of the Fungi. 10th Edition, Wallingford.

Krogh, A., Larsson, B., von Heijne, G., Sonnhammer, E.L.L., 2001. Predicting transmembrane protein topology with a hidden markov model: application to complete genomes11Edited by F. Cohen. J Mol Biol 305, 567–580. https://doi.org/10.1006/jmbi.2000.4315

Li, J., Yu, L., Tian, Y., Zhang, K.-Q., 2012. Molecular Evolution of the Deuterolysin (M35) Family Genes in *Coccidioides*. PLoS One 7, e31536. https://doi.org/10.1371/journal.pone.0031536

Li, J., Zhang, K.-Q., 2014. Independent Expansion of Zincin Metalloproteinases in Onygenales Fungi May Be Associated with Their Pathogenicity. PLoS One 9, e90225. https://doi.org/10.1371/journal.pone.0090225

Livak, K.J., Schmittgen, T.D., 2001. Analysis of Relative Gene Expression Data Using Real-Time Quantitative PCR and the 2−ΔΔCT Method. Methods 25, 402–408. https://doi.org/10.1006/meth.2001.1262

Looi, H.K., Toh, Y.F., Yew, S.M., Na, S.L., Tan, Y.-C., Chong, P.-S., Khoo, J.S., Yee, W.-Y., Ng, K.P., Kuan, C.S., 2017. Genomic insight into pathogenicity of dematiaceous fungus *Corynespora cassiicola*. PeerJ 5, e2841. https://doi.org/10.7717/peerj.2841

Lopez, D., Ribeiro, S., Label, P., Fumanal, B., Venisse, J.S., Kohler, A., de Oliveira, R.R., Labutti, K., Lipzen, A., Lail, K., Bauer, D., Ohm, R.A., Barry, K.W., Spatafora, J., Grigoriev, I. V., Martin, F.M., Pujade-Renaud, V., 2018. Genome-Wide Analysis of *Corynespora cassiicola* Leaf Fall Disease Putative Effectors. Front Microbiol 9. https://doi.org/10.3389/fmicb.2018.00276

Lv, J., Zhou, J., Chang, B., Zhang, Yihao, Feng, Z., Wei, F., Zhao, L., Zhang, Yalin, Feng, H., 2022. Two Metalloproteases VdM35-1 and VdASPF2 from *Verticillium dahliae* Are Required for Fungal Pathogenicity, Stress Adaptation, and Activating Immune Response of Host. Microbiol Spectr 10. https://doi.org/10.1128/spectrum.02477-22

Lynch, M., Conery, J.S., 2000. The Evolutionary Fate and Consequences of Duplicate Genes. Science (1979) 290, 1151–1155. https://doi.org/10.1126/science.290.5494.1151

MacKenzie, K.J., Sumabat, L.G., Xavier, K. V., Vallad, G.E., 2018. A Review of *Corynespora cassiicola* and Its Increasing Relevance to Tomato in Florida. Plant Health Prog 19, 303–309. https://doi.org/10.1094/PHP-05-18-0023-RV

McAuley, K.E., Jia-Xing, Y., Dodson, E.J., Lehmbeck, J., Østergaard, P.R., Wilson, K.S., 2001. A quick solution: ab initio structure determination of a 19 kDa metalloproteinase using ACORN. Acta Crystallogr D Biol Crystallogr 57, 1571–1578. https://doi.org/10.1107/S090744490101335X

Mistry, J., Chuguransky, S., Williams, L., Qureshi, M., Salazar, G.A., Sonnhammer, E.L.L., Tosatto, S.C.E., Paladin, L., Raj, S., Richardson, L.J., Finn, R.D., Bateman, A., 2021. Pfam: The protein families database in 2021. Nucleic Acids Res 49, D412–D419. https://doi.org/10.1093/nar/gkaa913

Nakadai, T., Nasuno, S., Iguchi, N., 1973. Purification and properties of neutral proteinase II from *Aspergillus oryzae*. Agric Biol Chem 37, 2703-2708. https://doi.org/10.1080/00021369.1973.10861072

Naumann, T.A., Price, N.P.J., 2012. Truncation of class IV chitinases from *Arabidopsis* by secreted fungal proteases. Mol Plant Pathol 13, 1135–1139. https://doi.org/10.1111/j.1364-3703.2012.00805.x

Nguyen, L.-T., Schmidt, H.A., von Haeseler, A., Minh, B.Q., 2015. IQ-TREE: A Fast and Effective Stochastic Algorithm for Estimating Maximum-Likelihood Phylogenies. Mol Biol Evol 32, 268–274. https://doi.org/10.1093/molbev/msu300

Ohm, R.A., Feau, N., Henrissat, B., Schoch, C.L., Horwitz, B.A., Barry, K.W., Condon, B.J., Copeland, A.C., Dhillon, B., Glaser, F., Hesse, C.N., Kosti, I., LaButti, K., Lindquist, E.A., Lucas, S., Salamov, A.A., Bradshaw, R.E., Ciuffetti, L., Hamelin, R.C., Kema, G.H.J., Lawrence, C., Scott, J.A., Spatafora, J.W., Turgeon, B.G., de Wit, P.J.G.M., Zhong, S., Goodwin, S.B., Grigoriev, I. V., 2012. Diverse Lifestyles and Strategies of Plant Pathogenesis Encoded in the Genomes of Eighteen Dothideomycetes Fungi. PLoS Pathog 8, e1003037. https://doi.org/10.1371/journal.ppat.1003037

Ökmen, B., Kemmerich, B., Hilbig, D., Wemhöner, R., Aschenbroich, J., Perrar, A., Huesgen, P.F., Schipper, K., Doehlemann, G., 2018. Dual function of a secreted fungalysin metalloprotease in *Ustilago maydis*. New Phytologist 220, 249–261. https://doi.org/10.1111/nph.15265

Pan, L., Wen, S., Yu, J., Lu, L., Zhu, X., Zhang, Z., 2020. Genome-Wide Identification of M35 Family Metalloproteases in *Rhizoctonia cerealis* and Functional Analysis of RcMEP2 as a Virulence Factor during the Fungal Infection to Wheat. Int J Mol Sci 21, 2984. https://doi.org/10.3390/ijms21082984

Petersen, T.N., Brunak, S., von Heijne, G., Nielsen, H., 2011. SignalP 4.0: discriminating signal peptides from transmembrane regions. Nat Methods 8, 785–786. https://doi.org/10.1038/nmeth.1701

Plissonneau, C., Blaise, F., Ollivier, B., Leflon, M., Carpezat, J., Rouxel, T., Balesdent, M.-H., 2017. Unusual evolutionary mechanisms to escape effector-triggered immunity in the fungal phytopathogen *Leptosphaeria maculans*. Mol Ecol 26, 2183–2198. https://doi.org/10.1111/mec.14046

Rambaut, A., 2009. FigTree v1. 3.1. http://tree. bio. ed. ac. uk/software/figtree/.

Rawlings, N.D., Barrett, A.J., Thomas, P.D., Huang, X., Bateman, A., Finn, R.D., 2018. The MEROPS database of proteolytic enzymes, their substrates and inhibitors in 2017 and a comparison with peptidases in the PANTHER database. Nucleic Acids Res 46, D624–D632. https://doi.org/10.1093/nar/gkx1134

Rocha, V.D., Dal'Sasso, T.C.S., Costa, M.D.B.L., Oliveira, L.O., 2023. Unveiling the Evolutionary History of the Pectin Methylesterase (Pme) Gene Family in the Dothideomycetes Class of Fungi. Available at SSRN: https://ssrn.com/abstract=4443733 or http://dx.doi.org/10.2139/ssrn.4443733

Rondon, MN., Lawrence, K., 2021. The fungal pathogen *Corynespora cassiicola*: A review and insights for target spot management on cotton and Soya bean. Journal of Phytopathology 169, 329–338. https://doi.org/10.1111/jph.12992

Rozas, J., Ferrer-Mata, A., Sánchez-DelBarrio, J.C., Guirao-Rico, S., Librado, P., Ramos-Onsins, S.E., Sánchez-Gracia, A., 2017. DnaSP 6: DNA Sequence Polymorphism Analysis of Large Data Sets. Mol Biol Evol 34, 3299–3302. https://doi.org/10.1093/molbev/msx248

Sánchez-Vallet, A., Fouché, S., Fudal, I., Hartmann, F.E., Soyer, J.L., Tellier, A., Croll, D., 2018. The Genome Biology of Effector Gene Evolution in Filamentous Plant Pathogens. Annu Rev Phytopathol 56, 21–40. https://doi.org/10.1146/annurev-phyto-080516-035303

Sánchez-Vallet, A., Mesters, J.R., Thomma, B.P.H.J., 2015. The battle for chitin recognition in plant-microbe interactions. FEMS Microbiol Rev 39, 171–183. https://doi.org/10.1093/femsre/fuu003

Sekine H., 1973. Neutral proteinase II of *Aspergillus sojae*: An enzyme specifically active on protamine and histone. Agric Biol Chem 37 1765-1767. https://doi.org/10.1080/00021369.1973.10860907

Schoch, C.L., Crous, P.W., Groenewald, J.Z., Boehm, E.W.A., Burgess, T.I., de Gruyter, J., de Hoog, G.S., Dixon, L.J., Grube, M., Gueidan, C., Harada, Y., Hatakeyama, S., Hirayama, K., Hosoya, T., Huhndorf, S.M., Hyde, K.D., Jones, E.B.G., Kohlmeyer, J., Kruys, Å., Li, Y.M., Lücking, R., Lumbsch, H.T., Marvanová, L., Mbatchou, J.S., McVay, A.H., Miller, A.N., Mugambi, G.K., Muggia, L., Nelsen, M.P., Nelson, P., Owensby, C.A., Phillips, A.J.L., Phongpaichit, S., Pointing, S.B., Pujade-Renaud, V., Raja, H.A., Plata, E.R., Robbertse, B., Ruibal, C., Sakayaroj, J., Sano, T., Selbmann, L., Shearer, C.A., Shirouzu, T., Slippers, B., Suetrong, S., Tanaka, K., Volkmann-Kohlmeyer, B., Wingfield, M.J., Wood, A.R., Woudenberg, J.H.C., Yonezawa, H., Zhang, Y., Spatafora, J.W., 2009. A class-wide phylogenetic assessment of Dothideomycetes. Stud Mycol 64, 1–15. https://doi.org/10.3114/sim.2009.64.01

Shiu, S.H., Byrnes, J.K., Pan, R., Zhang, P., Li, W.H., 2006. Role of positive selection in the retention of duplicate genes in mammalian genomes. Proceedings of the National Academy of Sciences 103, 2232–2236. https://doi.org/10.1073/pnas.0510388103

Stanke, M., Morgenstern, B., 2005. AUGUSTUS: a web server for gene prediction in eukaryotes that allows user-defined constraints. Nucleic Acids Res 33, W465–W467. https://doi.org/10.1093/nar/gki458

Sumabat, L.G., Kemerait, R.C., Kim, D.K., Mehta, Y.R., Brewer, M.T., 2018. Clonality and geographic structure of host-specialized populations of *Corynespora cassiicola* causing emerging target spot epidemics in the southeastern United States. PLoS One 13, e0205849. https://doi.org/10.1371/journal.pone.0205849

Tatsumi, H., Murakami, S., Tsuji, R.F., Ishida, Y., Murakami, K., Masaki, A., Kawabe, H., Arimura, H., Nakano, E., Motaf, H., 1991. Cloning and expression in yeast of a cDNA clone encoding *Aspergillus oryzae* neutral protease II, a unique metalloprotease. Mol Gen Genet 228, 97–103. https://doi.org/10.1007/BF00282453

Voglmayr, H., Jaklitsch, W.M., 2017. *Corynespora*, *Exosporium* and *Helminthosporium* revisited - New species and generic reclassification. Stud Mycol 87, 43–76. https://doi.org/10.1016/j.simyco.2017.05.001

Wijayawardene, N.N., Hyde, K.D., Rajeshkumar, K.C., Hawksworth, D.L., Madrid, H., Kirk, P.M., Braun, U., Singh, R. V., Crous, P.W., Kukwa, M., Lücking, R., Kurtzman, C.P., Yurkov, A., Haelewaters, D., Aptroot, A., Lumbsch, H.T., Timdal, E., Ertz, D., Etayo, J., Phillips, A.J.L., Groenewald, J.Z., Papizadeh, M., Selbmann, L., Dayarathne, M.C., Weerakoon, G., Jones, E.B.G., Suetrong, S., Tian, Q., Castañeda-Ruiz, R.F., Bahkali, A.H., Pang, K.-L., Tanaka, K., Dai, D.Q., Sakayaroj, J., Hujslová, M., Lombard, L., Shenoy, B.D., Suija, A., Maharachchikumbura, S.S.N., Thambugala, K.M., Wanasinghe, D.N., Sharma, B.O., Gaikwad, S., Pandit, G., Zucconi, L., Onofri, S., Egidi, E., Raja, H.A., Kodsueb, R., Cáceres, M.E.S., Pérez-Ortega, S., Fiuza, P.O., Monteiro, J.S., Vasilyeva, L.N., Shivas, R.G., Prieto, M., Wedin, M., Olariaga, I., Lateef, A.A., Agrawal, Y., Fazeli, S.A.S., Amoozegar, M.A., Zhao, G.Z., Pfliegler, W.P., Sharma, G., Oset, M., Abdel-Wahab, M.A., Takamatsu, S., Bensch, K., de Silva, N.I., De Kesel, A., Karunarathna, A., Boonmee, S., Pfister, D.H., Lu, Y.-Z., Luo, Z.-L., Boonyuen, N., Daranagama, D.A., Senanayake, I.C., Jayasiri, S.C., Samarakoon, M.C., Zeng, X.-Y., Doilom, M., Quijada, L., Rampadarath, S., Heredia, G., Dissanayake, A.J., Jayawardana, R.S., Perera, R.H., Tang, L.Z., Phukhamsakda, C., Hernández-Restrepo, M., Ma, X., Tibpromma, S., Gusmao, L.F.P., Weerahewa, D., Karunarathna, S.C., 2017. Notes for genera: Ascomycota. Fungal Divers 86, 1–594. https://doi.org/10.1007/s13225-017-0386-0

Zhang, J., Bayram Akcapinar, G., Atanasova, L., Rahimi, M.J., Przylucka, A., Yang, D., Kubicek, C.P., Zhang, R., Shen, Q., Druzhinina, I.S., 2016. The neutral metallopeptidase NMP1 of *Trichoderma guizhouense* is required for mycotrophy and self-defence. Environ Microbiol 18, 580–597. https://doi.org/10.1111/1462-2920.12966

Zhang, X., Huang, H., Wu, B., Xie, J., Viljoen, A., Wang, W., Mostert, D., Xie, Y., Fu, G., Xiang, D., Lyu, S., Liu, S., Li, C., 2021. The M35 Metalloprotease Effector FocM35_1 Is Required for Full Virulence of *Fusarium oxysporum* f. sp. *cubense* Tropical Race 4. Pathogens 10, 670. https://doi.org/10.3390/pathogens10060670

Zhang, Y., Crous, P.W., Schoch, C.L., Hyde, K.D., 2012. Pleosporales. Fungal Divers 53, 1–221. https://doi.org/10.1007/s13225-011-0117-x

Zipfel, C., 2014. Plant pattern-recognition receptors. Trends Immunol 35, 345–351. https://doi.org/10.1016/j.it.2014.05.004

SUPPLEMENTARY MATERIAL

Genome-wide survey and molecular evolution of the Deuterolysin metalloprotease (M35) gene family in the Dothideomycetes class of fungi

Table S1. List of fungal species, with assembled genome size (GZ), number of predicted genes (PG) in each genome, number of predicted Deuterolysin Metalloprotease (M35) genes, and number of M35 (putative effectors and putative non-effectors).

							Prediction from this study		
Species (Isolate)	**Alias**	**Class**	**Order**	**GZ (Mb)**	**#PG**	**Reference**	**# M35 genes**	**# putative effector M35s**	**# putative non-effector M35s**
Aaosphaeria arxii (CBS 175.79)	Aaoar	Dothideomycetes	Pleosporales	38.9	14,203	Haridas et al. 2020	3	2	1
Acidomyces richmondensis (BFW)	Aciri	Dothideomycetes	Capnodiales	29.9	11,202	Mosier et al. 2016	0	0	0
Alternaria alternata (BMP0270)	Altal	Dothideomycetes	Pleosporales	33.0	13,469	Dang et al. 2015	2	2	0
Amniculicola lignicola (CBS 123094)	Amnli	Dothideomycetes	Pleosporales	49.6	15,590	Haridas et al. 2020	2	1	1
Aplosporella prunicola (CBS 121.167)	Aplpr	Dothideomycetes	Botryosphaeriales	32.8	12,579	Haridas et al. 2020	1	0	1
Ascochyta rabiei (ArDII)	Ascra	Dothideomycetes	Pleosporales	34.7	10,596	Verma et al. 2016	0	0	0
Aulographum hederae	Aulhe	Dothideomycetes	Aulographales	32.0	12,127	Haridas et al. 2020	1	0	1
Baudoinia compniacensis (UAMH 10762 (4089826))	Bauco	Dothideomycetes	Capnodiales	21.9	10,513	Ohm et al. 2012	0	0	0
Bimuria novae-zelandiae (CBS 107.79)	Bimnz	Dothideomycetes	Pleosporales	78.2	16,681	Haridas et al. 2020	3	3	0
Botryosphaeria dothidea	Botdo	Dothideomycetes	Botryosphaeriales	43.5	14,998	Marsberg et al. 2017	7	0	7
Byssothecium circinans (CBS 675.92)	Bysci	Dothideomycetes	Pleosporales	49.3	15,785	Haridas et al. 2020	2	2	0
Cenococcum geophilum (1.58)	Cenge	Dothideomycetes	Mytilinidiales	177.6	14,748	Peter et al. 2016	0	0	0
Cercospora zeae-maydis	Cerzm	Dothideomycetes	Capnodiales	46.6	12,020	Haridas et al. 2020	4	2	2
Cladosporium fulvum	Clafu	Dothideomycetes	Capnodiales	61.1	14,127	de Wit et al. 2012	2	1	1
Clathrospora elynae (CBS 161.51)	Clael	Dothideomycetes	Pleosporales	37.4	13,617	Haridas et al. 2020	2	1	1
Clohesyomyces aquaticus	Cloaq	Dothideomycetes	Pleosporales	49.7	15,810	Mondo et al. 2017	3	3	0
Cochliobolus heterostrophus (C5)	Coche	Dothideomycetes	Pleosporales	36.5	13,336	Ohm et al. 2012	0	0	0
Corynespora cassiicola (CCP)	Corca	Dothideomycetes	Pleosporales	44.8	17,166	Lopez et al. 2018	3	3	0
Cucurbitaria berberidis (CBS 394.84)	Cucbe	Dothideomycetes	Pleosporales	32.9	12,439	Haridas et al. 2020	2	1	1
Delitschia confertaspora (ATCC 74209)	Delco	Dothideomycetes	Pleosporales	31.2	10,171	Haridas et al. 2020	1	1	0
Delphinella strobiligena (CBS 735.71)	Delst	Dothideomycetes	Dothideales	29.2	10,337	Haridas et al. 2020	0	0	0
Didymella exigua (CBS 183.55)	Didex	Dothideomycetes	Pleosporales	34.4	12,394	Haridas et al. 2020	1	0	1
Diplodia seriata (DS831)	Dipse	Dothideomycetes	Botryosphaeriales	37.1	9,343	Morales-Cruz et al. 2015	6	5	1
Dissoconium aciculare	Disac	Dothideomycetes	Capnodiales	26.5	10,299	Haridas et al. 2020	0	0	0
Dothidotthia symphoricarpi	Dotsy	Dothideomycetes	Pleosporales	34.4	11,790	Haridas et al. 2020	3	3	0
Dothistroma septosporum (NZE10)	Dotse	Dothideomycetes	Capnodiales	30.2	12,580	De Wit et al. 2012	0	0	0
Elsinoe ampelina (CECT 20119)	Elsam	Dothideomycetes	Myriangiales	28.3	10,209	Haridas et al. 2020	0	0	0
Eremomyces bilateralis (CBS 781.70)	Erebi	Dothideomycetes	Eremomycetales	26.9	9,881	Haridas et al. 2020	2	1	1
Glonium stellatum (CBS 207.34)	Glost	Dothideomycetes	Mytilinidiales	40.5	14,362	Peter et al. 2016	1	1	0
Hysterium pulicare	Hyspu	Dothideomycetes	Hysteriales	38.4	12,352	Ohm et al. 2012	1	0	1
Karstenula rhodostoma (CBS 690.94)	Karrh	Dothideomycetes	Pleosporales	44.9	12,469	Haridas et al. 2020	3	3	0
Lentithecium fluviatile	Lenfl	Dothideomycetes	Pleosporales	54.7	16,742	Haridas et al. 2020	2	1	1
Lepidopterella palustris	Leppa	Dothideomycetes	Mytilinidiales	45.7	13,870	Peter et al. 2016	1	1	0
Leptosphaeria maculans	Lepma	Dothideomycetes	Pleosporales	44.9	12,469	Rouxel et al 2011	2	2	0
Lindgomyces ingoldianus (ATCC 200398)	Linin	Dothideomycetes	Pleosporales	69.0	15,956	Haridas et al. 2020	1	1	0
Lineolata rhizophorae (ATCC 16933)	Linrh	Dothideomycetes	Lineolatales	31.1	10,230	Haridas et al. 2020	1	1	0

Continued Table S1

Lizonia empirigonia (CBS 542.76)	Lizem	Dothideomycetes	Pleosporales	51.5	12,467	Haridas et al. 2020	3	3	0
Lophiostoma macrostomum	Lopma	Dothideomycetes	Pleosporales	42.6	16,160	Haridas et al. 2020	1	1	0
Lophiotrema nucula (CBS 627.86)	Lopnu	Dothideomycetes	Pleosporales	48.6	18,117	Haridas et al. 2020	2	1	1
Lophium mytilinum (CBS 269.34)	Lopmy	Dothideomycetes	Mytilinidiales	43.4	15,153	Haridas et al. 2020	1	1	0
Macrophomina phaseolina (MS6)	Macph	Dothideomycetes	Botryosphaeriales	48.9	13,806	Islam et al. 2012	4	3	1
Macroventuria anomochaeta (CBS 525.71)	Macan	Dothideomycetes	Pleosporales	33.3	12,954	Haridas et al. 2020	3	0	3
Massarina eburnea (CBS 473.64)	Maseb	Dothideomycetes	Pleosporales	38.2	12,935	Haridas et al. 2020	3	3	0
Massariosphaeria phaeospora (CBS 611.86)	Masph	Dothideomycetes	Pleosporales	42.1	14,021	Haridas et al. 2020	1	1	0
Melanomma pulvis-pyrius	Melpu	Dothideomycetes	Pleosporales	42.1	15,881	Haridas et al. 2020	3	3	0
Microthyrium microscopicum (CBS 115976)	Micmi	Dothideomycetes	Microthyriales	37.1	12,494	Haridas et al. 2020	3	0	3
Myriangium duriaei (CBS 260.36)	Myrdu	Dothideomycetes	Myriangiales	25.7	10,685	Haridas et al. 2020	0	0	0
Mytilinidion resinicola (CBS 304.34)	Mytre	Dothideomycetes	Mytilinidiales	47.3	16,794	Haridas et al. 2020	1	1	0
Neofusicoccum parvum (UCRNP2)	Neopa	Dothideomycetes	Botryosphaeriales	42.6	10,366	Blanco-Ulate et al. 2013	3	2	1
Paraconiothyrium sporulosum (AP3s5-JAC2a)	Parsp	Dothideomycetes	Pleosporales	38.5	14,745	Zeiner et al. 2016	4	3	1
Patellaria atrata	Patat	Dothideomycetes	Patellariales	28.7	9,794	Haridas et al. 2020	1	1	0
Periconia macrospinosa (DSE2036)	Perma	Dothideomycetes	Pleosporales	55.0	18,750	Knapp et al. 2018	2	2	0
Phoma tracheiphila (IPT5)	Photr	Dothideomycetes	Pleosporales	34.2	13,209	Haridas et al. 2020	2	1	1
Phyllosticta citricarpa (CBS 127454)	Phyci	Dothideomycetes	Botryosphaeriales	29.0	11,088	Guarnaccia et al. 2019	1	1	0
Piedraia hortae (CBS 480.64)	Pieho	Dothideomycetes	Capnodiales	16.9	7,572	Haridas et al. 2020	0	0	0
Pleomassaria siparia	Plesi	Dothideomycetes	Pleosporales	43.2	13,486	Haridas et al. 2020	3	3	0
Polychaeton citri	Polci	Dothideomycetes	Capnodiales	27.2	10,582	Haridas et al. 2020	1	1	0
Polyplosphaeria fusca (CBS 125425)	Polfu	Dothideomycetes	Pleosporales	37.0	15,194	Haridas et al. 2020	3	1	2
Pseudocercospora eumusae (CBS 114824)	Pseeu	Dothideomycetes	Capnodiales	47.1	12,632	Chang et al. 2016	3	3	0
Pseudovirgaria hyperparasitica (CBS 121739)	Psehy	Dothideomycetes	Acrospermales	35.4	11,232	Haridas et al. 2020	4	3	1
Pyrenophora tritici-repentis	Pyrtr	Dothideomycetes	Pleosporales	37.8	12,141	Manning et al. 2013	1	1	0
Rhizodiscina lignyota (CBS 133067)	Rhili	Dothideomycetes	Aulographales	33.4	12,801	Haridas et al. 2020	1	1	0
Rhytidhysteron rufulum	Rhyru	Dothideomycetes	Hysteriales	40.2	12,117	Ohm et al. 2012	2	0	2
Saccharata proteae (CBS 121410)	Sacpr	Dothideomycetes	Botryosphaeriales	31.4	9,234	Haridas et al. 2020	0	0	0
Septoria musiva (SO2202)	Sepmu	Dothideomycetes	Capnodiales	29.4	10,233	Ohm et al. 2012	1	1	0
Setomelanomma holmii (CBS 110217)	Setho	Dothideomycetes	Pleosporales	39.2	14,389	Haridas et al. 2020	1	1	0
Setosphaeria turcica (Et28A)	Settu	Dothideomycetes	Pleosporales	43.0	12,028	Ohm et al. 2012	0	0	0
Stagonospora nodorum (SN15)	Stano	Dothideomycetes	Pleosporales	37.2	12,380	Hane et al. 2007	2	2	0
Teratosphaeria nubilosa (CBS 116005)	Ternu	Dothideomycetes	Capnodiales	28.4	10,998	Haridas et al. 2020	0	0	0
Tothia fuscella (CBS 130266)	Totfu	Dothideomycetes	Venturiales	36.8	13,685	Haridas et al. 2020	3	2	1
Trematosphaeria pertusa (CBS 122368)	Trepe	Dothideomycetes	Pleosporales	47.7	17,306	Haridas et al. 2020	2	2	0
Venturia inaequalis	Venin	Dothideomycetes	Venturiales	55.1	13,233	Deng et al. 2017	4	4	0
Verruconis gallopava	Verga	Dothideomycetes	Venturiales	31.8	11,357	Teixeira et al. 2017	1	1	0
Verruculina enalia (CBS 304.66)	Veren	Dothideomycetes	Pleosporales	61.2	13,748	Haridas et al. 2020	1	1	0
Viridothelium virens	Virvi	Dothideomycetes	Trypetheliales	32.2	11,858	Haridas et al. 2020	1	1	0

Continued Table S1

Westerdykella ornata (CBS 379.55)	Wesor	Dothideomycetes	Pleosporales	27.0	10,410	Haridas et al. 2020	1	1	0
Zasmidium cellare (ATCC 36951)	Zasce	Dothideomycetes	Capnodiales	38.2	16,015	Haridas et al. 2020	1	1	0
Zopfia rhizophila	Zoprh	Dothideomycetes	Pleosporales	152.8	21,730	Haridas et al. 2020	2	2	0
Zymoseptoria tritici	Zymtr	Dothideomycetes	Capnodiales	39.7	10,933	Goodwin et al. 2011	1	1	0
Aspergillus fumigatus (A1163)	Aspfu	Eurotiomycetes	Eurotiales	29.2	9,916	Fedorova et al. 2008	3	2	1
Aspergillus nidulans	Aspni	Eurotiomycetes	Eurotiales	30.5	10,608	Arnaud et al. 2012	4	4	0
						Total	146	107	39

Table S2. List of *Corynespora* isolates, with host species, country of origin, assembled genome size (GZ), number of predicted genes (PG) in each genome, number of predicted Deuterolysin Metalloprotease (M35) genes, and number of M35 (putative effectors and putative non-effectors).

								Prediction from this study		
Species (isolate)	**BioSample**	**BioProject**	**Assembly**	**Host species**	**Country**	**GZ (Mb) – [Reference]**	**#PG – [Reference]**	**# M35 genes**	**# putative effector M35s**	**# putative non-effector M35s**
Corynespora cassiicola (777AA)	SAMN08330686	PRJNA428435	GCA_002976175.1	*Glycine max*	Brazil	41.7 [Lopez et al., 2018]	14,873 [Dal'Sasso et al., 2022]	3	2	1
Corynespora cassiicola (ATI11)	SAMN08330687	PRJNA428435	GCA_002976025.1	*Cucumis sativus*	Brazil	41.1 [[Lopez et al., 2018]]	14,497 [Dal'Sasso et al., 2022]	2	1	1
Corynespora cassiicola (C7_L008)	SAMEA103891068	PRJEB19843	GCA_900169545.1	-	-	42.5 [-]	14,569 [Dal'Sasso et al., 2022]	3	2	1
Corynespora cassiicola (CAL-4)	SAMN12086008	PRJNA549429	GCA_006523515.1	*Gossypium hirsutum*	USA	47.5 [-]	19,239 [Dal'Sasso et al., 2022]	3	2	1
Corynespora cassiicola (CBS12925)	SAMN08330688	PRJNA428435	GCA_002976015.1	*Cucumis sativus*	Brazil	40.8 [Lopez et al., 2018]	14,403 [Dal'Sasso et al., 2022]	3	2	1
Corynespora cassiicola (CCAM1)	SAMN08330689	PRJNA428435	GCA_002975975.1	*Hevea brasiliensis*	Cameroon	42.3 [Lopez et al., 2018]	14,634 [Dal'Sasso et al., 2022]	3	2	1
Corynespora cassiicola (CCAM2)	SAMN08330690	PRJNA428435	GCA_002976125.1	*Hevea brasiliensis*	Cameroon	41.9 [Lopez et al., 2018]	14,785 [Dal'Sasso et al., 2022]	3	2	1
Corynespora cassiicola (CCAM3)	SAMN08330691	PRJNA428435	GCA_002975935.1	*Hevea brasiliensis*	Cameroon	42.7 [Lopez et al., 2018]	15,022 [Dal'Sasso et al., 2022]	3	2	1
Corynespora cassiicola (CCAM4)	SAMN08330692	PRJNA428435	GCA_002975955.1	*Hevea brasiliensis*	Cameroon	42.3 [Lopez et al., 2018]	14,545 [Dal'Sasso et al., 2022]	3	2	1
Corynespora cassiicola (CCI13)	SAMN08330693	PRJNA428435	GCA_002975895.1	*Hevea brasiliensis*	Côte d'Ivoire	41.9 [Lopez et al., 2018]	14,847 [Dal'Sasso et al., 2022]	3	2	1
Corynespora cassiicola (CCI6)	SAMN08330694	PRJNA428435	GCA_002975915.1	*Hevea brasiliensis*	Côte d'Ivoire	42.0 [Lopez et al., 2018]	14,905 [Dal'Sasso et al., 2022]	3	2	1
Corynespora cassiicola (CGAB1)	SAMN08330695	PRJNA428435	GCA_002975825.1	*Hevea brasiliensis*	Gabon	41.2 [Lopez et al., 2018]	14,635 [Dal'Sasso et al., 2022]	2	1	1
Corynespora cassiicola (CGAB2)	SAMN08330696	PRJNA428435	GCA_002975875.1	*Hevea brasiliensis*	Gabon	41.2 [Lopez et al., 2018]	14,638 [Dal'Sasso et al., 2022]	2	1	1
Corynespora cassiicola (CIND3)	SAMN08330697	PRJNA428435	GCA_002975845.1	*Hevea brasiliensis*	India	41.7[Lopez et al., 2018]	14,733 [Dal'Sasso et al., 2022]	3	2	1
Corynespora cassiicola (CLN16)	SAMN08330698	PRJNA428435	GCA_002975795.1	*Hevea brasiliensis*	Malaysia	41.7 [Lopez et al., 2018]	14,803 [Dal'Sasso et al., 2022]	3	2	1
Corynespora cassiicola (CSB16)	SAMN08330699	PRJNA428435	GCA_002976145.1	*Hevea brasiliensis*	Malaysia	40.7 [Lopez et al., 2018]	14,489 [Dal'Sasso et al., 2022]	2	2	0
Corynespora cassiicola (CSRI1)	SAMN08330700	PRJNA428435	GCA_002975815.1	*Hevea brasiliensis*	Sri Lanka	40.6 [Lopez et al., 2018]	14,327 [Dal'Sasso et al., 2022]	2	2	0
Corynespora cassiicola (CSRI2)	SAMN08330701	PRJNA428435	GCA_002975775.1	*Hevea brasiliensis*	Sri Lanka	40.8 [Lopez et al., 2018]	14,391 [Dal'Sasso et al., 2022]	2	2	0
Corynespora cassiicola (CSRI5)	SAMN08330702	PRJNA428435	GCA_002975755.1	*Hevea brasiliensis*	Sri Lanka	41.7 [Lopez et al., 2018]	14,736 [Dal'Sasso et al., 2022]	3	2	1
Corynespora cassiicola (CTHA1)	SAMN08330703	PRJNA428435	GCA_002975725.1	*Hevea brasiliensis*	Thailand	41.3 [Lopez et al., 2018]	14,432 [Dal'Sasso et al., 2022]	3	3	0
Corynespora cassiicola (CTHA2)	SAMN08330704	PRJNA428435	GCA_002976105.1	*Hevea brasiliensis*	Thailand	40.8 [Lopez et al., 2018]	14,424 [Dal'Sasso et al., 2022]	2	2	0
Corynespora cassiicola (CTHA3)	SAMN08330705	PRJNA428435	GCA_002975705.1	*Hevea brasiliensis*	Thailand	40.4 [Lopez et al., 2018]	14,616 [Dal'Sasso et al., 2022]	3	3	0
Corynespora cassiicola (CTHA4)	SAMN08330706	PRJNA428435	GCA_002975685.1	*Hevea brasiliensis*	Thailand	40.7 [Lopez et al., 2018]	14,410 [Dal'Sasso et al., 2022]	3	3	0
Corynespora cassiicola (CTHA5)	SAMN08330707	PRJNA428435	GCA_002975655.1	*Hevea brasiliensis*	Thailand	40.9 [Lopez et al., 2018]	14,461 [Dal'Sasso et al., 2022]	3	2	1
Corynespora cassiicola (CTHA6)	SAMN08330708	PRJNA428435	GCA_002976085.1	*Hevea brasiliensis*	Thailand	40.9 [Lopez et al., 2018]	14,444 [Dal'Sasso et al., 2022]	3	2	1
Corynespora cassiicola (CVa5)	SAMN12086010	PRJNA549429	GCA_006523535.1	*Gossypium hirsutum*	USA	45.3 [-]	15,347 [Dal'Sasso et al., 2022]	3	2	1
Corynespora cassiicola (E139)	SAMN08330709	PRJNA428435	GCA_002975665.1	*Hevea brasiliensis*	Brazil	42.8 [Lopez et al., 2018]	14,648 [Dal'Sasso et al., 2022]	3	2	1
Corynespora cassiicola (E55)	SAMN08330710	PRJNA428435	GCA_002976075.1	*Hevea brasiliensis*	Brazil	40.5 [Lopez et al., 2018]	14,352 [Dal'Sasso et al., 2022]	2	1	1
Corynespora cassiicola (E79)	SAMN08330711	PRJNA428435	GCA_002976045.1	*Hevea brasiliensis*	Brazil	42.5 [Lopez et al., 2018]	14,373 [Dal'Sasso et al., 2022]	3	3	0
Corynespora cassiicola (EDIG)	SAMN08330712	PRJNA428435	GCA_002975615.1	*Cucumis sativus*	Brazil	41.2 [Lopez et al., 2018]	14,743 [Dal'Sasso et al., 2022]	2	1	1
Corynespora cassiicola (GSO2)	SAMN08330713	PRJNA428435	GCA_002975635.1	*Vernonia cinerea*	Brazil	41.8 [Lopez et al., 2018]	15,072 [Dal'Sasso et al., 2022]	3	2	1
Corynespora cassiicola (IA)	SAMN08330714	PRJNA428435	GCA_002975535.1	*Cucumis sativus*	Brazil	41.6 [Lopez et al., 2018]	14,793 [Dal'Sasso et al., 2022]	3	2	1
Corynespora cassiicola (India_Hevea)	SAMN10434155	PRJNA505742	SRR8196886	*Hevea brasiliensis*	India	42.9 [Dal'Sasso et al., 2022]	14,404 [Dal'Sasso et al., 2022]	3	2	1
Corynespora cassiicola (JQ)	SAMN08330715	PRJNA428435	GCA_002975595.1	*Cucumis sativus*	Brazil	41.6 [Lopez et al., 2018]	14,815 [Dal'Sasso et al., 2022]	3	2	1

Continued Table S2

Corynespora cassiicola (LPO7)	SAMN08330716	PRJNA428435	GCA_002975495.1	*Piper hispidinervum*	Brazil	42.2 [Lopez et al., 2018]	14,535 [Dal'Sasso et al., 2022]	1	1	0
Corynespora cassiicola (PB)	SAMN08330717	PRJNA428435	GCA_002975575.1	*Cucumis sativus*	Brazil	41.6 [Lopez et al., 2018]	14,801 [Dal'Sasso et al., 2022]	3	2	1
Corynespora cassiicola (RUD)	SAMN08330718	PRJNA428435	GCA_002975505.1	*Glycine max*	Brazil	41.6 [Lopez et al., 2018]	14,858 [Dal'Sasso et al., 2022]	3	2	1
Corynespora cassiicola (SS1)	SAMN08330719	PRJNA428435	GCA_002975995.1	*Hevea brasiliensis*	Malaysia	40.7 [Lopez et al., 2018]	14,378 [Dal'Sasso et al., 2022]	2	2	0
Corynespora cassiicola (TCl3)	SAMN12086019	PRJNA549429	GCA_006519745.1	*Solanum lycospersium*	USA	46.0 [-]	14,986 [Dal'Sasso et al., 2022]	2	1	1
Corynespora cassiicola (TSB1)	SAMN08330720	PRJNA428435	GCA_002975555.1	*Hevea brasiliensis*	Malaysia	40.9 [Lopez et al., 2018]	14,435 [Dal'Sasso et al., 2022]	2	2	0
Corynespora cassiicola (Tscotton1)	SAMN06706475	PRJNA382361	SRR5435235	*Gossypium hirsutum*	USA	42.1 [Dal'Sasso et al., 2022]	14,988 [Dal'Sasso et al., 2022]	3	2	1
Corynespora cassiicola (UM591)	SAMN02981578	PRJNA236064	GCA_000603925.1	*Homo sapiens*	Malaysia	41.3 [Looi et al., 2016]	14,695 [Dal'Sasso et al., 2022]	3	3	0
Corynespora cassiicola (CCP)	SAMN05660679	PRJNA234811	GCA_003016335.1	*Hevea brasiliensis*	Philippines	44.8 [Lopez et al., 2018]	17,166 [Lopez et al., 2018]	3	3	0
Corynespora cassiicola (CC_29)	SAMN18718492	PRJNA721456	GCA_019202905.1	*Glycine max*	Brazil	44.7 [Dal'Sasso et al., 2021]	18,487 [Dal'Sasso et al., 2021]	3	2	1
Corynespora cassiicola (CC01)	SAMN17150876	PRJNA687613	GCA_016906425.1	*Hevea brasiliensis*	China	47.1 [Li et al., 2021]	15,606 [this study]	3	2	1
Corynespora cassiicola (YN49)	SAMN17150874	PRJNA687612	GCA_016906405.1	*Hevea brasiliensis*	China	45.1 [Li et al., 2021]	15,005 [this study]	2	2	0
Corynespora cassiicola (ZM170522)	SAMN17573700	PRJNA694745	GCA_022059125.1	*Hevea brasiliensis*	China	44.4 [Xu et al., 2021]	14,467 [this study]	3	3	0
Corynespora cassiicola (ZM160181)	SAMN17573614	PRJNA694745	GCA_022496115.1	*Fragaria x ananassa*	China	44.9 [-]	15,257 [this study]	3	2	1
Corynespora cassiicola (HG20101029)	SAMN09258516	PRJNA473037	GCA_023647615.1	*Cucumis sativus*	China	42.7 [Gao et al., 2020]	14,599 [this study]	3	2	1
Corynespora cassiicola (SAR-9)	SAMN12086012	PRJNA549429	GCA_023653695.1	*Glycine max*	USA	47.6 [-]	20,522 [this study]	2	1	1
Corynespora cassiicola (SMR2)	SAMN12086013	PRJNA549429	GCA_023653595.1	*Glycine max*	USA	48.4 [-]	21,607 [this study]	3	2	1
Corynespora cassiicola (FIM4)	SAMN12086011	PRJNA549429	GCA_023653765.1	*Gossypium hirsutum*	USA	49.1 [-]	22,414 [this study]	3	2	1
Corynespora cassiicola (CC1551)	SAMN12086017	PRJNA549429	GCA_023653545.1	*Solanum lycospersium*	USA	50.1 [-]	22,587 [this study]	2	1	1
Corynespora cassiicola (TCf2)	SAMN12086018	PRJNA549429	GCA_023653535.1	*Solanum lycospersium*	USA	50.8 [-]	22,751 [this study]	2	1	1
Corynespora cassiicola (Ssta1)	SAMN12086014	PRJNA549429	GCA_023653575.1	*Glycine max*	USA	45.0 [-]	15,596 [this study]	3	2	1
Corynespora cassiicola (CM13)	SAMN12086009	PRJNA549429	GCA_024500335.1	*Gossypium hirsutum*	USA	53.3 [-]	18,721 [this study]	3	2	1
Corynespora cassiicola (STNa-1)	SAMN12086015	PRJNA549429	GCA_024500205.1	*Glycine max*	USA	50.9 [-]	25,819 [this study]	2	1	1
Corynespora cassiicola (CC1343)	SAMN12086016	PRJNA549429	GCA_024500185.1	*Solanum lycospersium*	USA	54.1 [-]	20,620 [this study]	3	2	1
Corynespora cassiicola (CC_08)	-	-	-	*Commelina benghalensis*	Brazil	Dal'Sasso et al., (unpublished)	Dal'Sasso et al., (unpublished)	4	2	2
Corynespora cassiicola (CC_10)	-	-	-	*Lantana camara*	Brazil	Dal'Sasso et al., (unpublished)	Dal'Sasso et al., (unpublished)	3	2	1
Corynespora cassiicola (CC_28)	-	-	-	*Plectranthus barbatus*	Brazil	Dal'Sasso et al., (unpublished)	Dal'Sasso et al., (unpublished)	3	3	0
Corynespora smithii (CBS139925)	-	-	-	-	-	Dal'Sasso et al., (unpublished)	Dal'Sasso et al., (unpublished)	2	1	1
							Total	167	120	47

Table S3. Description of primer sequences used for RT-qPCR analysis of Deuterolysin Metalloprotease (M35) genes in *Corynespora cassiicola* (isolate CC_29).

Gene name	Gene ID (CC_29)	Sequences 5'- 3'	References
Cc_M35_1.1	CC_29_g9669	F: ATCTAGCACTAGCAGCACGG R: TTGCAGTTTGTCGAGGTGGT	This study
Cc_M35_1.2	CC_29_g9929	F: CCCCTGACTCCCCTGATGTA R: CAGCGAGGGGAAGTGGTATC	This study
Cc_M35_2.1	CC_29_g1451	F: ATTCTTCCTCCGGCATCGAC R: CGGAAGTTCGACTGGAGGAC	This study
β-tubulin	CC_29_g4872	F: CAGACCGGTCAATGCGGTAA R: GCCATTGTAGACGCCGGATC	Dal'Sasso et al. 2022

Table S4. Amino acid sequence alignment of two conserved segments for 146 Deuterolysin Metalloprotease (M35) proteins across Dothideomycetes. The alignment was generated by MAFFT v7.453. Arrows indicate amino acid positions, using the protein Aspnid_1387 of *Aspergilus nidulans* as a reference sequence. Code-color: yellow, zinc-binding amino acid residues; blue, catalytic amino acid residues. Protein ID with highlight in red: a putative non-effector M35.

	Segments	
Protein ID	**I**	**II**
	304 ↑	316 ↑
Aspnid_1385	HEFTH	GTDDLG-YG
Aspnid_8700	HEFTH	GTDDLG-YG
Aspfu_106035	HEFTH	GTDDYA-YG
Aspfu_108913	HEFTH	GTEDLG-YG
Bysci_142124	HEATH	GTDDHG-YG
Aaoar_394903	HEVTH	GTDDLG-YG
Maseb_535422	HEVTH	GTDDLG-YG
Perma_715261	HESTH	GTDDLG-YG
Karrh_463384	HEVTH	GTRDLG-YG
Parsp_1140357	HETTH	GTDDLG-YG
Bimnz_651240	HEVTH	GTGDLG-CG
Trepe_95520	HEVTH	GTQDYG-YG
Melpu_368415	HEMTH	GTDDYGTYG
Plesi_427021	HEMTH	GTEDYSTYG
Lopnu_574243	HETTH	GTSDYGVYG
Polfu_497999	HEMTH	GTSDYGVYG
Zoprh_652785	HETTH	GTSDYGAYG
Cloaq_629136	HEVTH	GTSDYGVYG
Lenfl_423058	HETMH	GADDLG-YG
Corca_494700	HEVTH	GTSDYGGYG
Clael_449453	HEMTH	GTSDYGGYG
Photr_17034	HEMTH	GTSDYGGYG
Lepmu_1271	HEMTH	GTSDYGGYG
Cucbe_320887	HETTH	GTSDYGGYG
Lizem_80288	HEMTH	GTSDYGGYG
Stano_7319	HEMTH	GTSDYGGYG
Macan_444410	HEMTH	GTSDYGGYG
Botdo_292495	HEMTH	GTTDQGAYG
Dipse_1466	HEMTH	GTTDQGAYG
Botdo_292212	HESTH	GTDDLG-YG
Macph1_2190	HESTH	GTDDLG-YG
Dipse_3186	HEATH	GTDDLG-YG
Aplpr_288850	HEFTH	GTDDLG-YG
Botdo_291212	HETTH	GTSDYGGYG
Macph_6055	HEVTH	GTSDYGGYG
Dipse_3833	HEMTH	GTSDYNGYG
Neopa_6977	HEMTH	GTDDFGGYG
Patat_976660	HEYTH	GTDDYA-YG
Virvi_536766	HEFTH	GTQDLG-YG
Rhili_71564	HEMTH	GTLDLG-YG
Totfu_116987	HEFTH	GTEDYA-YG
Venin_14452	HEYTH	GTEDNG-YG
Verga_116235	HEFTH	GTEDNG-YG

Continued Table S4

Botdo_296886	HEFTH	GTDDLG-YG
Dipse_6541	HEFTH	GTDDLG-YG
Neopa_5102	HEFTH	GTDDLG-YG
Macph_1714	HEFTH	GTDDLG-YG
Bysci_522142	HEETH	GTDDLG-YG
Maseb_514950	HEETH	GTDDLG-YG
Corca_410347	HEETH	GTDDYA-YG
Karrh_438693	HEETH	GTDDLG-YG
Parsp_1136914	HEETH	GTDDLG-YG
Bimnz_628904	HEETH	GTDDLG-YG
Lenfl_362847	HEETH	GTDDLG-YG
Trepe_562941	HEETH	GTDDIA-YG
Lopnu_510827	HEETH	GTDDLG-YG
Polfu_512870	HEETH	GTDDLG-YG
Linin_382046	HEETH	GTDDLG-YG
Cloaq_494373	HEETH	GTDDLG-YG
Lopma_722262	HEETH	GTDDIA-YG
Masph_173269	HEETH	GTDDFA-YG
Melpu_356703	HEETH	GTQDLG-YG
Wesor_448473	HEETH	GTDDLG-YG
Veren_618044	HEETH	GTDDLA-YG
Clael_431175	HEETH	GTQDLG-YG
Stano_3840	HEETH	GTQDNG-YG
Photr_374527	HEEAH	GTDDLG-YG
Cucbe_365220	HEEAH	GTDDLG-YG
Dotsy_380859	HEETH	GTDDLG-YG
Lepmu_2697	HEETH	GTDDLG-YG
Setho_119530	HEETH	GTEDLG-YG
Lizem_119044	HEETH	GTDDLG-YG
Macan_366018	HEETH	GTDDLG-YG
Didex_421595	HEETH	GTDDLG-YG
Zoprh_692496	HEETH	GTDDLG-YG
Plesi_533089	HEETH	GTEDNG-YG
Amnli_580729	HEEAH	GTDDLG-YG
Delco_49401	HEETH	GTDDLA-YG
Aaoar_442081	HEETH	GTDDLA-YG
Hyspu_112234	HENTH	GTQDYA-YG
Rhyru_110711	HETTH	GTDDYA-YG
Glost_419775	HENTH	GTQDYA-YG
Leppa_317930	HENTH	GTEDYG-YG
Mytre_432170	HESTH	GTDDNA-YG
Lopmy_449080	HESTH	GTDDNA-YG
Perma_584626	HEMTH	GTDDLG-YG
Cerzm_91873	HEETH	GTDDLG-YG
Pseeu_837	HEETH	GTQDYG-YG
Pseeu_838	HEETH	GTQDYG-YG
Clafu_184653	HEETH	GTQDYG-YG
Zasce_48379	HEETH	GTDDYA-YG
Clafu_185858	HEETH	GTEDFA-YG
Cerzm_115587	HEKTH	GTDDYA-YG
Sepmu_149143	HEKTH	GTDDYA-YG
Pseeu_10574	HEETH	GTEDYA-YG
Polci_314507	HEETH	GTEDNG-YG
Cerzm_48618	HETTH	NTVDYA-YG
Altal_113526	HETTH	STQDLA-YG

Continued Table S4

Linrh_383136	HEMTH	GTDDNA-YG
Polfu_517549	HEMTH	GTDDYGTYG
Cloaq_633927	HEMTH	GTDDYGTYE
Aulhe_308457	HEFAH	GTQDLG-YG
Erebi_464438	HEFTH	GTNDNG-YG
Aaoar_389579	HEFTH	GTDDYGVYG
Psehy_165348	HESTH	GTDDYG-YG
Phyci_627813	HEMTH	GTIDIG-YG
Micmi_413312	HEYTH	GTQDLA-YG
Totfu_705093	HEMTH	ETDDKT-MG
Totfu_698912	HEMTH	STDDFGHYG
Venin_21517	HEMTH	ATDDFGHYG
Micmi_426174	HETTH	STVDFNNYG
Corca_655616	HELTH	ATTDFA-YG
Botdo_290783	HELSH	PARDYA-IG
Macph_537	HELSH	RCQDFA-VG
Dipse_5710	HELAH	PARDYA-YG
Neopa_6444	HELTH	ATDDFA-AE
Aspnid_2159	HEYAH	GTEDIA-YG
Aspnid_9591	HELAH	ET-----YG
Aspfu_102465	HELAH	ET-----YG
Psehy_535466	HEMSH	ATGDYA-YG
Psehy_135362	HEFAH	WIVDVA-YF
Pytr_06872	HEMTH	ICSDYA-YG
Cerzm_103453	HELTH	TCDDLA-YG
Zymtr_39241	HEMAH	GCADYA-YF
Altal_119013	HEMTH	GTNDYG-YG
Dotsy_422152	HEMTH	GTDDYG-YG
Lizem_165069	HEMTH	GTEDYG-YG
Karrh_527022	HEFTH	GTTDYA-YG
Parsp_1191399	HEMTH	GTTDYA-YG
Bimnz_529613	HEMTH	GTGDYG-YG
Maseb_147769	HEMTH	GTDDWG-YG
Melpu_381455	HEFTH	GTDDWA-YG
Plesi_450899	HEMTH	GTTDWA-YG
Botdo_289873	HEVSH	ETRDWG-FL
Dipse_1285	HEMTH	ATDDIRHDK
Venin_15820	HELTH	STDDLA-YD
Botdo_298250	HEFLH	AARDYGHLW
Erebi_454198	HELMH	GLMDYA-YT
Venin_18283	HELTH	VTTDIT-YE
Micmi_454111	HELTH	PTVDHC-QG
Dotsy_429075	HEFSH	RLLDYA-YG
Rhyru_113199	HEYSH	AKQDWA-YG
Macan_414708	HEMHH	--TDYA-YG
Psehy_513790	HELTH	DDEDNP-YG
Parsp_1262851	HELTH	-TDDHT-YN
Amnli_536872	HELFH	DDADRC-YG

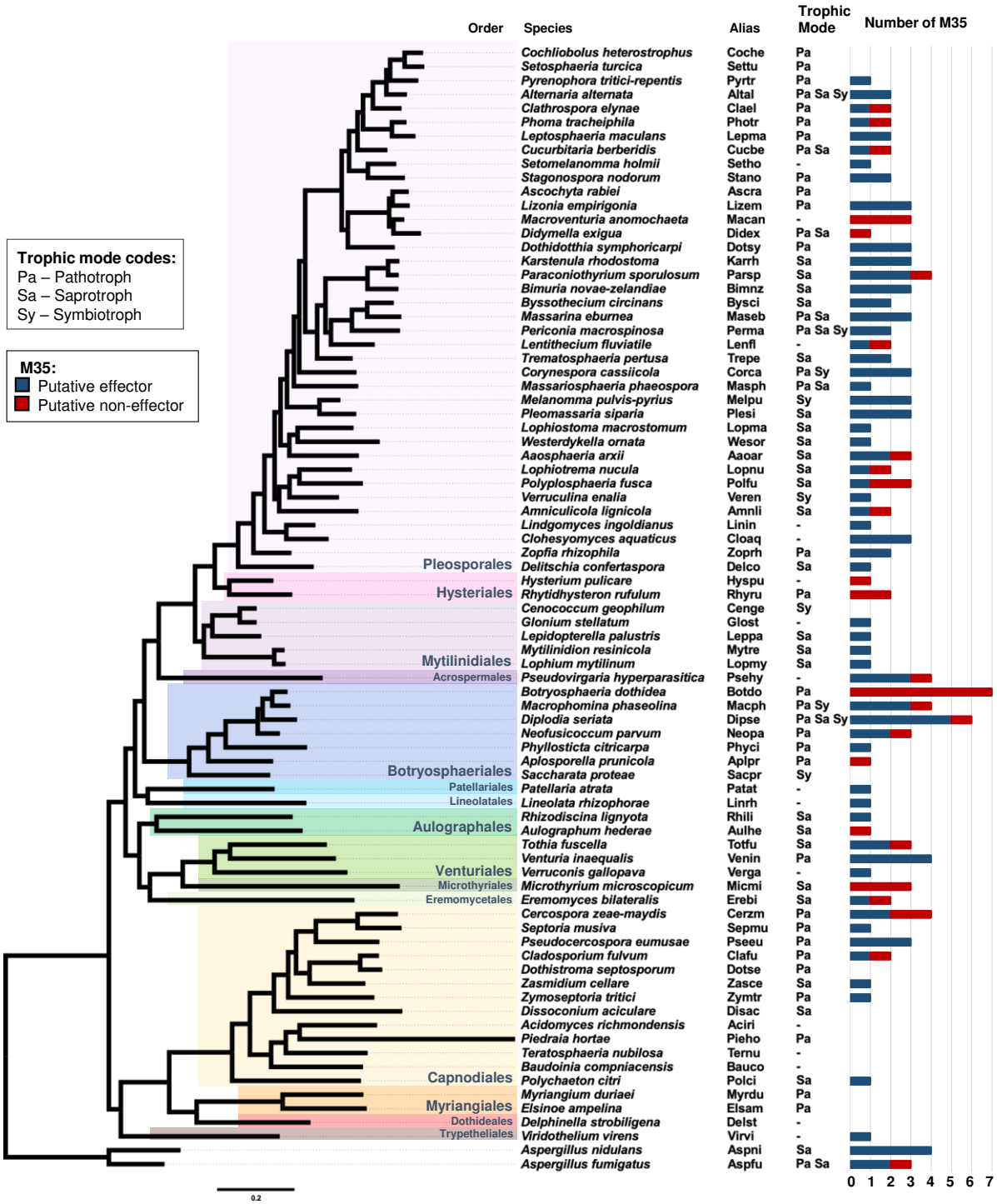

Figure S1. Distribution of putative effector M35s and putative non-effector M35s among 79 species across the Dothideomycetes class of fungi. The Maximum-likelihood consensus tree was based on a dataset of 1851 single-copy ortholog proteins. Phylogenomic tree, Alias, and Trophic Modes are from a previous study (Dal Sasso et al. 2023).

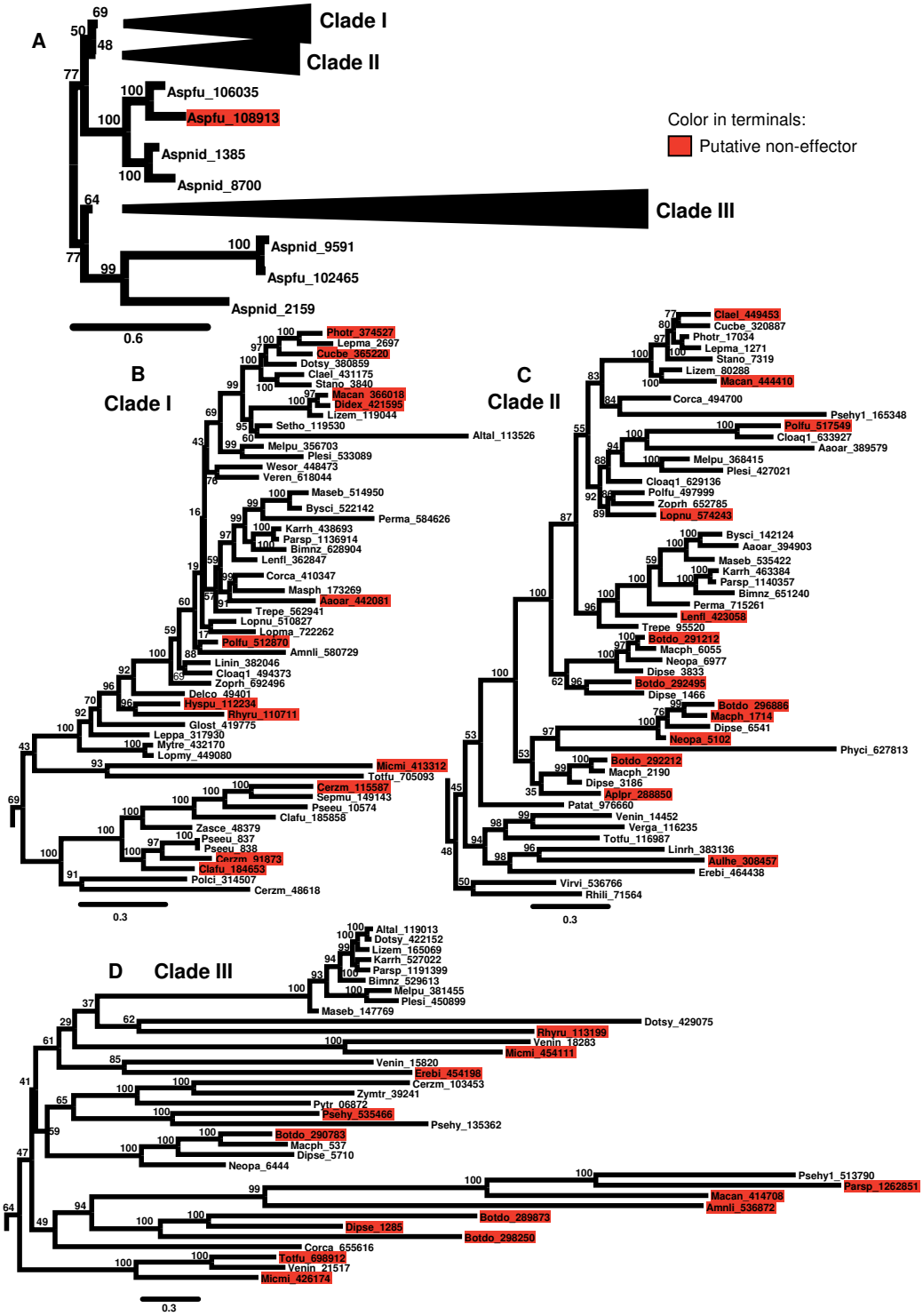

Figure S2. Maximum likelihood tree of the Deuterolysin Metalloprotease (M35) gene family across the Dothideomycetes. The analysis was based on the full set of 146 protein sequences of M35s obtained from 65 species across the Dothideomycetes class of fungi, with *Aspergillus nidulans* and *A. fumigatus* as outgroups. **A**. Overview of the unrooted consensus showing three major clades (collapsed into triangles) with low bootstrap values (<70). **B-D**. Expanded views show the internal composition of each clade. **B**. Clade I. **C**. Clade II. **D**. Clade III. Nodal support values are given as bootstrap values above the branches. Branch lengths are drawn to scale. Scale bar corresponds to the expected number of substitutions per site. Red terminals indicate putative non-effector M35s.

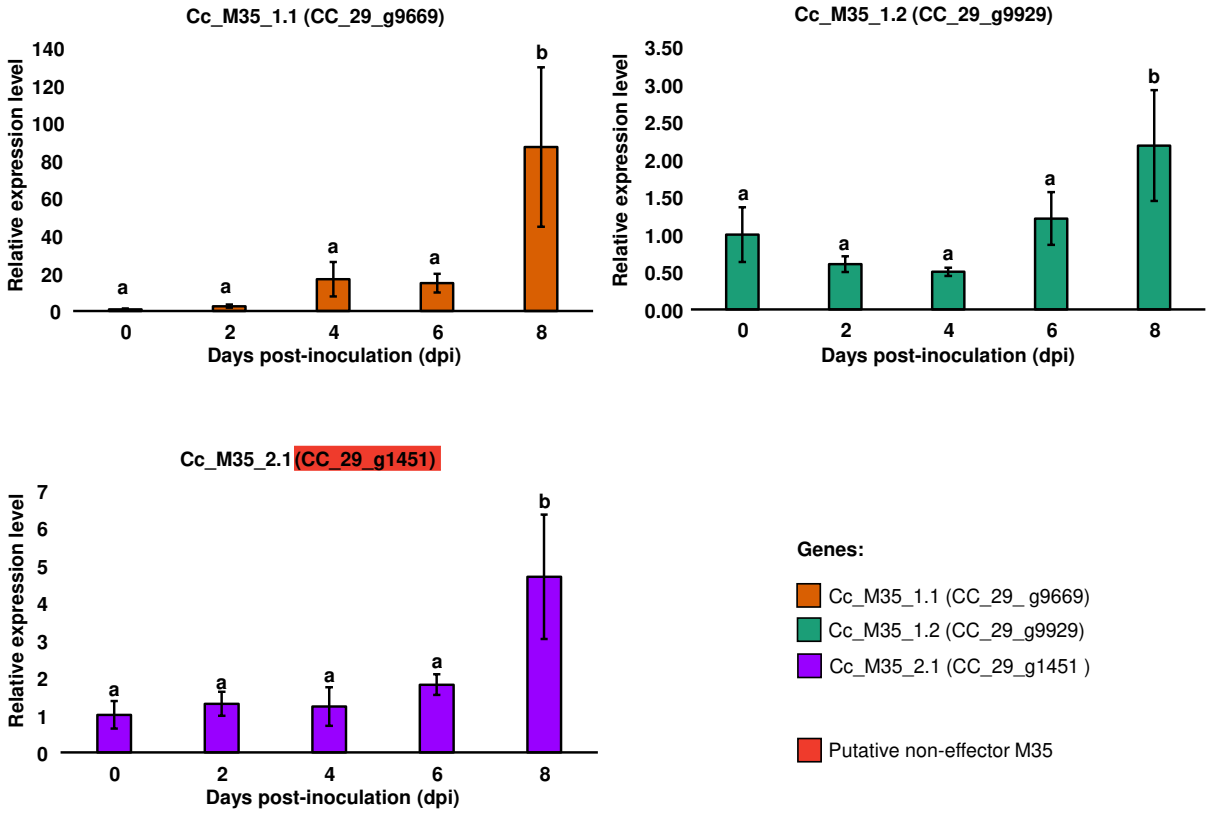

Figure S3. Relative expression levels of three Deuterolysin Metalloprotease (M35) genes of *Corynespora cassiicola* isolate CC_29 on soybean leaves, during 0, 2, 4, 6, and 8 days post-inoculation (dpi), respectively. Data were obtained from the RT-qPCR analyses. The relative expression levels were calculated using the $2^{-\Delta\Delta Ct}$ method, with four biological replicates for each time point. The constitutive β-tubulin gene of *C. cassiicola* was used as an endogenous control. The relative expression level was calibrated and set as 1 at 0 dpi. The letters above bars indicate statistically significant differences according to Tukey's test (p-value < 0.05). Error bars show the standard error of the mean. Levels of expression were color-coded according to the three M35 genes, as indicated.

REFERENCES

Arnaud, M.B., Cerqueira, G.C., Inglis, D.O., Skrzypek, M.S., Binkley, J., Chibucos, M.C., Crabtree, J., Howarth, C., Orvis, J., Shah, P., Wymore, F., Binkley, G., Miyasato, S.R., Simison, M., Sherlock, G., Wortman, J.R., 2012. The *Aspergillus* Genome Database (AspGD): recent developments in comprehensive multispecies curation, comparative genomics and community resources. Nucleic Acids Res 40, D653–D659. https://doi.org/10.1093/nar/gkr875

Blanco-Ulate, B., Rolshausen, P., Cantu, D., 2013. Draft Genome Sequence of *Neofusicoccum parvum* Isolate UCR-NP2, a Fungal Vascular Pathogen Associated with Grapevine Cankers. Genome Announc 1, e00339-13. https://doi.org/10.1128/genomeA.00339-13

Chang, T.-C., Salvucci, A., Crous, P.W., Stergiopoulos, I., 2016. Comparative Genomics of the Sigatoka Disease Complex on Banana Suggests a Link between Parallel Evolutionary Changes in *Pseudocercospora fijiensis* and *Pseudocercospora eumusae* and Increased Virulence on the Banana Host. PLoS Genet 12, e1005904. https://doi.org/10.1371/journal.pgen.1005904

Dal'Sasso, T.C.S., Rocha, V.D., Rody, H.V.S., Costa, M.D.B.L., Oliveira, L.O., 2022. The necrosis- and ethylene-inducing peptide 1-like protein (NLP) gene family of the plant pathogen *Corynespora cassiicola*. Curr Genet 68, 645–659. https://doi.org/10.1007/s00294-022-01252-0

Dal'Sasso, T.C.S., Rody, H.V.S., Grijalba, P.E., Oliveira, L.O., 2021. Genome sequences and in silico effector mining of *Corynespora cassiicola* CC_29 and *Corynespora olivacea* CBS 114450. Arch Microbiol 203, 5257–5265. https://doi.org/10.1007/s00203-021-02456-7

Dang, H.X., Pryor, B., Peever, T., Lawrence, C.B., 2015. The *Alternaria* genomes database: a comprehensive resource for a fungal genus comprised of saprophytes, plant pathogens, and allergenic species. BMC Genomics 16, 239. https://doi.org/10.1186/s12864-015-1430-7

De Wit, P.J.G.M., van der Burgt, A., Ökmen, B., Stergiopoulos, I., Abd-Elsalam, K.A., Aerts, A.L., Bahkali, A.H., Beenen, H.G., Chettri, P., Cox, M.P., Datema, E., de Vries, R.P., Dhillon, B., Ganley, A.R., Griffiths, S.A., Guo, Y., Hamelin, R.C., Henrissat, B., Kabir, M.S., Jashni, M.K., Kema, G., Klaubauf, S., Lapidus, A., Levasseur, A., Lindquist, E., Mehrabi, R., Ohm, R.A., Owen, T.J., Salamov, A., Schwelm, A., Schijlen, E., Sun, H., van den Burg, H.A., van Ham, R.C.H.J., Zhang, S., Goodwin, S.B., Grigoriev, I. V., Collemare, J., Bradshaw, R.E., 2012. The Genomes of the Fungal Plant Pathogens *Cladosporium fulvum* and *Dothistroma septosporum* Reveal Adaptation to Different Hosts and Lifestyles But Also Signatures of Common Ancestry. PLoS Genet 8, e1003088. https://doi.org/10.1371/journal.pgen.1003088

Deng, C.H., Plummer, K.M., Jones, D.A.B., Mesarich, C.H., Shiller, J., Taranto, A.P., Robinson, A.J., Kastner, P., Hall, N.E., Templeton, M.D., Bowen, J.K., 2017. Comparative analysis of the predicted secretomes of Rosaceae scab pathogens *Venturia inaequalis* and *V. pirina* reveals expanded effector families and putative determinants of host range. BMC Genomics 18, 339. https://doi.org/10.1186/s12864-017-3699-1

Fedorova, N.D., Khaldi, N., Joardar, V.S., Maiti, R., Amedeo, P., Anderson, M.J., Crabtree, J., Silva, J.C., Badger, J.H., Albarraq, A., Angiuoli, S., Bussey, H., Bowyer, P., Cotty, P.J., Dyer, P.S., Egan, A., Galens, K., Fraser-Liggett, C.M., Haas, B.J., Inman, J.M., Kent, R., Lemieux, S., Malavazi, I., Orvis, J., Roemer, T., Ronning, C.M., Sundaram, J.P., Sutton, G., Turner, G., Venter, J.C., White, O.R., Whitty, B.R., Youngman, P., Wolfe, K.H., Goldman, G.H., Wortman, J.R., Jiang, B., Denning, D.W., Nierman, W.C., 2008. Genomic Islands in the Pathogenic Filamentous Fungus *Aspergillus fumigatus*. PLoS Genet 4, e1000046. https://doi.org/10.1371/journal.pgen.1000046

Gao, S., Zeng, R., Xu, L., Song, Z., Gao, P., Dai, F., 2020. Genome sequence and spore germination-associated transcriptome analysis of *Corynespora cassiicola* from cucumber. BMC Microbiol 20, 199. https://doi.org/10.1186/s12866-020-01873-w

Goodwin, S.B., Ben M'Barek, S., Dhillon, B., Wittenberg, A.H.J., Crane, C.F., Hane, J.K., Foster, A.J., Van der Lee, T.A.J., Grimwood, J., Aerts, A., Antoniw, J., Bailey, A., Bluhm, B., Bowler, J., Bristow, J., van der Burgt, A., Canto-Canché, B., Churchill, A.C.L., Conde-Ferràez, L., Cools, H.J., Coutinho, P.M., Csukai, M., Dehal, P., De Wit, P., Donzelli, B., van de Geest, H.C., van Ham, R.C.H.J., Hammond-Kosack, K.E., Henrissat, B., Kilian, A., Kobayashi, A.K., Koopmann, E., Kourmpetis, Y., Kuzniar, A., Lindquist, E., Lombard, V., Maliepaard, C., Martins, N., Mehrabi, R., Nap, J.P.H., Ponomarenko, A., Rudd, J.J., Salamov, A., Schmutz, J., Schouten, H.J., Shapiro, H., Stergiopoulos, I., Torriani, S.F.F., Tu, H., de Vries, R.P., Waalwijk, C., Ware, S.B., Wiebenga, A., Zwiers, L.-H., Oliver, R.P., Grigoriev, I. V., Kema, G.H.J., 2011. Finished Genome of the Fungal Wheat Pathogen *Mycosphaerella graminicola* Reveals Dispensome Structure, Chromosome Plasticity, and Stealth Pathogenesis. PLoS Genet 7, e1002070. https://doi.org/10.1371/journal.pgen.1002070

Guarnaccia, V., Gehrmann, T., Silva-Junior, G.J., Fourie, P.H., Haridas, S., Vu, D., Spatafora, J., Martin, F.M., Robert, V., Grigoriev, I. V., Groenewald, J.Z., Crous, P.W., 2019. *Phyllosticta citricarpa* and sister species of global importance to *Citrus*. Mol Plant Pathol 20, 1619–1635. https://doi.org/10.1111/mpp.12861

Hane, J.K., Lowe, R.G.T., Solomon, P.S., Tan, K.-C., Schoch, C.L., Spatafora, J.W., Crous, P.W., Kodira, C., Birren, B.W., Galagan, J.E., Torriani, S.F.F., McDonald, B.A., Oliver, R.P., 2007. Dothideomycete–Plant Interactions Illuminated by Genome Sequencing and EST Analysis of the Wheat Pathogen *Stagonospora nodorum*. Plant Cell 19, 3347–3368. https://doi.org/10.1105/tpc.107.052829

Haridas, S., Albert, R., Binder, M., Bloem, J., LaButti, K., Salamov, A., Andreopoulos, B., Baker, S.E., Barry, K., Bills, G., Bluhm, B.H., Cannon, C., Castanera, R., Culley, D.E., Daum, C., Ezra, D., González, J.B., Henrissat, B., Kuo, A., Liang, C., Lipzen, A., Lutzoni, F., Magnuson, J., Mondo, S.J., Nolan, M., Ohm, R.A., Pangilinan, J., Park, H.-J., Ramírez, L., Alfaro, M., Sun, H., Tritt, A., Yoshinaga, Y., Zwiers, L.-H., Turgeon, B.G., Goodwin, S.B., Spatafora, J.W., Crous, P.W., Grigoriev, I.V., 2020. 101 Dothideomycetes genomes: A test case for predicting lifestyles and emergence of pathogens. Stud Mycol 96, 141–153. https://doi.org/10.1016/j.simyco.2020.01.003

Islam, M.S., Haque, M.S., Islam, M.M., Emdad, E.M., Halim, A., Hossen, Q.M.M., Hossain, M.Z., Ahmed, B., Rahim, S., Rahman, M.S., Alam, M.M., Hou, S., Wan,

X., Saito, J.A., Alam, M., 2012. Tools to kill: Genome of one of the most destructive plant pathogenic fungi *Macrophomina phaseolina*. BMC Genomics 13, 493. https://doi.org/10.1186/1471-2164-13-493

Knapp, D.G., Németh, J.B., Barry, K., Hainaut, M., Henrissat, B., Johnson, J., Kuo, A., Lim, J.H.P., Lipzen, A., Nolan, M., Ohm, R.A., Tamás, L., Grigoriev, I. V., Spatafora, J.W., Nagy, L.G., Kovács, G.M., 2018. Comparative genomics provides insights into the lifestyle and reveals functional heterogeneity of dark septate endophytic fungi. Sci Rep 8, 6321. https://doi.org/10.1038/s41598-018-24686-4

Li, B., Yang, Y., Cai, J., Liu, X., Shi, T., Li, C., Chen, Y., Xu, P., Huang, G., 2021. Genomic Characteristics and Comparative Genomics Analysis of Two Chinese *Corynespora cassiicola* Strains Causing Corynespora Leaf Fall (CLF) Disease. Journal of Fungi 7, 485. https://doi.org/10.3390/jof7060485

Looi, H.K., Toh, Y.F., Yew, S.M., Na, S.L., Tan, Y.C., Chong, P.-S., Khoo, J.-S., Yee, W.-Y., Ng, K.P., Kuan, C.S., 2017. Genomic insight into pathogenicity of dematiaceous fungus *Corynespora cassiicola*. PeerJ 5, e2841. https://doi.org/10.7717/peerj.2841

Lopez, D., Ribeiro, S., Label, P., Fumanal, B., Venisse, J.S., Kohler, A., de Oliveira, R.R., Labutti, K., Lipzen, A., Lail, K., Bauer, D., Ohm, R.A., Barry, K.W., Spatafora, J., Grigoriev, I. V., Martin, F.M., Pujade-Renaud, V., 2018. Genome-Wide Analysis of *Corynespora cassiicola* Leaf Fall Disease Putative Effectors. Front Microbiol 9, 276. https://doi.org/10.3389/fmicb.2018.00276

Manning, V.A., Pandelova, I., Dhillon, B., Wilhelm, L.J., Goodwin, S.B., Berlin, A.M., Figueroa, M., Freitag, M., Hane, J.K., Henrissat, B., Holman, W.H., Kodira, C.D., Martin, J., Oliver, R.P., Robbertse, B., Schackwitz, W., Schwartz, D.C., Spatafora, J.W., Turgeon, B.G., Yandava, C., Young, S., Zhou, S., Zeng, Q., Grigoriev, I. V, Ma, L.-J., Ciuffetti, L.M., 2013. Comparative Genomics of a Plant-Pathogenic Fungus, *Pyrenophora tritici-repentis*, Reveals Transduplication and the Impact of Repeat Elements on Pathogenicity and Population Divergence. G3 Genes|Genomes|Genetics 3, 41–63. https://doi.org/10.1534/g3.112.004044

Marsberg, A., Kemler, M., Jami, F., Nagel, J.H., Postma-Smidt, A., Naidoo, S., Wingfield, M.J., Crous, P.W., Spatafora, J.W., Hesse, C.N., Robbertse, B., Slippers, B., 2017. *Botryosphaeria dothidea*: a latent pathogen of global importance to woody plant health. Mol Plant Pathol 18, 477–488. https://doi.org/10.1111/mpp.12495

Mondo, S.J., Dannebaum, R.O., Kuo, R.C., Louie, K.B., Bewick, A.J., LaButti, K., Haridas, S., Kuo, A., Salamov, A., Ahrendt, S.R., Lau, R., Bowen, B.P., Lipzen, A., Sullivan, W., Andreopoulos, B.B., Clum, A., Lindquist, E., Daum, C., Northen, T.R., Kunde-Ramamoorthy, G., Schmitz, R.J., Gryganskyi, A., Culley, D., Magnuson, J., James, T.Y., O'Malley, M.A., Stajich, J.E., Spatafora, J.W., Visel, A., Grigoriev, I. V, 2017. Widespread adenine N6-methylation of active genes in fungi. Nat Genet 49, 964–968. https://doi.org/10.1038/ng.3859

Morales-Cruz, A., Amrine, K.C.H., Blanco-Ulate, B., Lawrence, D.P., Travadon, R., Rolshausen, P.E., Baumgartner, K., Cantu, D., 2015. Distinctive expansion of gene families associated with plant cell wall degradation, secondary metabolism,

and nutrient uptake in the genomes of grapevine trunk pathogens. BMC Genomics 16, 469. https://doi.org/10.1186/s12864-015-1624-z

Mosier, A.C., Miller, C.S., Frischkorn, K.R., Ohm, R.A., Li, Z., LaButti, K., Lapidus, A., Lipzen, A., Chen, C., Johnson, J., Lindquist, E.A., Pan, C., Hettich, R.L., Grigoriev, I. V., Singer, S.W., Banfield, J.F., 2016. Fungi Contribute Critical but Spatially Varying Roles in Nitrogen and Carbon Cycling in Acid Mine Drainage. Front Microbiol 7. https://doi.org/10.3389/fmicb.2016.00238

Ohm, R.A., Feau, N., Henrissat, B., Schoch, C.L., Horwitz, B.A., Barry, K.W., Condon, B.J., Copeland, A.C., Dhillon, B., Glaser, F., Hesse, C.N., Kosti, I., LaButti, K., Lindquist, E.A., Lucas, S., Salamov, A.A., Bradshaw, R.E., Ciuffetti, L., Hamelin, R.C., Kema, G.H.J., Lawrence, C., Scott, J.A., Spatafora, J.W., Turgeon, B.G., de Wit, P.J.G.M., Zhong, S., Goodwin, S.B., Grigoriev, I. V., 2012. Diverse Lifestyles and Strategies of Plant Pathogenesis Encoded in the Genomes of Eighteen Dothideomycetes Fungi. PLoS Pathog 8, e1003037. https://doi.org/10.1371/journal.ppat.1003037

Peter, M., Kohler, A., Ohm, R.A., Kuo, A., Krützmann, J., Morin, E., Arend, M., Barry, K.W., Binder, M., Choi, C., Clum, A., Copeland, A., Grisel, N., Haridas, S., Kipfer, T., LaButti, K., Lindquist, E., Lipzen, A., Maire, R., Meier, B., Mihaltcheva, S., Molinier, V., Murat, C., Pöggeler, S., Quandt, C.A., Sperisen, C., Tritt, A., Tisserant, E., Crous, P.W., Henrissat, B., Nehls, U., Egli, S., Spatafora, J.W., Grigoriev, I. V., Martin, F.M., 2016. Ectomycorrhizal ecology is imprinted in the genome of the dominant symbiotic fungus *Cenococcum geophilum*. Nat Commun 7, 12662. https://doi.org/10.1038/ncomms12662

Rouxel, T., Grandaubert, J., Hane, J.K., Hoede, C., Van De Wouw, A.P., Couloux, A., Dominguez, V., Anthouard, V., Bally, P., Bourras, S., Cozijnsen, A.J., Ciuffetti, L.M., Degrave, A., Dilmaghani, A., Duret, L., Fudal, I., Goodwin, S.B., Gout, L., Glaser, N., Linglin, J., Kema, G.H.J., Lapalu, N., Lawrence, C.B., May, K., Meyer, M., Ollivier, B., Poulain, J., Schoch, C.L., Simon, A., Spatafora, J.W., Stachowiak, A., Turgeon, B.G., Tyler, B.M., Vincent, D., Weissenbach, J., Amselem, J., Quesneville, H., Oliver, R.P., Wincker, P., Balesdent, M.H., Howlett, B.J., 2011. Effector diversification within compartments of the *Leptosphaeria maculans* genome affected by repeat-induced point mutations. Nat Commun 2. https://doi.org/10.1038/ncomms1189

Teixeira, M.M., Moreno, L.F., Stielow, B.J., Muszewska, A., Hainaut, M., Gonzaga, L., Abouelleil, A., Patané, J.S.L., Priest, M., Souza, R., Young, S., Ferreira, K.S., Zeng, Q., da Cunha, M.M.L., Gladki, A., Barker, B., Vicente, V.A., de Souza, E.M., Almeida, S., Henrissat, B., Vasconcelos, A.T.R., Deng, S., Voglmayr, H., Moussa, T.A.A., Gorbushina, A., Felipe, M.S.S., Cuomo, C.A., de Hoog, G.S., 2017. Exploring the genomic diversity of black yeasts and relatives (*Chaetothyriales*, *Ascomycota*). Stud Mycol 86, 1–28. https://doi.org/10.1016/j.simyco.2017.01.001

Verma, S., Gazara, R.K., Nizam, S., Parween, S., Chattopadhyay, D., Verma, P.K., 2016. Draft genome sequencing and secretome analysis of fungal phytopathogen *Ascochyta rabiei* provides insight into the necrotrophic effector repertoire. Sci Rep 6, 24638. https://doi.org/10.1038/srep24638

Xu, C., Xue, C., Hou, M., Geng, Y., Zang, R., Wu, H., Zhang, M., 2021. Nanopore/Illumina Hybrid Genome Sequence Resource for *Corynespora cassiicola* Strain XJ Infecting Rubber Tree in China. Plant Dis 105, 3727–3731. https://doi.org/10.1094/PDIS-03-21-0458-A

Zeiner, C.A., Purvine, S.O., Zink, E.M., Paša-Tolić, L., Chaput, D.L., Haridas, S., Wu, S., LaButti, K., Grigoriev, I. V., Henrissat, B., Santelli, C.M., Hansel, C.M., 2016. Comparative Analysis of Secretome Profiles of Manganese(II)-Oxidizing Ascomycete Fungi. PLoS One 11, e0157844. https://doi.org/10.1371/journal.pone.0157844

GENERAL CONCLUSIONS

GENERAL CONCLUSIONS

Our study provides a basis for understanding the evolutionary history of two gene families (PME and M35) across a broad range of species within the Dothideomycetes class of fungi.

The PME family size was small, with a maximum of 5 members per genome among Dothideomycetes species. There were three major PME clades across the Dothideomycetes. Each PME clade was shaped largely by independent evolutionary patterns. Notably, two clades (PME1 and PME2) have experienced ancient duplications and sequent gene retention events. In contrast, the third clade (PME3) has undergone biased gene loss. The phylogenic analyses suggest an ancient origin for PME in *C. cassiicola*. The five PME haplogroups in *C. cassiicola* seem to be under distinct selective constraints. The gene CC_29_g7533 (Cc_PME2.3) in *C. cassiicola* exhibited the highest expression levels during from six to eight days post-inoculation on soybean leaves.

For the M35 family, the large variation in the number of members suggests the occurrence of gene duplications and gene losses across the Dothideomycetes. The putative effector M35s were widespread among the Dothideomycetes. In *C. cassiicola*, sub-clades (Cc_M35_1.1 and Cc_M35_2.1) exhibited signals of biased gene retention, while Cc_M35_1.2 and Cc_M35_2.2 likely have undergone gene loss. The gene CC_29_g9669, a representative of the sub-clade Cc_M35_1.1, displayed the highest relative expression levels throughout the soybean infection, whereas other genes showed low expression levels.